DISSERTATION

submitted to the
Combined Faculty for the Natural Sciences and for Mathmetics
of the Ruperto-Carola University of Heidelberg, Germany
for the degree of
Doctor of Natural Sciences

presented by
MS in Chemistry: Robina Shaheen
born in Faisalabad, Pakistan
Oral examination: 28.10.2005

Investigation of the Oxygen Isotope Exchange Between Carbon Dioxide and Ozone via $O(^1D)$

Referees: **Prof. Dr. Thomas Röckmann**

Prof. Dr. Wolfgang Krätschmer

Erklärung gemäß § 7(3) b) und c) der Promotionsordnung:

a) Ich erkläre hiermit, dass ich die vorgelegte Dissertation selbst verfasst und mich dabei keineranderen als der von mir ausdrücklich bezeichneten Quellen bedient habe.

b) Ich erkläre hiermit, dass ich an keiner anderen Stelle ein Prüfungsverfahren beantragt bzw. die Dissertation in dieser oder anderer Form bereits anderweitig als Prüfungsarbeit verwendet oder einer anderen Fakultät als Dissertation vorgelegt habe.

Robina Shaheen

Abstract

Carbon dioxide in the middle atmosphere shows an increasing enrichment in the heavy oxygen isotopes with altitude which preferential enrichment for ^{17}O according to $\delta^{17}O = 1.7\ \delta^{18}O$. This is contrary to tropospheric CO_2 where $\delta^{17}O \sim 0.5\delta^{18}O$. These isotope enrichments are transferred from O_3 into CO_2, but details of the mechanism are not understood yet. A systematic study was carried out using O_2 and CO_2 gases of different isotopic composition. Results show the existence of a photochemical isotope equilibrium between O_2 and CO_2, which is independent of the initial isotopic composition and shows equal enrichments for ^{17}O and ^{18}O. Additional experiments were conducted to investigate the effect of temperature, pressure and O_2/CO_2 ratio. Data revealed that the magnitude of enrichment at photochemical equilibrium depends on pressure and on O_2/CO_2 ratios with a decrease in enrichment at higher pressures. Also, the enrichment in CO_2 showed a positive temperature dependence. The measurement of asymmetric O_3 in one experiment yields additional insight into the isotope exchange mechanism and shows the absence of anomalous fractionation steps in the CO_3^* intermediate. The experimental data were modeled with the chemical kinetics software Facsimile. In addition, a large set of new measurements of the isotopic composition of stratospheric CO_2 are presented, extending the earlier data down to the tropopause.

Zusammenfassung

In der mittleren Atmosphäre zeigt Kohlendioxid eine Anreicherung in den schweren Sauerstoffisotopen, die mit der Höhe zunimmt wobei ^{17}O bevorzugt in CO_2 zu finden ist. Es ergibt sich der ungewöhnliche Zusammenhang $\delta^{17}O = 1.7\delta^{18}O$. Für troposphärisches CO_2 dagegen gilt: $\delta^{17}O \sim 0.5\ \delta^{18}O$. Diese Isotopenanreicherungen werden von O_3 in CO_2 übertragen, aber die Details des Isotopentransfers sind noch nicht verstanden. In dieser Arbeit wurde eine systematische Studie unter Verwendung von O_2 und CO_2 unterschiedlicher Isotopenzusammensetzung durchgeführt. Die Ergebnisse zeigen ein photochemisches Isotopengleichgewicht zwischen O_2 und CO_2, das unabhängig von der anfänglichen Isotopenzusammensetzung ist und ähnliche Anreicherungen für ^{17}O und ^{18}O aufweist. Weitere Experimente zum Einfluss von Temperatur, Druck und Mischungsverhältnis wurden durchgeführt. Die Anreicherungen im photochemischen Gleichgewicht sind abhängig vom Druck und dem O_2/CO_2 Verhältnis und nehmen mit zunehmendem Druck ab. Sie zeigen außerdem eine positive Temperaturabhängigkeit. Die Messung von asymmetrischem Ozon in

einem Experiment liefert zusätzliche Einsichten in den Isotopenaustauschprozess und zeigt, dass keine anomalen Isotopeneffekte im intermediären CO_3^* Komplex auftreten. Die experimentellen Daten wurden mit der Software Facsimile modelliert. Zusätzlich werden neue Isotopenmessungen von stratosphärischem CO_2 vorgestellt, die die vorhandenen Messungen bis zur Tropopause vervollständigen.

Who created seven heavens in harmony.
Thou can't see no fault in Beneficent One's creation; then look again:
can't thou see any rift.
(Al-Quran 67:3)

Table of Contents

1 Introduction

The study of atmospheric dynamics such as stratosphere-troposphere exchange and stratospheric mixing processes has focused on concentration measurements of inert trace gases with long life time such as CO_2, N_2O and halogenated compounds such as SF_6, CF_4 and the chlorofluorocarbons (CFCs) [Boering et al.1996, Maiss et al. 1996]. Mass independent anomalies observed in the multi-oxygen isotopic measurements of stratospheric and mesospheric CO_2 offer another potential tracer of upper atmosphere dynamics [Boering et al. 2004, Alexander et al. 2001, Lämmerzahl et al. 2002, Thiemens et al. 1995a, b]. The anomaly can also be used as a tracer of terrestrial gross carbon fluxes on a decadal to millienial time scales[Hoag et al. 2005, Luz et al. 1999] because it is directly related to gross primary productivity. However, a prerequisite for the quantitative application of three-isotope technique to study stratospheric transport and chemistry is a thorough understanding of the anomalous isotope exchange mechanism, which is still missing.

Most isotopic fractionation processes such as diffusion, evaporation-condensation and kinetic effects depends on the masses of the molecules involved. For oxygen with three stable isotopes, this leads to a correlation between ^{17}O and ^{18}O as $\delta^{17}O \sim 0.5\delta^{18}O$. Here the commonly used delta (δ) values denote the relative deviations of the isotope ratios $^{17}O/^{16}O$ and $^{18}O/^{16}O$ (^{17}R and ^{18}R, respectively) in a sample (R_s) from a standard material (R_{st}) in permill (‰), e.g. $\delta^{17}O = (^{17}R_s/^{17}R_{st} -1)*1000‰$.

Fractionation processes which do not obey this relation are called "anomalous" or "mass independent" (for details see sec. 2.1.3). On a three isotope plot of $\delta^{17}O$ (ordinate) versus $\delta^{18}O$ (abscissa) mass dependent fractionation processes define a line with slope of ~0.5 that passes through the origin (Vienna Standard Mean Ocean Water). A mass independently fractionated compound will not lie on this mass dependent fractionation (MDF) line as shown in Figure 1.1.

Since the startling discovery of the anomalous fractionation in ozone [Mauersberger 1981, 1987], in the stratosphere and laboratory [Thiemens and Heidenreich 1983] anomalous compositions have been observed in many other atmospheric trace species such as N_2O, CO, HO_2, SO_4^{-2} [Brenninkmeijer et al.2003] (for details see sec. 2.1.3).

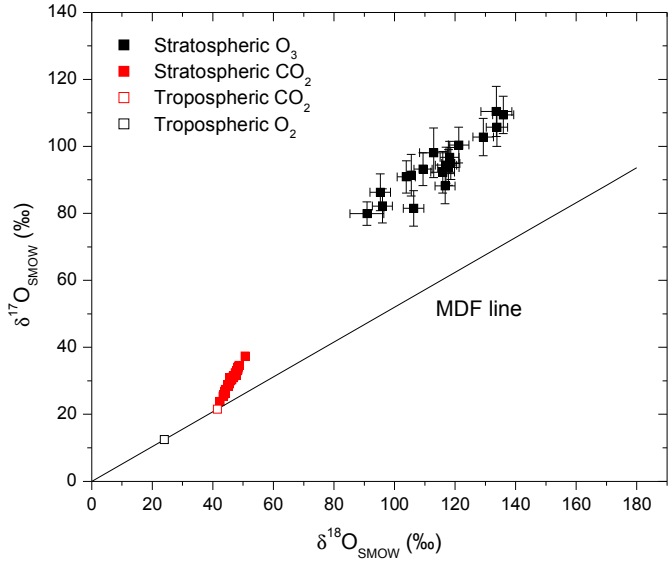

Figure 1.1: Three isotope plot with MDF line ($\delta^{17}O \sim 0.5\delta^{18}O$). Stratospheric ozone ($\delta^{17}O \sim 0.6\delta^{18}O$) [Krankowsky et al. 2000], stratospheric CO_2 ($\delta^{17}O \sim 1.6\delta^{18}O$) [Lämmerzahl et al. 2002]. Tropospheric CO_2 and O_2 are also shown for comparison.

Tropospheric CO_2 possesses a mass dependent isotopic composition (Figure 1.1) that is controlled by the biosphere, mostly through exchange with water within leaf stomata [Francy and Tans 1987] and soil water [Tans 1998]. However upon entering the stratosphere, CO_2 acquires a mass independent anomaly from O_3 via $O(^1D)$ through the following sequence of reactions:

$$O_3 + h\nu \rightarrow (O^1D) + O_2 \quad \lambda < 310\ nm \qquad (R1)$$

$$CO_2 + O(^1D) \rightarrow CO^*_3 \qquad (R2)$$

$$CO^*_3 \rightarrow CO_2 + O(^3P) \qquad (R3)$$

$$CO^*_3 \rightarrow CO_2 + O(^1D) \qquad (R4)$$

The surprising observation is that the isotope anomaly in stratospheric CO_2 is unique. In contrast to ozone and various other substances related to ozone, where the ^{17}O and ^{18}O enrichments are approximately equal, stratospheric CO_2 follows the relation $\delta^{17}O \sim 1.7\delta^{18}O$, which has the highest three isotope slope observed in a natural system [Lämmerzahl et al. 2002]. This means that ^{17}O is preferentially incorporated into CO_2 compared to ^{18}O.

1 Introduction

To date, at least four different mechanisms have been proposed to explain the oxygen isotope transfer from O_3 to CO_2.

(1). Simple statistical mixing between the CO_2 and $O(^1D)$ reservoirs according to R1- R3 [Yung et al. 1991, 1997].

(2). Isotope transfer according to R1-R3, including an additional mass dependent fractionation process in the formation or dissociation of the CO^*_3 complex (R2 and R3) [Barth and Zahn 1997].

(3). Isotope transfer according to R1-R3, including an additional mass independent fractionation process in the CO^*_3 complex [Wen and Thiemens 1993, Johnston et al. 2000].

(4). An additional (e.g. Mesospheric) source of the mass independent anomaly in stratospheric CO_2 [Thiemens et al., 1995].

The isotope exchange on the singlet surface (R4) has been identified only very recently [Perri et al. 2004] so this channel was not considered in the previous studies. Additionally, given that CO_2 is only a trace compound in air (mixing ratio at present ~ 380 ppm), it is unlikely that the non quenching channel is of relevance to the atmosphere.

From the molecular perspective, isotope transfer is governed by two important effects: first, the isotopic composition of $O(^1D)$ and second by possible fractionation mechanisms in the formation or dissociation of the CO^*_3 complex. If the former is known, the latter can be derived and thus a decision can be made between mechanisms 1-3 above. Unfortunately, the isotopic signature of $O(^1D)$ cannot be measured directly, and it is not clear how it is related to the isotopic composition of its source molecule O_3. Several aspects have to be considered here. First, it is well established that enrichment is not distributed randomly in the O_3 molecule but favors the terminal position (asymmetric O_3) at ambient temperatures due to the advantage of rate coefficients to form asymmetric molecules [Janssen et al. 1999, Tuzson 2005]. The $O(^1D)$ is expected to be formed entirely from the terminal oxygen atoms in O_3 [Sheppard and Walker 1983], and it may have at the outset, an isotope signature significantly different than that of the parent O_3 [Lyons 2001]. The intra molecular distribution of heavy oxygen in O_3 may be temperature dependent, and thus could be different for presently available laboratory measurements compared to stratospheric data. Furthermore, a possible fractionation in the UV photolysis of O_3 which may also be temperature and wavelength dependent, would further modify the isotopic composition of $O(^1D)$. Finally, isotope fractionation in the quenching of $O(^1D)$ with O_2 and other gases may alter the isotopic composition of the fraction of $O(^1D)$ that is available for reaction with CO_2.

Given the lack of information about $O(^1D)$, it is problematic to decide between mechanisms 1-3 above. For mechanism 1 to be true, the $O(^1D)$ from stratospheric O_3 must lie on the extrapolated fit line through the stratospheric CO_2 data, since a simple isotope mixing process proceeds along a straight line between the mixing reservoirs. Mechanism 2 selects a certain mass dependent line between CO^*_3 complex and isotopic composition of $O(^1D)$. For mechanism 3, $O(^1D)$ could lie anywhere on the three isotope plot in principle, and a fractionation mechanism in the CO^*_3 complex would bring it back to the extrapolated fit line (with any slopes for mechanism 3). Regarding mechanism 4, the fact that the extrapolation of stratospheric data precisely intersects the tropospheric isotopic values [Lämmerzahl et al. 2002] indicates that the mechanism actually involves tropospheric CO_2, which gets progressively enriched in the stratosphere. Nevertheless, a possible contribution of a mesospheric source at high altitudes cannot be exclude.

Three sets of laboratory experiments at room temperature have been published to date that investigate the isotopic exchange between CO_2 and $O(^1D)$ in detail. The first study used O_3-CO_2 mixtures that were irradiated with a Hg-pen ray lamp [Wen and Thiemens et al., 1993]. This study confirmed that isotope exchange occurs via (O^1D) but concluded that additional fractionation processes associated with the CO^*_3 intermediate must contribute. The second set of experiments started with O_2-CO_2 mixtures [Johnston et al., 2000]. Photolysis of O_2 was used to produce O_3, which upon photolysis yielded $O(^1D)$ to react with CO_2. These measurements reveal the temporal evolution and the final equilibrium isotopic compositions of the CO_2 and O_2 reservoirs. Although, this situation simulates the atmosphere to some extent where O_3 is recycled through the oxygen reservoir, the results showed a $\delta^{17}O$-$\delta^{18}O$ slope of one similar to the study of Wen and Thiemens[1993]. Recently, Chakraborty and Bhattacharya [2003] reported to have reproduced the stratospheric slope of 1.7 in similar experiments, but using initial gases of slightly different isotopic composition. However, there are certain artifacts in their experimental data which will be discussed in detail. Furthermore, no plausible explanation is given to justify the observed results in the light of previous experiments.

1.1 Objectives

Given all those open questions, a systematic investigation of the isotope exchange mechanism is carried out in the present work to understand the isotope exchange process in the laboratory in more detail and to provide information about the relevant parameters that determine the

observed three-isotope slope in the atmosphere.

The first objective was to investigate the photochemical equilibrium point in a series of laboratory experiments. This included development of experimental techniques for complete oxygen isotope analysis of O_2 and CO_2 and setup of a laboratory photolysis reactor system. Our experimental technique allowed to directly analyze ^{17}O enrichments in CO_2 without assumptions on ^{13}C. We then employed a triangulation method to establish the photochemical isotope equilibrium using mass dependently and anomalously fractionated oxygen and CO_2 gases.

In subsequent measurements series, the effect of temperature and pressure on the CO_2 and O_3 isotope exchange at photochemical and isotope equilibrium were investigated in detail for the first time. Numerical simulations were carried out for the photochemical equilibrium experiments in order to deepen insight into the isotope exchange mechanism between CO_2 and O_3 via $O(^1D)$. Those simulations were then also employed to assess the effect of the results obtained in the laboratory to the atmospheric conditions.

Finally, an extraction and analysis system for complete oxygen isotope characterization of atmospheric CO_2 samples has been set up. Using this system, we have analyzed a considerable number of stratospheric CO_2 samples, in particular extending existing data from samples obtained on balloon platforms down to the tropopause.

2 Background and Theory

In this section, basic theory behind isotope fractionation in equilibrium and kinetic isotope effect is described. An overview about tropospheric and stratospheric CO_2 is included in second section. Some important implications of stratospheric anomaly are briefly described. Last section of this chapter deals with the anomaly in O_3 formation and some observations of heavy isotope enrichments in stratospheric and tropospheric O_3.

2.1 Isotope effects

Stable isotope research in the earth science exploits subtle differences in reaction rate coefficients or equilibrium constants of chemical species that differ only in their isotopic composition, but are otherwise identical. These effects are denoted *kinetic isotope effects* if a reaction rate constant changes upon isotopic substitution, and *thermodynamic* (or *equilibrium*) *isotope effects* if the equilibrium constant is affected. Isotope effects can give rise to different isotope distributions of the same element in different substances or at non-equivalent positions within a single substance, and are called *intermolecular* or *intramolecular* isotope effects, respectively [Müller, 1994]. Often isotope effects are also referred to as (*isotope*) *fractionation* or (*isotope*) *discrimination*.

Many constituents of the earth´s atmosphere, oceans, soils, ice sheets or the earth´s crust, show characteristic variations of their isotopic composition which are caused by isotope effects. For elements heavier than hydrogen, these variations are of the order of 10^{-2} to 10^{-4} relative to the average isotopic composition on earth. Precise analytical measurements by mass spectrometry or infrared absorption spectroscopy allow to quantify these small differences. In a sense, this goes beyond the “traditional” view of chemistry which states that isotopically substituted molecules display the same chemical behavior because their electron configuration is identical.

The differences in physico-chemical properties of isotopic compounds (i.e. Chemical compounds consisting of molecules containing different isotopes of the same element [Mook 2000] are mainly due to the mass differences of the atomic nuclei. Hence, the translational, rotational and vibrational energy levels change and as a consequence also the partition functions. This causes heavier molecules to have lower mean velocities, lower collision frequencies and lower zero point energies. Such changes at the molecular level appear as a macroscopic isotope effects in a number of processes, for example

chemical conversions
isotope exchange reactions
photolysis
diffusion
gravitational separation
phase changes, such as evaporation, dissolution, etc.
chromatography

According to the theory of Bigeleisen and Mayer [1947], isotope effects in exchange reactions and equilibrium processes are expected to vary regularly with mass. This theory of so-called "mass dependent" isotope effects was extended later to kinetic reaction rates [Bigeleisen 1949; Bigeleisen and Wolfsberg 1958]. The Bigeleisen-Mayer theory predicts $^{17}O/^{16}O$ fractionation effects are about half as large as for $^{18}O/^{16}O$, but slight differences are expected for kinetic and equilibrium processes. In the following section, a brief summary of the fractionation laws for mass-dependent isotope effects and anomalous isotope effects is described.

2.1.1 Equilibrium mass-dependent isotope fractionation

The simplest possible exchange reaction is between diatomic molecules. Such a system serve very well to illustrate the physical principles involved in isotopic fractionation.

$$A^lX + B^hX \quad \overrightarrow{\leftarrow} \quad A^hX + B^lX \tag{2.1}$$

Superscripts *l* and *h* stand for light (e.g.^{16}O) and heavy istopes (e.g. ^{17}O or ^{18}O). In this example of monoatomic exchange, the fractionation factor $\alpha_{A/B}$ between the two substances AX and BX is simply the ratio of equilibrium constants at a given temperature relative to the highest temperature (classical) limit (k_∞), i.e.

$$\alpha_{\frac{A}{B}} = \frac{k}{k_\infty} = \frac{\frac{A^hX}{A^lX}}{\frac{B^hX}{B^lX}} = \frac{Q(A^hX)Q(B^lX)}{Q(A^lX)Q(B^hX)} \tag{2.2}$$

where Q stands for the total partition function of the particular isotopologue. The partition function is defined as

$$Q = \Sigma_i g_i \exp\left(\frac{-E_i}{kT}\right) \tag{2.3}$$

where summation is over all quantum states *i* accessible to the system. E_i is the energy of state *i* and g_i is the degeneracy of state *i*. The energy E_i is made up of a series of terms

$$E = E_{tr} + E_0 + E_{vib} + E_{anh} + E_{rot} + E_{rot-str} + E_{rot-vib} + T_e \tag{2.4}$$

where E_{tr} stands for translational energy; E_0 zero point energy; E_{vib} vibrational energy, from which is subtracted the zero point energy, in the harmonic approximation; E_{anh} anharmonic vibrational energy, without zero point energy; E_{rot} rotational energy; $E_{rot\text{-}vib}$ energy associated with rotational-vibrational interaction; and T_e electronic energy. Separation of nuclear and electronic motion corresponds to the Born-Oppenheimer approximation which is justified by the fact that the heavy nuclei remain in virtually fixed position while the electrons move. This is related to the assumption that the potential energy surface for the electronic ground state is the same for isotopically substituted molecules [Richet et al. 1977].

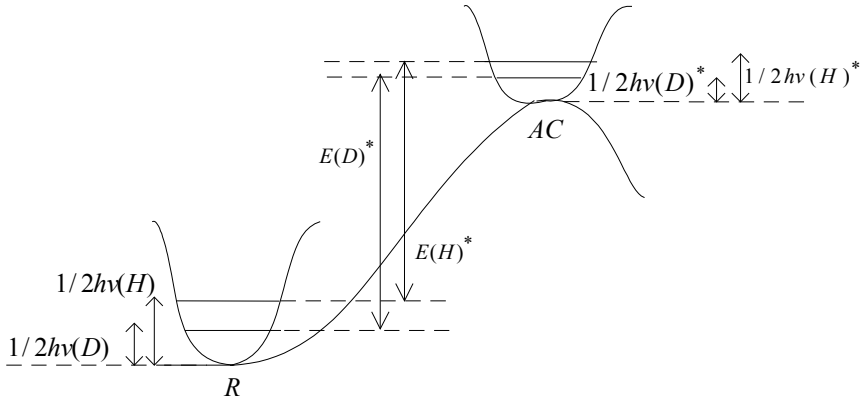

Figure 2.1: Stretching vibrations of RH in an unperturbed state, and upon formation of the activated complex in reaction RH + X → R + HX. Zero point energies of hydrogen and deuterium substituted molecules are shown as well as the activation energies for reaction involving both compounds. Here R and AC denotes reactants and activated complex.

Combining equation (2.1) and (2.4) and neglecting the term T_e because all of the molecules we are dealing with are overwhelmingly in their ground states, we can write

$$Q = Q_{tr} Q_0 Q_{vib} Q_{anh.} Q_{rot} Q_{rot-str} Q_{rot-vib} \tag{2.5}$$

It has been demonstrated [Richtet et al. 1977] that rotational-vibration interaction, rotational-stretching and anharmonicity correction contribution to the partition function ratio is too small that it can be ignored. Moreover, assuming that translational and rotational energy levels are

closely spaced, integration of the corresponding partition function is justified and the following expression for K can be derived for a diatomic molecules [Urey 1947]

$$K = \prod_{i=0}^{n} \left(M_i^{\frac{3}{2}} \frac{I_i}{\sigma_i} \frac{e^{\frac{-h\nu_i}{(2k_B T)}}}{1 - e^{\frac{-h\nu_i}{(2k_B T)}}} \right)^{\zeta_i} \tag{2.6}$$

Here M denotes molar mass, I moment of inertia, σ symmetry number, ν frequency of vibration and ζ is the stoichiometric coefficient.

Bigeleisen and Mayer [1947] deduce an equation similar to (2.6) in a rather simple way and split the ratio of partition function for two isotopologues into a "quantum mechanical" part *(f)* arising from molecular vibrations and a "classical" part:

$$\frac{Q(A^h X)}{Q(A^l X)} = f \left(\frac{m_h}{m_l} \right)^{\frac{3}{2}} \tag{2.7}$$

symmetry numbers have been omitted since they only represent the relative probabilities of forming symmetrical and unsymmetrical molecules and drop out in the final computation of α from k and k_∞ (2.2). The ratio of masses $(m_h/m_l)^{3/2}$ cancels for equilibrium constants in stoichiometrically balanced reaction, so that the fractionation factor is $\alpha_{A/B}$ = f (AX)/ f(BX). In case of oxygen we will have two fractionation factors, $^{17}\alpha_{A/B}$ and $^{18}\alpha_{A/B.}$ Following Urey [1947] and Bigeleisen [1955], it was shown that a simple relationship between $^{17}\alpha_{A/B}$ and $^{18}\alpha_{A/B}$ can be approximated [Matsuhisa et al. 1978; Weston 1999; Young et al., 2002].

$$\beta = \frac{\ln {}^{17}\alpha_{\frac{A}{B}}}{\ln {}^{18}\alpha_{\frac{A}{B}}} = \frac{1/m({}^{16}O) - 1/m({}^{17}O)}{1/m({}^{16}O) - 1/m({}^{18}O)} = 0.5305 \tag{2.8}$$

Eqn.(2.8) is rearranged to give $^{17}\alpha_{A/B} = (^{18}\alpha_{A/B})^{\beta}$. This relationship is valid for any oxygen carrying species, the equilibrium value of β is not sensitive to the masses of surrounding atoms. However, it relies on a number of assumptions made during the derivation of eqn. (2.8) e.g. high temperature or treating the molecular vibrations as harmonic oscillator so that the vibrational frequencies depend only on the masses of the isotopes.

The partition functions depend on temperature, and so do the equilibrium constants. In fact, the distribution of stable isotopes between different reservoirs at equilibrium is an almost perfect thermometer. This has allowed an accurate reconstruction of the climate history of the earth to be assembled, using for example the $\delta^{18}O$ of carbonate shells in the ocean, and the

$\delta^{18}O$ of ancient water in the Antarctic and Greenland glaciers. The first example depends on the equilibrium between aqueous and carbonate CO_2 and the second, on the difference in the chemical potential of H_2O and $H_2{}^{18}O$ in the liquid and gas phase.

2.1.2 Kinetic mass-dependent isotope fractionation

Equilibrium partitioning of isotopes between compounds depends upon zero-point energy differences that reflect the net effect of numerous vibrational modes. These differences do not arise in the limit of classical mechanics. Kinetic fractionation, on the other hand, can result from motions that are described satisfactorily by classical mechanics. A generalized functional form for the kinetic mass-dependent fractionation law can be derived from the classical part of the partition function ratio in equation (2.7). However, before describing such a law, it is useful to illustrate the way that kinetic fractionation differs from equilibrium fractionation using a simple example.

If molecules comprising a gas do not interact apart from collision, then kinetic energies are the same (treating the gas as ideal). In this case we can calculate the mass fractionation law for three isotope comprising isotopologues of these molecules. Imagine, e.g. collecting the molecules based on their relative velocities. The number of isotopic molecules collected will be proportional to the velocities and the velocities a function of mass, such that

$$KE = \frac{1}{2} m_1 v_1{}^2 = \frac{1}{2} m_2 v_2{}^2 = \frac{1}{2} m_3 v_3{}^2 \tag{2.9}$$

where subscripts 1,2 and 3 designate the three isotopes in descending order of masses, KE is the kinetic energy of the molecules, m is the mass of the indicated isotopologue, and v is the velocity of the isotopologue. The isotope fractionation factor α can be equated with the ratio of the velocities of the molecules relative to a condition in which the velocities o are equal, leading to

$$\frac{\ln \alpha_{2/1}}{\ln \alpha_{3/1}} = \frac{\ln (v_2/v_1)}{\ln (v_3/v_1)} = \frac{\ln (m_1/m_2)}{\ln (m_1/m_3)} \tag{2.10}$$

Eqn. (2.10) shows that the mass fractionation law in these circumstances is $\alpha_{2/1} = \alpha^{\beta}_{3/1}$ where the exponent β is

$$\beta = \frac{\ln (m_1/m_2)}{\ln (m_1/m_3)} \tag{2.11}$$

Eqn (2.11) is evaluated using the molecular masses. The exponent β in this kinetic process is different from that derived for equilibrium isotope partitioning (2.8).

2.1.3 Anomalous or mass independent isotope fractionation

Most of the process that have been considered up to this point have a simple mass relation. For these mechanisms, the relative effect of say an ^{18}O substitution will be twice the effect of a ^{17}O substitution. For example the mass dependent isotopic fractionation of oxygen containing molecules thus varies between $\delta^{17}O/\delta^{18}O \approx 0.529$ for atomic oxygen and $\delta^{17}O/\delta^{18}O \approx 0.5$ for high molecular mass species [Johnson et al. 2002]. However, mass independent fractionation (MIF) denotes processes that give rise to change in isotopic composition that is not mass dependent. This definition is a bit misleading since it might imply that such isotope effects occur without accompanying changes of mass. Obviously this is not the case. What was meant is rather an isotope effect deviating from usual mass dependent fractionation laws. Unconventional or anomalous are probably preferable descriptions of this kind of effect which is dependent on mass indeed. The magnitude of this anomaly is generally defined as $\Delta^{17}O = \delta^{17}O - 0.516\,\delta^{18}O$ (see sec. 2.1.4).

Anomalous isotope effects may arise from changes of nuclear properties upon isotopic substitution (such as nuclear spin, size or shape). These isotopic changes can cause shifts in the electronic spectra as well as vibrational and rotational energy levels [Bigeleisen 1996, Fujii et al. 1998]. Moreover, stellar nucleosynthesis, radioactive decay or natural nuclear reactors (such as in Oklo, Gabon) may cause exceptional isotopic variations. In fact, anomalous isotope effects were first detected in meteorites [Clayton et al., 1973] and ascribed to nucleosynthetic processes.

Gas-phase ozone formation in an electrical discharge was the first chemical reaction in which anomalous oxygen isotope ratios were detected [Thiemens and Heidenreich III, 1983]. Other reactions with unconventional isotope effects were reviewed by Weston [1999] and include O_3 formation by O_2 photolysis, photolytic and thermal dissociation of O_3, electrodissociation of CO_2, reaction of CO+ OH, formation of S_2F_{10} by an electric discharge in SF_4, photo polymerisation of CS_2 and ion molecule reactions of the type $A^+ + A \rightarrow A^+_2$.

In the atmosphere, oxygen isotope anomalies were first reported for stratospheric O_3 [Mauersberger, 1981]. Subsequent measurements found similar anomalies in tropospheric O_3 and showed that ^{17}O enrichment was about 0.7 times the corresponding ^{18}O enrichment in both

stratosphere and troposphere [Krankowsky et al. 1995, 2000]. Ozone is a key trace gas for both tropospheric and stratospheric chemistry and may transfer its oxygen isotope anomaly to other atmospheric trace gases and aerosoles, including CO_2 [Lämmerzahl et al. 2002; Thiemens et al. 1991], CO [Röckmann et al. 1998 a] N_2O [Cliff and Thiemens 1997, Röckmann et al. 2001, Kaiser et al. 2003], sulphate [Lee and Theimens, 2001] and nitrate [Michalski et al. 2001]. Next to O_3 formation, reaction of CO+OH [Röckmann et al. 1998b] and H + O_2 [Savarino and Theimens, 1999b] are other primary sources of excess ^{17}O in tropospheric gases, namely CO and HO_x.

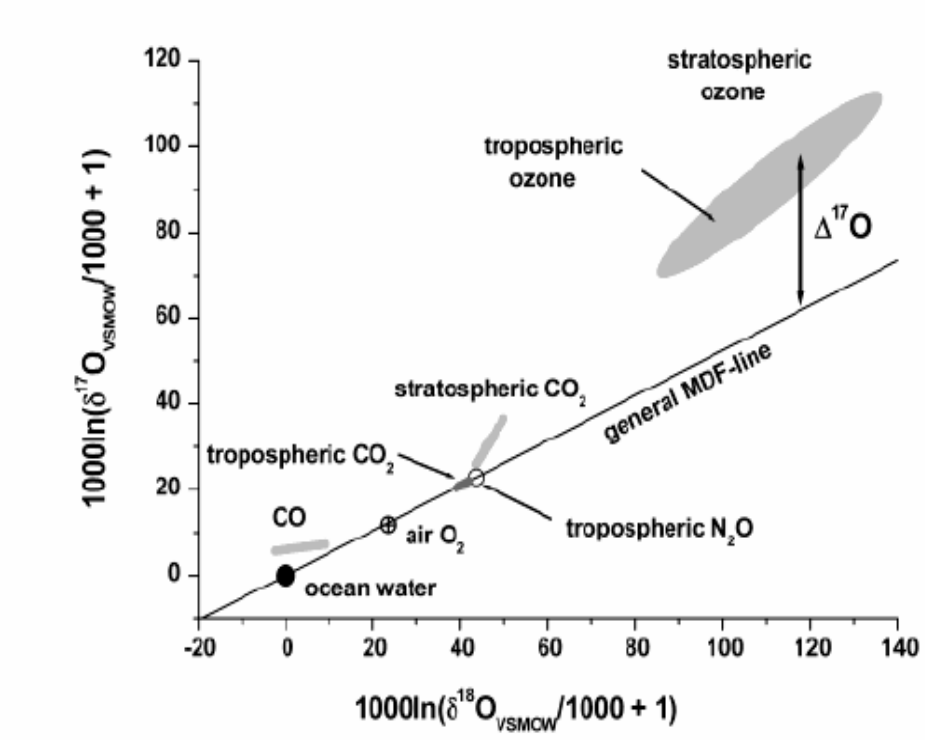

Figure 2.2: Schematic picture of the general mass-dependent relationship with ln(1+ $\delta^{17}O$/1000) plotted against ln(1+ $\delta^{18}O$/1000) using V-SMOW as reference. For small d values, or as a general approximation, at times $\delta^{17}O$ is plotted directly against $\delta^{18}O$. The typical composition for V-SMOW representing ocean water, atmospheric oxygen. CO, N_2O (arrow tip), stratospheric CO_2, tropospheric and stratospheric O_3 are shown as a general guide [Brenninkmeijer et al., 2003].

2.1.4 Mass dependent fractionation line: slope and $\Delta^{17}O$ definition

It was postulated by Craig [1957], from the established theoretical basis of the quantitative effects of isotopic substitution under equilibrium [Urey 1947; Bigeleisen and Mayer 1947] and kinetic [Bigeleisen 1949] conditions that fractionation of the three oxygen isotopes between entities a and b during chemical or physical fractionation should be described by $(^{17}R_a/^{17}R_b) = (^{18}R_a/^{18}R_b)^{0.5}$, where $^{17}R_a$ and $^{18}R_a$ refers to the respective $^{17}O/^{16}O$ and $^{18}O/^{16}O$ in a; b is a reference material. On this basis, $\alpha_{17/16} = (\alpha_{18/16})^{0.5}$ from the definition of the respective fractionation factors. The value of the exponent term was refined by Matsuhisa et al. [1978], who calculated the logarithmic reduced partition function ratios $\ln(Q_{17}/Q_{16})/ \ln(Q_{18}/Q_{16})$, equivalent to the fractionation factor ratios, for a number of oxygen compounds and exchange reactions. A range of 0.520 to 0.528 was reported for equilibrium conditions, whereas calculations for diffusion processes indicated greater variation, from 0.500 to 0.523. A value of 0.52 was chosen (for the quartz-water system) as a compromise between theory and experimental measurements on terrestrial rocks and waters. This is the origin of the proportionality factor in the well known identity $\delta^{17}O = 0.52\ \delta^{18}O$. However, it is generally recognized [Clayton and Mayeda, 1996] that this linear relationship between $\delta^{17}O$ and $\delta^{18}O$ is an approximation derived from the power law, $\alpha_{17/16} = (\alpha_{18/16})^{0.52}$

Li and Meijer [1998] used high precision measurements of the oxygen three-isotope distribution in natural waters to establish that the respective fractionation factors do follow a power law relationship, $(^{17}R_a/^{17}R_b) = (^{18}R_a/^{18}R_b)^{\lambda}$ where λ was determined empirically to be 0.5281 ± 0.0015.

However, in the case of oxygen from extraterrestrial reservoirs, where mass dependent fractionation line may be offset parallel to that of the bulk silicate earth, a further terms is required to quantify the offset:

$$\frac{^{17}R_a}{^{17}R_b} = [1 + k_{a,b}]\left(\frac{^{18}R_a}{^{18}R_b}\right)^{\lambda} \qquad (2.12)$$

In this case, b refers specifically to a material which lies on the terrestrial fractionation line, whilst $k_{a,b}$ is a measure of the offset between the terrestrial line and that associated with the SNC meteorite (the parent body of which is, most probably Mars) has been accurately characterized by Franchi et al. [1999], although not in this format. Equation ((2.12) is also applicable to the identification of terrestrial oxygen reservoirs which lie off the bulk earth fractionation line; tropospheric O_2 is an example. Such an offset may be indicative of mass

independently fractionated component, or the result of a specific fractionation process characterized by a λ value which is distinct from that which describes the oxygen three-isotope distribution in terrestrial rocks and waters. In terms of δ values, as generally measured rather than absolute ratios, (2.12) becomes:

$$1+\frac{^{17}\delta O}{1000}=[1+k_{a,b}](1+\frac{^{18}\delta O}{1000})^{\lambda} \tag{2.13}$$

Taking logarithm of the equalities in (2.9) and scaling up by a factor of 10^3 gives

$$1000\ln(1+\frac{^{17}\delta O}{1000})=\lambda\,1000\ln(1+\frac{^{18}\delta O}{1000})+1000\ln[1+k_{a,b}] \tag{2.14}$$

Thus a plot of $10^3\ln(1+10^{-3}\,\delta^{17}O)$ against $10^3\ln(1+10^{-3}\,\delta^{18}O)$ should produce a straight line of slope λ and intercept corresponding to $10^3\ln[1 + K_{a,b}]$. The respective ordinate and abscissa axis scales are essentially unchanged from those of a corresponding $\delta^{17}O$ versus $\delta^{18}O$ plot; also any offset on the ordinate axis will be of similar magnitude to that given by the established definition of $\Delta^{17}O$, i.e., $\delta^{17}O = 0.52\,\delta^{18}O$, if $\lambda \sim 0.52$. The use of a similar equation to (2.13), for the accurate determination of linear fractionation slopes in the sulphur multiple isotope has already been reported [Hulston and Thode 1965]. If $\Delta^{17}O$ is now defined as $1000k_{a,b}$ the following applies

$$\Delta^{17}O=1000\,k_{a,b}\simeq 1000\ln[1+k_{a,b}]=1000\ln(1+\frac{^{17}\delta O}{1000})-\lambda\,1000\ln(1+\frac{^{18}\delta O}{1000}) \tag{2.15}$$

Using the well-known identity that

$$\ln(1+x)=x+\frac{1}{2}x^2+\frac{1}{3}x^3+.....\simeq x\ where\ x\ll 1 \tag{2.16}$$

it is readily apparent that the right-hand terms of (2.15) may be approximated to give

$$\Delta^{17}O\simeq{}^{17}\delta O-\lambda'{}^{18}\delta O \tag{2.17}$$

This is the usual representation of $\Delta^{17}O$, with $\lambda' = 0.52$. A distinction is made here between λ and λ', for two reasons: firstly, λ' is not independent of the range of sample δ values. In fact, it increasingly diverges from λ as the sample data set includes points of greater $\delta^{17}O$ and $\delta^{18}O$. Secondly, λ is independent of the isotopic composition of the reference material, λ' is not. This is of particular significance when sample isotopic data are reported with respect to a reference material which does not fit on the same mass dependent line or where the isotopic composition of the reference material is not well characterized. It should be noted, however,

that the value of $\Delta^{17}O$ as give either by (2.5) or (2.3) is dependent on the isotopic composition of the reference material, relative to which the δ values are reported.

2.2 CO_2 in the atmosphere

The importance of CO_2 in regulating the earth's temperature has long been recognized [Arrhenius, 1896]. Because CO_2 is an importance green house gas and an essential ingredient in photosynthetic processes, it plays a critical role in maintaining the earth's habitability.

Pioneering efforts to monitor the atmospheric CO_2 concentration were made by Keeling in 1957 at Mauna Loa, Hawaii and at South Pole [Keeling et al. 1989]. It indicated a steady increase in CO_2 and was attributed to human activities such as fossil fuel combustion and deforestation. Since this CO_2 alarm, numerous sites for CO_2 monitoring have been established all over the world. The principal aim of this global net work is to document the abundance of CO_2 in the remote atmosphere [http://www.cmdl.noaa.gov/ccg/co2] and to gain a better insight into the sources and sinks of this important atmospheric green house gas, by using the spatial and temporal variations of CO_2 in combination with atmospheric models [Tans et al. 1990]. Results of these efforts have indicated that over the last few decades atmospheric CO_2 concentration have increased from ~ 315 ppm to ~370 ppm at an annual rate of about 1.6 parts per million by volume (ppmv) or slightly less than 0.5% as shown in Figure 2.3.

$\delta^{13}C$, a measure of the relative abundance of the two stable isotopes, ^{13}C and ^{12}C, in atmosphere gives in principle possibilities for the partitioning of atmospheric CO_2 uptake by land and ocean[Keeling et al. 1989, 1995; Francy et al., 1995]. The principle of using $\delta^{13}C$ to separate between two components of the carbon budget relies on the fractionation during photosynthesis by C_3 plants, which discriminate against ^{13}C. This fractionation leads to biospheric carbon being depleted in ^{13}C by about 18% relative to the atmosphere. In contrast, exchange with the ocean involve relatively small fractionation effects. Changes in the $^{13}C/^{12}C$ ratio of atmospheric CO_2 thus indicate the extent to which concurrent CO_2 variations can be ascribed to variations in biospheric uptake. The calculation also requires specification of the turnover times of carbon in the ocean and on land, because fossil fuel burning implies a continuous release of isotopically light carbon to the atmosphere. This leads to a lowering of the atmospheric $^{13}C/^{12}C$ isotope ratio, which takes years to centuries to work its way through the carbon cycle [Keeling et al. 1980; Tans et al. 1993; Ciais et al. 1995a, b].

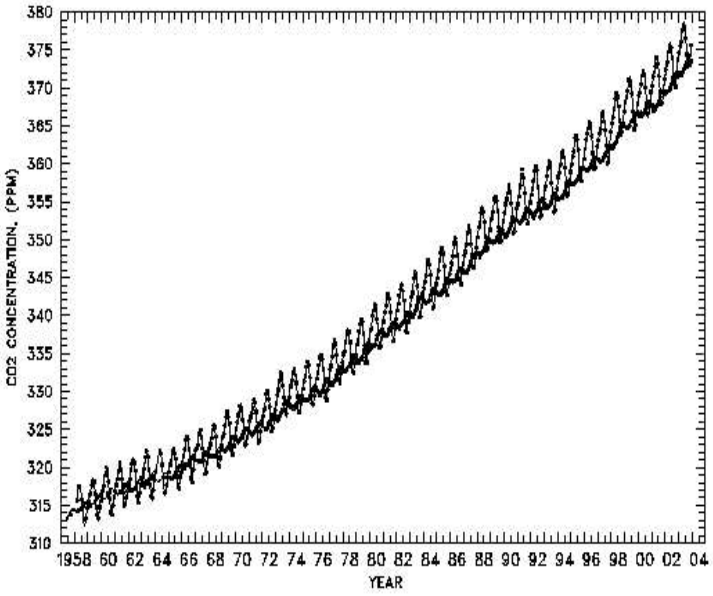

Figure 2.3: Time trend in the concentration of atmospheric CO_2 measured at Mauna Loa observatory, Hawai (20^oN, 156^oW) and at the South Pole. The former record is distinguished by its pronounced seasonal cycle.

Similarly $\delta^{18}O$ of CO_2 is being used to measure the gross carbon fluxes among the three reservoirs (atmosphere, biosphere, and ocean). Francy and Tans [1987] first suggested that isotopic exchange between CO_2 and water in the chloroplasts of leaves during photosynthesis largely determine tropospheric $\delta^{18}O$ of CO_2. While ~1/3 of atmospheric CO_2 entering leaves is assimilated, the remainder diffuses back out with a new $\delta^{18}O$ value determined largely by $\delta^{18}O$ of leaf-H_2O. related This isotope exchange was then related to gross primary productivity (GPP) in a model which include a large number of isotopic, physical, hydrological and biological variables [Farquhar et al. 1993]. Subsequent modeling studies confirmed that land bioata are the primary determinant of $\delta^{18}O(CO_2)$ [Ciais et al. 1997; Cuntz et al. 2003a, b]. Among the current aims of modeling efforts is to use $\delta^{18}O$ observations of CO_2 and H_2O to improve estimates of GPP and respiration, both locally and globally [Cuntz et al. 2003a, b; Riley et al. 2003].

On a global scale, isotopic exchange with vegetation and respiration processes produce an isotopic enrichment in ^{18}O, while exchange with soils acts to decrease the ^{18}O content. The mean $\delta^{18}O$ of tropospheric CO_2 is enriched by 41.5‰ relative to VSMOW, with only small seasonal and geographical variations of less than 4 ‰ [Farquhar et al. 1993, Trolier et al. 1996]. It is important to point out here for clarification that all these processes involved, fractionate the heavier isotopes in a mass dependent fashion i.e. $^{17}O = 0.5\ \delta^{18}O$ because they

arise from differences in chemical and physical properties which are dependent on mass. For example, equilibrium isotope effects and kinetic isotope effects are all produced by atomic or molecular mass differences (see sec.2.1).

2.2.1 Stratospheric CO_2

CO_2 is essentially an inert gas in the lower atmosphere, its isotopic composition will not change during upward transport from the troposphere into the stratosphere. Measurements of stratospheric and mesospheric samples, however, revealed a significant enrichment in the heavy oxygen isotopes of CO_2 above tropospheric values.

The enrichment in $\delta^{18}O$ of stratospheric CO_2 (2-7‰) was first reported by Gamo et al. [1989] However, Thiemens et al, [1991, 1995b] extended this information to $\delta^{17}O$ along with $\delta^{18}O$. The measured enrichment of heavy oxygen isotopes in CO_2 showed a steady increase with altitude reaching a maximum of $\delta^{17}O$ = 40.5 ‰ and $\delta^{18}O$ = 54.9‰ at 60 km. Thus the additional enrichment in relation to tropospheric values was stronger for ^{17}O (~ + 20 ‰) than for ^{18}O(~ + 15‰) but this data show some scatter. However, very precise measurements of stratospheric CO_2 with a very tight relationship $\delta^{17}O/\delta^{18}O = 1.7 \pm 0.03$ have been reported by Lämmerzahl et al. [2002] as shown in Figure 2.4.

The fact that stratospheric CO_2 is mass independently fractionated ($\Delta^{17}O > 0$) showed that the enrichment cannot be the result of dynamics, due to the fact that this mechanism would be strictly mass dependent. Young et al. [1991] proposed an isotopic exchange between CO_2 and O_3 via $O(^1D)$ to account for observed isotopic enrichment in stratospheric CO_2 because a variety of measurements showed enrichment in $\delta^{17}O$ (~70 - 80 ‰) and $\delta^{18}O$ (~90 -120 ‰) for ozone [Mauersberger et al. 1993;Krankowsky et al. 1995].

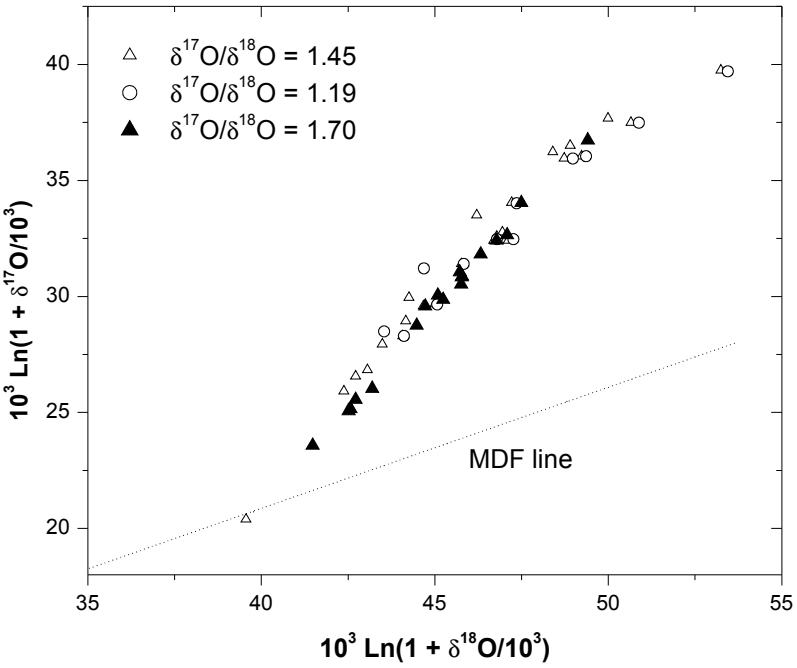

Figure 2.4: Three isotope plot of stratospheric and mesospheric CO_2 samples obtained using rocket [Thiemens et al. 1995b, Zipf and Erdmann 1994] and baloon [Lämmerzahl et al. 2002].

2.2.2 Implication of the stratospheric CO_2 anomaly

It has been pointed out in previous section that using $\delta^{18}O_{CO2}$ as a constraint on terrestrial GPP requires estimates and/ or detailed modeling of $\delta^{18}O$ values for numerous water pools which can be difficult to ascertain. $\delta^{18}O$ of leaf water, e.g., depends on plant anatomy, the vertical distribution of $\delta^{18}O_{H2O}$ in soils, the humidity in the canopy and its $\delta^{18}O$, and other factors such as precipitation and temperature. Recently, Hoag et al. [2005] proposed to use ^{17}O anomaly as a tracer of terrestrial gross carbon fluxes. There is no stratospheric sink for $\Delta^{17}O_{CO2}$, anomalous CO_2 produced in the stratosphere is transported to the troposphere where the isotope anomaly is destroyed by isotopic exchange with water and diluted by inputs of non anomalous CO_2. Importantly, as $\Delta^{17}O$ does not depend directly on values for $\delta^{18}O$ and or $\delta^{17}O$ of soils and leaf water and may therefore, be easier to link it directly to GPP and to deconvolve the response of GPP to inter annual changes in e.g., temperature and precipitation. Moreover, $\Delta^{17}O$ of O_2 has been proposed as a constraint on GPP on millienial time scales

[Luz et al. 1999], whereas $\Delta^{17}O_{CO2}$ may provide information on annual to decadal time scales [Hoag et al. 2005].

Secondly, as CO_2 is the most abundant trace gas in the stratosphere and its enrichment increases linearly ($\delta^{17}O = 1.7\ \delta^{18}O$) with altitude, its anomaly may provide information about $O(^1D)$ density [Lämmerzahl et al. 2002] provided details of the mechanism are known.

Thirdly, CO_2 near the tropopause has mass dependent signature but as CO_2 is transported to the upper part of the stratosphere, it is subjected to isotope exchange with O_3. Thus "aged" CO_2 becomes enriched, progressing towards isotopic equilibrium at higher altitude. The enrichment of CO_2 can be used to measure the age of the air parcel because at higher altitude, tracers like N_2O and CH_4 loses their utility because of photolysis and oxidation [Alexander et al. 2001].

2.3 Ozone

Ozone, although it is a minor species in the earth atmosphere, is of considerable importance to mankind by virtue of its acting as shield over the biosphere against lethal UV radiation from the sun. The name ozone is derived from a Greek word “Ozein” meaning smell because of its particular odour. Ozone is largely confined to a layer between 30 to 50 km above sea level depending on altitude. Soon after the discovery of ozone in the upper atmosphere, Chapman proposed a mechanism for its formation.

The Chapman reactions are

$$O_2 + h\nu \rightarrow O + O \qquad (R2.1) \quad \lambda < 253\ nm$$

$$O + O_2 + M \rightarrow O_3 + M \qquad (R2.2)$$

$$O_3 + h\nu \rightarrow O + O_2 \qquad (R2.3)$$

$$O + O_3 \rightarrow O_2 + O_2 \qquad (R2.4)$$

Here M is the third body required to carry of the excess energy of the association process. The rapid cycle composed of R2.2 and R2.3 does not of course destroy ozone, it merely transfer an oxygen atom between a free state and a state in which it is bound to an oxygen molecule. Destruction of ozone by R2.4 is insignificant, however catalytic processes can accelerate R4.4.

$$X + O_3 \rightarrow XO + O_2 \qquad (R2.5)$$

$$XO + O \rightarrow X + O_2 \qquad (R2.6)$$

$$\text{net: } O + O_3 \rightarrow 2O_2 \qquad (X = OH, NO, Cl)$$

The ozone molecule forms an open triangle and has a binding energy of 1.1 eV. This low

energy compared to O_2 (5.1 eV) or N_2 (9.8eV) makes O_3 a very reactive molecule. There are three stable oxygen isotopes- ^{16}O, ^{17}O, and ^{18}O, so the O_3 molecule can carry a large variety of isotope combinations. In the atmosphere, however, only $^{49}O_3$ and $^{50}O_3$ have any significant abundance since ^{18}O is by a factor of almost 500 and ^{17}O by a factor of 2500 lower than ^{16}O [Mauersberger et al. 2003]. Because of its triangular geometry the singly-substituted heavy oxygen atom can be found in the apex or at either end of the triangle. In the first case, such an O_3 molecule is called symmetric; when heavy oxygen atom is located at either end, the molecule is asymmetric.

2.3.1 Isotope effect in ozone

The suggestion that atmospheric O_3 might be enhanced in ^{18}O was made by Cicerone and McCrumb[1980], who first realized that $^{34}O_2$ might be preferentially photolyzed in earth's atmosphere owing to opacity effects in the Schumann-Runge band region. The photolysis rate for $^{34}O_2$ was estimated to be up to a factor of 10 more rapid than that of $^{32}O_2$, with the relative difference largest between 50 and 60 km. They noted that preferential photo dissociation of $^{34}O_2$ might not be reflected in the O_3 isotope composition owing to isotopic dilution associated with the Chapman reactions. More refined calculations performed on the problem [Blake et al. 1984; Omidvar and Fredrick, 1987] showed that preferential photolysis of $^{34}O_2$ should be significantly less than estimated by Cicerone and McCrumb[1980]. What preferential photolysis there is, should occur mainly in the mesosphere.

Kaye and Strobel [1983] pointed out that the O atom exchange reaction, should be sufficiently fast in the upper atmosphere that any additional ^{18}O produced by the preferential photolysis of $^{34}O_2$ would be redistributed e.g.

$$^{18}O + {}^{16}O^{16}O \rightarrow {}^{18}O^{16}O + {}^{16}O \qquad \text{(R2.7)}$$

$$^{17}O + {}^{16}O^{16}O \rightarrow {}^{17}O^{16}O + {}^{16}O \qquad \text{(R2.8)}$$

These fast equilibrium processes determine after photolysis the distribution of atomic oxygen in gas mixture such as air. Exchange recycle O-atoms numerous times through O_2 before ozone is formed in a three body collision. Because of the different zero point energies of the O_2 molecules that participate in the exchange reactions, the rate coefficients of the different channels are higher for exothermic processes which proceed from left to right in R2.7 and R2.8 and lower for endothermic that are right to left. Thus the distribution of the three oxygen atoms is governed by exchange which will lower ^{18}O and ^{17}O compared to what would be

expected from just statistically distributed O-isotopes in molecular oxygen.

However, first measurements of isotope ratios in the stratosphere and in laboratory environment were met with surprise since an unusually large enrichment and not a depletion in the two heavy isotopomers $^{49}O_3$ and $^{50}O_3$ was observed [Mauersberger et al. 1981, 87; Thiemens and Heidenreich 1983]. Oxygen mixture enriched in heavier isotopes were employed heavily for the ozone formation with the aim to get some additional information about the unusual isotope effect in ozone formation[Yang and Epstein 1987a, b]. Unluckily, isotope analysis was done on molecular oxygen which has been obtained from the product ozone after chemical reaction, information contained in O_3 isotopologue was lost. A successful measurement of O_3 isotopologue formation from heavy oxygen was carried out by Morton et al. [1989] and Mauersberger et al. [1993]. The results of these investigations showed that homonuclear ozone isotopologue were depleted in a standard fashion, with $^{54}O_3$ being depleted most (- 4.6%). Heteronuclear molecules were strongly enriched, and the highest enrichment of about 18% resided in $^{16}O^{17}O^{18}O$. All other isotopologues were about two third as much enriched as $^{16}O^{17}O^{18}O$. The data on$^{16}O_2{}^{17}O$ and $^{16}O_2{}^{18}O$ agreed well with measurements in natural oxygen and thus confirmed that the ozone isotope effect is independent of the isotope composition of the oxygen. The multi-isotope measurements suggested that molecular symmetry could play the dominating role in ozone formation, which was later shown to be misleading [Anderson et al. 1997].

The fundamental quantity which best describes a chemical reaction is the rate coefficient which may be pressure or temperature dependent and in either case can be related to a specific isotope formation channel. To investigate symmetry effects or other parameters influencing ozone formation, a number of experiments were performed by Mauersberger group [Anderson etal. 1989; Janssen et al., 1999; Günther et al. 1999, 2000]. Rate coefficients were determined relative to standard $^{48}O_3$ formation channel as shown in Table 2.1.

The large difference between 0.92 and 1.53 of the two asymmetric $^{18}O^{16}O^{16}O$, $^{16}O^{18}O^{18}O$ eliminated a symmetry driven explanation for the ozone isotope effects. The experiments, using tunable diode laser technique showed that the ozone formation process is dominated by end-on reactions and not by insertion [Janssen et al. 1999]. Relative rate coefficients of asymmetric molecules of $^{50}O_3$ had linear relationship with the zero point energy difference (Δ ZPE). The relative rate coefficients for exothermic processes were found to be low whereas for endothermic processes the rates were higher. The rates of symmetric molecules, however,

were below the straight line by ~20 % .

Table 2.1: Reaction channels of all measured oxygen isotope combinations leading to O_3 molecules. Rate coefficents [Mauersberger et al. 1999; Janssen et al., 1999] relative to the standard reaction of $^{48}O_3$.

Mass	Reaction	Relative rate coefficients
48	$^{16}O + {}^{16}O^{16}O \rightarrow {}^{16}O^{16}O^{16}O$	1
49	$^{17}O + {}^{16}O^{16}O \rightarrow {}^{17}O^{16}O^{16}O$	1.03[b]
50	$^{16}O + {}^{17}O^{17}O \rightarrow {}^{16}O^{17}O^{17}O$	1.23[b]
	$^{16}O + {}^{16}O^{18}O \rightarrow {}^{16}O^{16}O^{18}O$	1.45[c]
	$\rightarrow {}^{16}O^{18}O^{16}O$	1.08[c]
	$^{18}O + {}^{16}O^{16}O \rightarrow {}^{18}O^{16}O^{16}O$	0.92
	$\rightarrow {}^{16}O^{18}O^{16}O$	0.006
51	$^{17}O + {}^{17}O^{17}O \rightarrow {}^{17}O^{17}O^{17}O$	1.02
52	$^{16}O + {}^{18}O^{18}O \rightarrow {}^{16}O^{18}O^{18}O$	1.50
	$\rightarrow {}^{18}O^{16}O^{18}O$	0.029
	$^{18}O + {}^{16}O^{18}O \rightarrow {}^{18}O^{16}O^{18}O$	1.04[c]
	$\rightarrow {}^{18}O^{18}O^{16}O$	0.92[c]
	$^{18}O + {}^{17}O^{17}O \rightarrow {}^{18}O^{17}O^{17}O$	1.03[b]
53	$^{17}O + {}^{18}O^{18}O \rightarrow {}^{17}O^{18}O^{18}O$	1.31[b]
54	$^{18}O + {}^{18}O^{18}O \rightarrow {}^{18}O^{18}O^{18}O$	1.03

b: These rates may contain small contributions from the subsequent symmetric molecules.

c: For those reactions which involve heteronuclear oxygen molecules the relative reaction probability is shown while relative rate coefficients may be obtained by dividing the quoted number by two.

2.3.2 Pressure and temperature effect

The ozone formation itself is a highly temperature dependent process, increasing with decreasing temperature. The effect of temperature and pressure on the magnitude of enrichment in $^{49}O_3$ and $^{50}O_3$ was measured by using visible light photolysis of ozone in an oxygen bath gas of known isotopic composition [Morton et al. 1990]. Through rapid isotope exchange reactions, the atoms equilibrate with the molecular oxygen and reform O_3 molecules. The newly formed O_3 acquires an isotopic composition that depends only on the bath gas isotopic composition and the isotope fractionation mechanism in the formation as

well as in photolytic destruction of O_3. Large temperature-dependent enrichment at a constant oxygen pressure of 50 Torr were observed. Delta values increased from $\delta^{17}O$ = 3.6% and $\delta^{18}O$ = 2.6% at 130 K to $\delta^{17}O$ = 11.7% and $\delta^{18}O$ = 14.6 % at 361 K with an overall uncertainty of 0.6%. The % enrichment for O_3 is defined as $[(R_s/R_{std}) -1] \times 100$
where R = $^{34}O_2/^{32}O_2$ or $^{33}O_2/^{32}O_2$.
Similarly, pressure dependency in O_3 formation was characterized at 321 K between 5.0 and 1000 Torr. Enrichment values of $\delta^{17}O$ = 11.2% and $\delta^{18}O$ = 12.9% were observed in the low pressure regimes, and they decreased to $\delta^{17}O$ = 7.5% and $\delta^{18}O$ = 7.9% at 1000 Torr (again overall uncertainty of 0.6% for reported enrichments). Results of these measurements are reported in chapter 7.
Ozone was also generated at pressure well below 10 mb [Bains-Sahota and Thiemen, 1987]. The magnitude of enrichment decreased and rather a depletion was measured at very low pressure. It was concluded that O_3 formation is a gas phase process and as the mean free path in the gas decreased, heterogeneous chemistry begun which ultimately eliminated the fractionation in O_3 and resulting O_3 showed a normal mass dependency in heavier isotopes.

2.3.3 Ozone in atmosphere

Ozone in the troposphere is only present in ppb and thus samples are difficult to collect and analyze. However, a comprehensive set of nearly 50 tropospheric ozone samples with average enrichment values 7.1% for $^{49}O_3$ and 9.1% for $^{50}O_3$ has been reported [Krankowsky et al. 1995]. These values agree well with the laboratory data when temperature and pressure correction is applied. No isotopic data for O_3 have been obtained in the tropopause (between 10 and 15 km). Stratospheric O_3 showed overall enrichment of 5 to 10% for $^{49}O_3$ and 6 to 12% for $^{50}O_3$ [Krankowsky et al. 2000].

3 Experimental Techniques

The most precise technique presently available for isotope ratio measurement is isotope ratio mass spectrometry (IRMS). This technique has been employed in our experiments to measure the isotopic composition of CO_2, O_2 and O_3 (after conversion to O_2). The general principle and the inlet system for traditional off line measurements is presented in section 3.1. The limitations for traditional measurements to determine the ^{17}O content of CO_2 are mentioned in section 3.2, together with the CeO_2 exchange method that has been used in this work for those measurements. Section 3.3 presents the analytical setup for preparation of CO_2 gases with different isotopic compositions from O_2. To study the mechanism of isotope exchange between CO_2 and O_3 via $O(^1D)$, we used a line source (Hg-pen ray lamp) and the system employed is presented in section 3.4.

The Photolysis rates $J(O_3)$ and $J(O_2)$ of the Hg-pen ray lamp were measured using O_3 and O_2 in a specially designed cell (section 3.5), because knowledge of those values is important for modeling the isotope exchange.

To determine the oxygen isotope composition of CO_2 in atmospheric air samples, it is necessary to first separate CO_2 from the bulk air. For this purpose a special extraction system has been developed which is discussed in sec 3.6. For atmospheric CO_2 measurements, it is also crucial to apply a correction for N_2O, which is contained in the sample and has the same isotopic masses as CO_2, but with very different isotopomer composition. The correction procedure is described in section 3.7.

3.1 Isotope Ratio Mass Spectrometry

3.1.1 Principle

In mass spectrometer, atoms or molecules are ionized in the ion source (e.g. by electron impact) and accelerated in an electric field. Usually first passing through electric focusing lenses and slits, the ions are subjected to a magnetic force by a magnetic field:

$$\vec{F} = -(ne)\vec{v}\,\vec{B} \tag{3.1}$$

where e is the elementary electric charge, ν the particle velocity and B the magnetic field strength. n is the number of electrons removed in the ionization, and is usually one as double

or higher ionization rarely occurs. As the direction of the force points perpendicularly to both velocity and magnetic field, the ions are forced on a circular trajectory with radius

$$R = m\frac{v}{eB} \tag{3.2}$$

where m is the mass of the particle. Therefore, the trajectory of a particle can be altered by either changing its velocity (by means of electric field) or the magnitude of the magnetic field. However, by keeping both v and B constant, particles of different masses can be separated and they leave the magnetic field on different trajectories. In isotope ratio mass spectrometer, the charged particles of different masses are detected on Faraday cups which are grounded via an electric resistor. An incoming particle neutralizes its electric charge with a free electron of the detector cup. As this charge is replaced from ground, a current flows through the resistor which is used to measure the signal strength of the particle beam.

Though a number of different mass spectrometer types exist (e.g. quadruople, time of flight), the work described in this thesis has been exclusively performed on a dipole mass spectrometer (Thermo Finnigan, Delta Plus^{XL}) with multiple cup detectors as shown in Figure 3.1. These isotope ratio mass spectrometers are specially designed for high stability which enables isotope ratio measurements with very high precision.

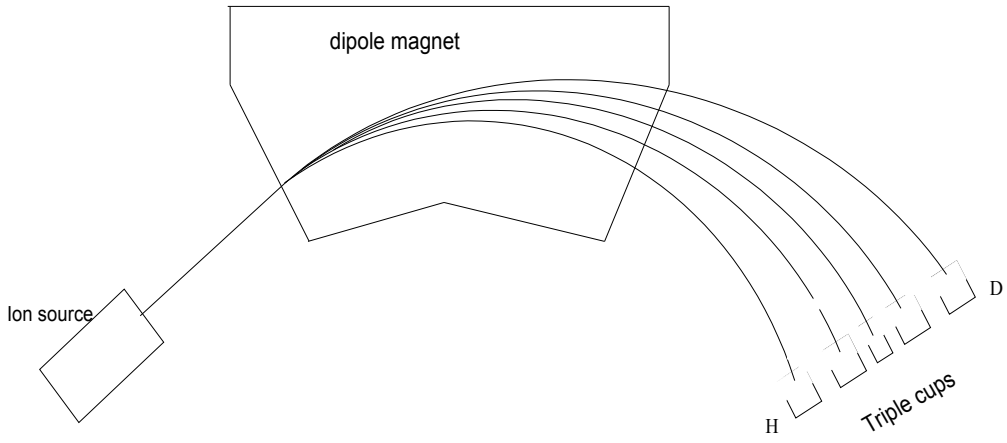

Figure 3.1: Ion trajectories in the Delta Plus^{XL} isotope ratio mass spectrometer. CO_2 signal (mass 44, 45, 46) is measured on the three central cups. The outer two cups are for deuterium and hydrogen measurement.

Absolute isotope ratio determinations are cumbersome and have to be performed on mass spectrometers which have been carefully calibrated by synthetic mixtures of essentially pure isotopes [Aregbe et al. 1998]. However, relative measurements of isotopes are much easier. If sample and reference material are treated in exactly the same way (identical treatment or "IT" principle [Werner and Brand 2001]), mass discrimination effects that occur for instance in the inlet capillary or the ion source are both for sample and reference and are cancelled.. To enable comparison between results from different laboratories and to allow for some degree of traceability of results, isotope ratios are reported relative to a common international standard using δ notation

$$\delta(‰) = [\frac{R_s}{R_{st}} - 1] x\, 1000 \tag{3.3}$$

Here R_s and R_{st} are the ratios ($^{17}O/^{16}O$ or $^{18}O/^{16}O$) or $^{13}C/^{12}C$ in sample and standard.

We have reported $\delta^{17}O$ and $\delta^{18}O$ values with reference to Standard Mean Ocean Water (SMOW) and $\delta^{13}C$ on VPDB scale. However, in photochemical equilibrium experiments results are reported versus O_2 to facilitate the comparison of isotopic equilibrium point in various systems.

3.1.2 Sample Inlet

The gas sample is transferred to the ion source through a system of valves that alternatively switches between the sample and reference gas as shown in Figure 3.2.

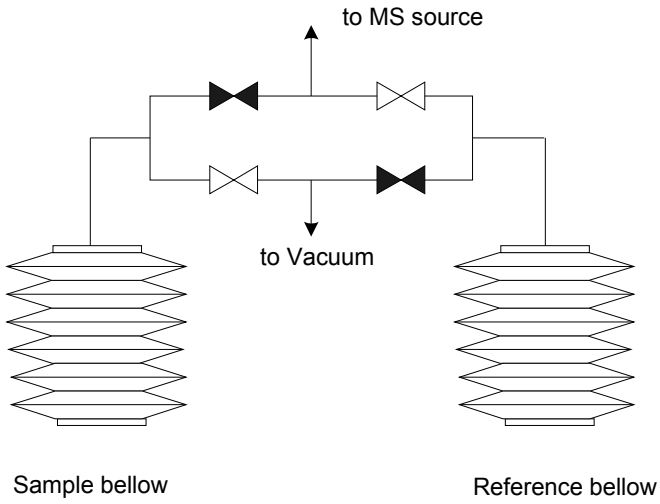

Figure 3.2: Working principle of a dual inlet system.

Sample and reference gases are stored in pressure adjustable bellows. Capillaries connect the bellows to a change over valve, which selects one of the two gases to flow into the mass spectrometer source. To adjust the signal intensity of both reference and sample gas to the same level, both are admitted from volume adjustable bellows. The principal advantage of dual inlet mass spectrometer is high precision and reproducibility of the signal, although gas samples needs to be prepared off line.

3.2 Analysis of CO_2 isotopes

Mass spectrometers to analyze CO_2 commonly register three ion beam currents corresponding to m/z 44, 45, 46 which are composed of various isotopomers as shown in Table 3.1. The most abundant molecule $^{12}C^{16}O^{16}O$ is recorded on m/z 44. The ^{13}C-bearing isotopologue dominates on m/z 45, whereas the ^{17}O-bearing isotopologue contribute only ~6.5%. Similarly, ^{18}O-bearing isotopologue prevails on m/z 46 because doubly substituted molecules have much lower abundances. From m/z 47 onwards, all isotopologues are double or triple substituted and have very low abundance, which are not used for analysis in standard applications, although modern analytical methods are now being developed.

Table 3.1: Isotopomers of Carbon dioxide

Mass	44	45	46	47	48	48
Isotopomer	$^{12}C^{16}O^{16}O$	$^{12}C^{17}O^{16}O$ $^{13}C^{16}O^{16}O$	$^{12}C^{18}O^{16}O$ $^{13}C^{17}O^{16}O$ $^{12}C^{17}O^{17}O$	$^{12}C^{17}O^{18}O$ $^{13}C^{17}O^{17}O$ $^{13}C^{18}O^{16}O$	$^{12}C^{18}O^{18}O$ $^{13}C^{17}O^{18}O$	$^{13}C^{18}O^{18}O$

Thus, only the three isotopologues of m/z 44, 45, 46 and consequently two independent molecular ratios ^{45}R and ^{46}R are generally available for high precision isotope ratio mass spectrometry, from which three independent isotope ratios ^{13}R, ^{17}R and ^{18}R have to be obtained. Here ^{n}R denotes the abundance ratio of the molecular or atomic species of mass n to the related molecular or atomic species of the most abundant mass. The underlying two equations to derive atomic from molecular ratios are not sufficient to solve for the three unknowns atomic ratios.

$$^{45}R = 2\,^{17}R + {}^{13}R \tag{3.4}$$

$$^{46}R = 2\,^{18}R + 2\,^{17}R\,^{13}R + (^{17}R)^2 \tag{3.5}$$

Therefore, an additional equation is needed. This equation is provided by the mass dependent fractionation equation mentioned in chapter 2. If a certain relation between ^{17}R and ^{18}R ratios is assumed, ^{13}R can be derived from ^{45}R. Based on theoretical considerations, the ^{17}O-correction of Craig [1957] is based on the following relationship between oxygen isotopes:

$$\frac{^{17}R}{^{17}R_{RM}} = \left(\frac{^{18}R}{^{18}R_{RM}}\right)^{0.5} \tag{3.6}$$

where $^{17}R_{RM}$ and $^{18}R_{RM}$ are oxygen isotope ratios in a reference material (RM). Later the ^{17}O-correction was refined [Santrock et al. 1985] using the relationship:

$$^{17}R = K\,(^{18}R)^{\lambda} \tag{3.7}$$

where K = $^{17}R_{RM}$ $(^{18}R_{RM})^{-\lambda}$. This relationship describes the mass-dependent isotopic fractionation of oxygen isotopes and is valid for most known chemical processes (for details about λ see sec. 2.1.4). Substituting ^{17}R from eqn (3.7), ^{18}R can be calculated from eqns (3.4) and (3.5) by numerical solution of the equation:

$$-3\,K^2(^{18}R)^{2\lambda} + 2\,R^{45}(^{18}R)^{\lambda} + 2\,^{18}R - ^{46}R = 0 \tag{3.8}$$

^{17}R is then calculated from eqn (3.7) and finally ^{13}R is determined as

$$^{13}R = ^{45}R - 2\,^{17}R \tag{3.9}$$

However, the application of eqn (3.7) is only adequate for mass dependently fractionated gas. For CO_2 gas of anomalous oxygen isotopic composition, all three unknowns (^{13}R as well as ^{17}R and ^{18}R) have to be determined, which is impossible from eqn (3.4) and (3.5) only. Therefore, the exact ^{13}R value of CO_2 must be determined independently.

In view of the importance to quantify the mass independent isotope effect in atmospheric CO_2 three other techniques have been developed:

i) Decomposition of CO_2 with BrF_5 at ~800°C for 48h [Bhattacharya and Thiemens 1989].

ii) Conversion of CO_2 to methane and water followed by decomposition of water to H_2 and O_2 [Brenninkmeijer and Röckmann 1998].

iii) Complete oxygen isotope exchange of a CO_2 sample with CeO_2 and measurements of the isotope exchange before and after exchange [Assonov and Brenninkmeijer 2002].

In the work presented here, we used CeO_2 equilibration method as described in the following subsection.

3.2.1 CeO_2 exchange system

The CeO_2 equilibration method consists of number of steps as shown in Figure 3.3. The CO_2 gas is isotopically analyzed by the mass spectrometer with the conventional IRMS method. After analysis, the remainder is frozen back into the sample bottle and transferred to the vacuum line. Hereafter, the CO_2 gas is introduced into the CeO_2 reaction tube by freezing into the cold finger at the inlet of the conversion oven at liquid nitrogen temperature (77K).

The CO_2 is istopically equilibrated with the excess O_2 of the CeO_2 at 650°C for 35min. As CeO_2 may adsorb some CO_2, it takes a long time to freeze all CO_2 from reaction tube. To facilitate recovery of CO_2, CO_2 is distilled into the U-tube (placed between the reaction tube and the vacuum line), after which it is isolated from the reactor and CO_2 qualitatively transferred into the sample bottle Figure 3.11. The equilibrated CO_2 is reanalyzed on the mass spectrometer. To minimize the error in the $\Delta^{17}O$ determinations, the time elapsed between two successive mass spectrometry measurements is kept as short as possible (45-60 min) so that mass spectrometer conditions are similar.

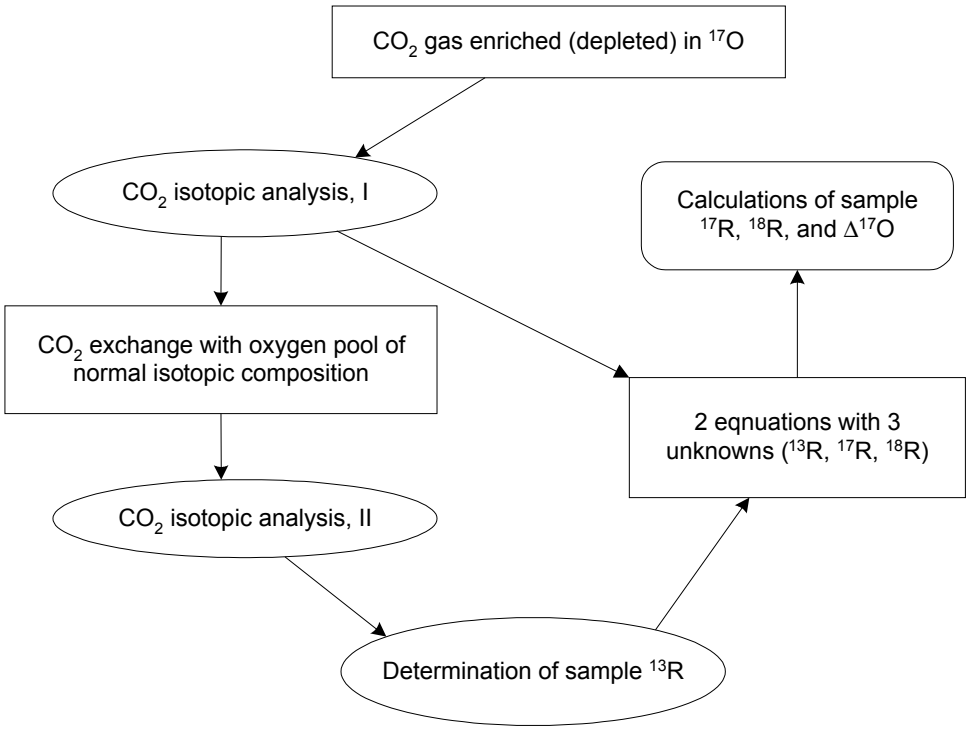

Figure 3.3: An approach to determine the $\Delta^{17}O$ value of CO_2

The key point of this analytical technique is that after complete equilibration, the oxygen isotopic composition of the CO_2 follows the mass dependent fractionation equation, i.e. the atomic isotope ratios can be derived from the molecular ratios with the formulation presented above.

In case of 100% CO_2 recovery or no fractionation in sampling handling and processing, the carbon isotopic composition is to be exactly the same before and after exchange (subscripts 1 and 2 denotes CO_2 analysis before and after isotopic equilibration with CeO_2).

$$^{13}R_1 = {}^{13}R_2 = {}^{13}R \tag{3.10}$$

This value of ^{13}R may then be used to calculate $^{17}R_1$ and $^{18}R_1$ of the initial CO_2 according to equations (3.4) and (3.5).

$$^{17}R_1 = 0.5\left({}^{45}R_1 - {}^{13}R\right) \tag{3.11}$$

$$^{18}R_1 = 0.5\left({}^{46}R_1 - 2\,{}^{13}R\,{}^{17}R_1 - \left({}^{17}R_1\right)^2\right) \tag{3.12}$$

$^{17}R_1$ and $^{18}R_1$ characterize the excess of ^{17}O, which is usually determined in linearized form as:

$$\Delta^{17}O = \delta^{17}O - 0.516\,\delta^{18}O \tag{3.13}$$

where $\delta^{17}O$ and $\delta^{18}O$ are the oxygen isotopic ratio expressed in δ-notation and 0.516 is the λ value in relationship (3.7). In fact, the λ value may vary between 0.500 – 0.5305 as pointed out in sect. 2.1.4.

3.2.2 Preparation of the CeO_2 reactant

Granulated CeO_2 (Merck #102263) is heated in air for ~10 h at ~900ºC to decompose sulphate impurities. The granulated CeO_2 is crushed, and 0.25-0.5mm fraction is used for the experiments. The amount of CeO_2 reactant (~10g) is chosen so that its oxygen stoichiometrically exceeds the oxygen of a typical CO_2 sample by a factor of ~1500. After filling the reaction tube CeO_2 is preconditioned by flushing with tank oxygen gas to fully replace the original oxygen of CeO_2 with oxygen of known isotopic composition. Oxygen gas is admitted to the reactor with an automated valve to a pressure of ~ 200mb, allowed to equilibrate with CeO_2 at 650ºC for 20 min and pumped away to a pressure of ~ 10^{-6}mb with a turbo molecular pump. This automated equilibration/ pumping cycle is repeated for several days until the CeO_2 has acquired a stable isotope composition. Before each CO_2 exchange

experiment, the CeO_2 is kept at 650°C under high vacuum for ~1h in order to remove excess oxygen.

3.2.3 Calibration of CeO_2 exchange system

The oxygen isotope exchange with CeO_2 was investigated using CO_2 of various isotopic compositions: (i) Lab CO_2 (ii) Light CO_2 (iii) CO_2 enriched in ^{17}O, prepared from synthetic O_2 mixture (iv) CO_2 enriched in both ^{17}O and ^{18}O .

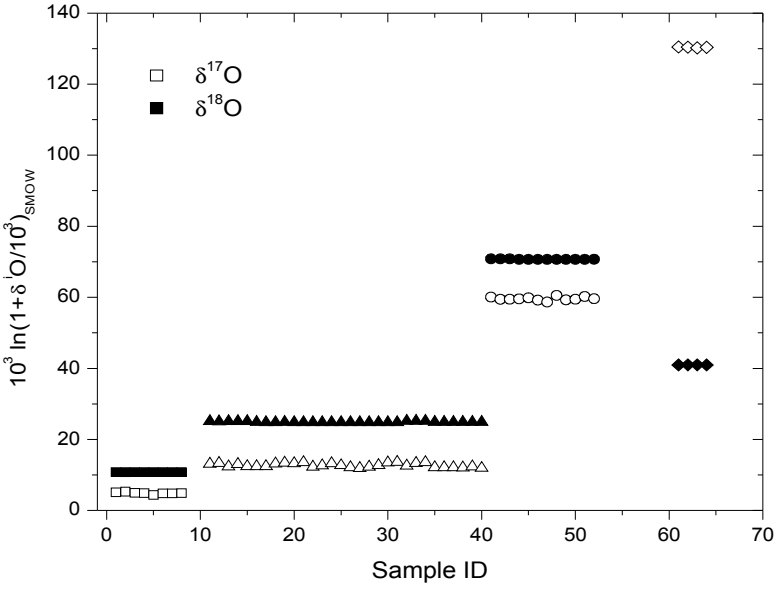

Figure 3.4: CO_2 of various isotopic compositions exchanged with CeO_2 at 650°C for 35 minutes. $\delta^{i}O = {}^{17}O$ or ${}^{18}O$. Open symbols $= {}^{17}O$ and closed symbols $= {}^{18}O$.

The results for this calibration with different CO_2 are shown in Figure 3.4. Reproducible results are obtained for all CO_2 gases. A typical scatter in $\Delta\ ^{17}O$ of $\pm$ 0.5 per mill was observed during all exchange experiments, which is taken as the analytical error. Several processes may contribute to this error:

i) The fact that CO_2 was analyzed on mass spectrometer twice, firstly for initial m/z 45, 46 signal, frozen back into the sample bottle, exchanged with CeO_2 and reanalyzed for mass dependent m/z 45, 46 signal to measure actual $\delta^{13}C$ values.

ii). Incomplete recovery during extraction or contamination during the reaction. Although 99.8 $\pm$ 0.5% recovery yield was confirmed for CO_2, there could be some contamination from viton rings used in the vacuum line, which can alter $\delta^{13}C$ and ultimately affects $\delta^{17}O$ values.

Nevertheless, with the stated errors, the CeO_2 exchange method can be used reliably to study the CO_2 and $O(^1D)$ exchange mechanism.

3.3 Production of MIF CO_2 from O_2

In order to calibrate the CeO_2 method for a wide range of isotopic compositions to be used in the CO_2 and O_3 isotope exchange experiments, CO_2 enriched in either ^{17}O or ^{18}O was prepared from the combustion of synthetic mixtures of oxygen enriched in ^{17}O and ^{18}O on activated charcoal. The ^{17}O and ^{18}O-enriched oxygen gas was prepared by mixing pure ^{17}O (90 atom %, Isotec. Inc. USA) and ^{18}O (99 atom %, Isotec. Inc. USA) with normal tank oxygen. Random distribution of heavy isotopes in the mixture was achieved by discharging the mixture for one hour.

The system to produce CO_2 from O_2 consisted of a pyrex glass reactor. Activated charcoal pellets were filled in a platinum mesh cup, which itself was placed inside a cup made out of sheathed thermocouple used as a heater element. The temperature was controlled with an additional thermocouple sensor as shown in Figure 3.5.

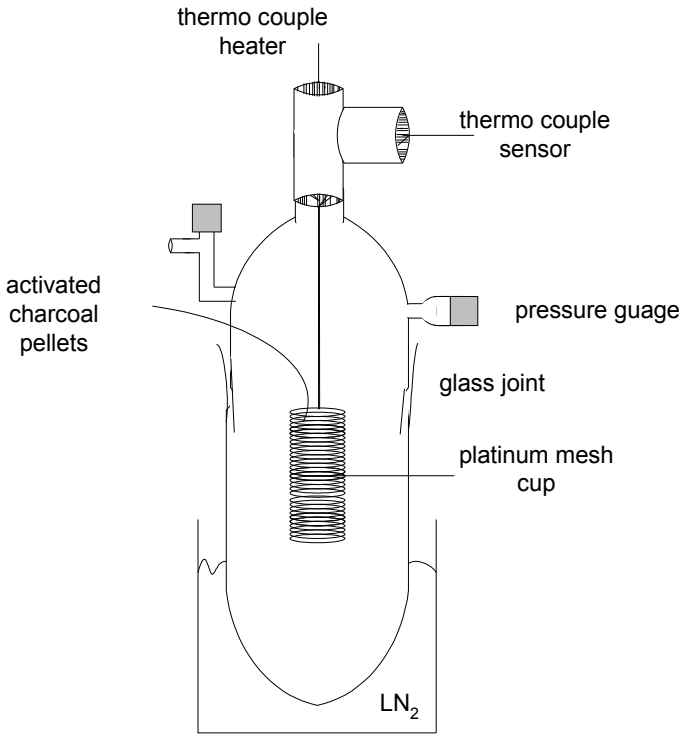

Figure 3.5: Setup to produce CO_2 from synthetic O_2 mixtures.

Before each combustion reaction the carbon reactor was degassed at ~ 800°C while being

evacuated. When oxygen was admitted to the evacuated system at ~ 650°C, it quickly reacted with carbon to form CO_2 which was trapped at the bottom at liquid nitrogen temperature. The conversion was monitored by a pressure guage connected to the reactor, and was complete when the pressure in the reactor was below 1mb and did not change any more. This final pressure was higher than the pressure observed prior to introduction of oxygen owing to CO production. After the conversion, the heating was switched off and the reactor was cooled to ~200°C to prevent the interaction of resultant CO_2 with the heated walls of reactor and prevent the formation of CO during the transfer of CO_2 to a sample bottle. The CO_2 produced was first dried over P_2O_5 and further purified in multiple freeze thawing cycles i.e. by pumping away non condensible components from CO_2 by freezing at liquid N_2 temperature.

Usually the charcoal pellets required conditioning before reproducible results could be obtained. Few O_2 aliquots (~ 3- 4) were combusted until the $\delta^{13}C$ values of the produced CO_2 became stable. After this treatment, the conversion reactor was ready for routine reactions.

To produce MIF CO_2 equally enriched in ^{17}O and ^{18}O, aliquots of CO_2 and O_2 (routinely used as mass spectrometer working standards) were mixed in a 2.2L bulb and the mixture was irradiated for ~72 h (can be adjusted according to the enrichment required in CO_2) with a Hg-pen ray lamp as shown in Figure 3.6. At the end of photolysis time CO_2, O_2 and O_3 were separated as described in sec. 3.4.

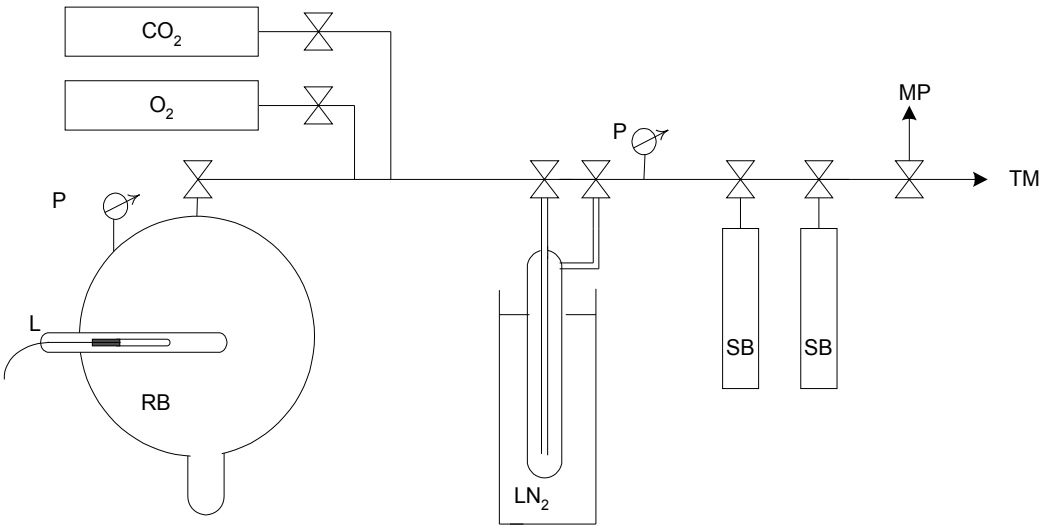

Figure 3.6: Laboratory setup to produce CO_2 enriched in ^{17}O and ^{18}O. RB= 2.1 L reaction bulb, L = Hg pen ray lamp, P = pressure sensor, SB = sample bottle, MP = membrane pump, TM = turbo molecular pump.

3.4 CO_2 and O_3 isotope exchange experiments

Ultra high purity CO_2 and O_2 (Messer Griesheim, > 99.998 %) were used in the experiment. Ozone was prepared by discharging oxygen in a commercial ozonizer (Orec V5-0, Osmonic Inc. USA). Typically the first reaction in the discharge kinetics is the dissociation of molecular oxygen by electron collisions. Ozone is mainly formed in a the three body reaction involving O and O_2. Side reactions of O atoms compete with O_3 formation. The main contribution to O_3 decomposition are collisions with atomic oxygen or with electrons.

A simplified list of the main reactions that govern ozone formation in an electric discharge is given below

$O_2 + e \rightarrow O + O + e$

$O + O_2 + M \rightarrow O_3 + M$

$O + O + M \rightarrow O_2 + M$

$O + O_3 \rightarrow 2O_2$

$O_3 + e \rightarrow O + O_2 + e$

The O_2-O_3 mixture thus produced was passed through a trap at liquid N_2 temperature allowing O_3 condensation while pumping away all the oxygen.

To study the isotope exchange reactions between CO_2 and O_3, different amounts of CO_2 and O_3 were mixed in a reaction cell. The mixture was irradiated with a Hg- pen ray lamp (Oriel instruments, Stratford, Connecticut) with primary emission peaks at 184.9 and 253.7 nm and a photon flux of approximately 10^{15} photons s^{-1}. The reactions at room temperature were carried out either in 250mL (named SR) or in 2.2 L (named LR) borosilicate reactors containing a Suprasil^{TM} finger in the center to place the lamp. For low temperature experiments the geometry of the reactor was modified to fit into the cryostat (Huber CE, Unistat 390W (-90 to +150^{o}C). The reactor used for low temperature experiments was 510mL (named MR). All the reactors were conditioned by exposing them to O_3 in contact for several days. The same treatment was given to the connecting tubing but for a shorter time. Teflon stoppers were used in the setup in order to avoid any contamination in the reaction products from Viton o-rings. The photolysis lamp was operated at a current of 10mA and nitrogen was circulated through the Suprasil finger to remove atmospheric oxygen and to prevent excessive heating.

Initially Oriel pen ray lamp (Hg-Ar) was used for irradiation. But in our photochemical

equilibrium experiments, the life time of Oriel lamp was found short so in latter experiments this lamp was replaced with a Puritech (Hg-Ar) pen ray lamp. Its emission intensity was also measured.

At the end of each experiment CO_2 and O_2 were cryogenically separated in a glass spiral trap fitted with a fiber glass thimble (Figure 3.7). During extraction small quantities of ozone were also condensed along with CO_2. The oxygen was collected over molecular sieve (13X) at 77 K. The O_3 was destroyed over hot Ni foil and CO_2 was separated from product oxygen cryogenically. In order to avoid any unwanted effects we heated O_3 and CO_2 mixture at 90 ± 5°C in the present experiments as some exchange between labeled CO_2 and O_3 at 200°C have bee reported [Katakis and Taube 1962]. Blank measurements with CO_2 and O_2 in all the reactors were also carried out to check any additional fractionation during handling of the samples. Isotopic material balance was observed in all experiments except in cases where large amount of O_3 were produced by photolysis which were not measured quantitatively.

Since, O_3 has a considerable vapor pressure at liquid N_2 temperature, it cannot be quantitatively trapped and partial recovery of O_3 can lead to significant fractionation [Krankowsky et al. 2003].

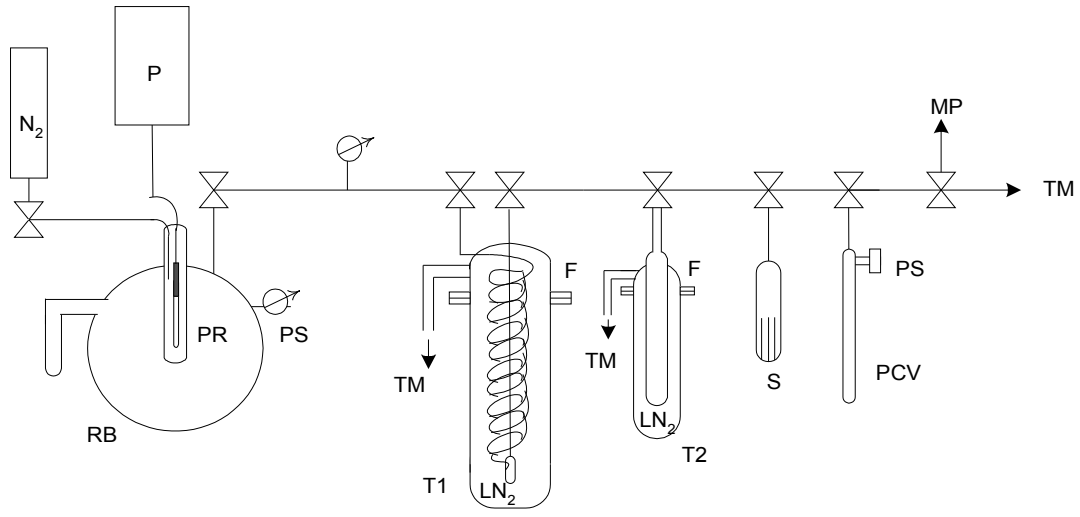

Figure 3.7: Laboratory setup for CO_2-O_3 isotope exchange including the novel trap to collect ozone at the triple point of N_2 (63K). RB = reaction bulb, PR = pen ray lamp, P = power supply for pen ray lamp, PS = pressure sensor, PCV = pre calibrated volume, F = air tight flange, TM = turbo molecular pump, MP = membrane pump, T1 and T2 = traps at triple point of N_2, S = sample vial with Ni- foil to collect O_3 and CO_2 for O_3 decomposition and bulk O_3 and CO_2 analysis.

In order to avoid a possible bias and to measure the O_3 isotopic composition precisely, the cold trap setup used for low temperature experiment was modified to allow the complete condensation of O_3 at triple point of nitrogen (63K) as shown in Figure 3.8. This temperature was achieved by pumping on the liquid nitrogen in a closed dewar system. At this temperature the O_3 vapor pressure is less than 10^{-6} mb. Thus O_3 and CO_2 were completely collected, while molecular O_2 was pumped away by keeping the total pressure in the trap below 150mb. When the pressure in the vacuum system dropped below 10^{-6} mb, the O_3 was evaporated by replacing the liquid nitogen with a water bath. The evaporated O_3 was collected in another cell at 63K to be transferred to the multi pass cell a of tunable diode laser to measure the enrichment in asymmetric isotopemer of O_3. Very recently, the first method world wide has been developed at our institute to measure the intramolecular distribution of oxygen isotopes in ozone with tunable diode laser system [Tuzson 2005]. This information about asymmetric isotopmer of O_3 is important as $O(^1D)$ is more likely produced from asymmetric O_3 [Sheppard and Walker 1983].

3.5 Photolysis constants

In order to model the isotope exchange process with the chemical kinetic program Facsimile (chapter 7), it is necessary to know the O_2 and O_3 photolysis constants for the lamps employed in the experiments.

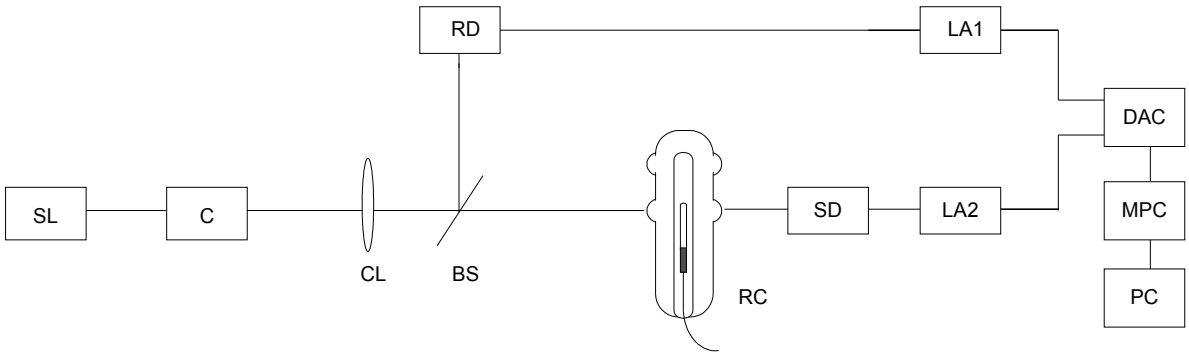

Figure 3.8: Scheme showing setup to measure photolysis rates. SL = source light (Oriel pen ray lamp), C = chopper, CL = collimating lens, BS = beam splitter, RD = reference detector, SD = sample detector, RC = Reaction cell, LA1& LA2= Lock in amplifiers, DAC = Digital analog converter, Multipurpose card, PC = computer with software Lab View.

In order to determine these parameters, the time evolution of O_3 formation and dissociation as a function of irradiation time was used to measure photolysis constant for the dissociation of oxygen (JO_2) and ozone (JO_3) using a setup shown in Figure 3.8. (for details reader is referred to Tuzson 2005).

3.5.1 Time profile of O_3 formation

In order to measure JO_2, oxygen gas was filled into a 300mL quartz reactor fitted with four quartz windows and a Suprasil finger for the placement of Hg pen ray lamp. The O_3 quantum yield measured in the initial stage just after the start of irradiation corresponded to the quantum yield of primary odd oxygen species, because the primarily produced odd-oxygen species reacted with O_2 to yield O_3. The O_3 yield in the later stage can be influenced by the subsequent catalytic O_3 reactions which are initiated by the photo absorption of the O_3 produced. Therefore primary O_3 quantum yield (3min), without any influence by subsequent catalytic O_3 reaction (initial 3 min) was used to estimate the O_3 concentration from the initial time profile as shown in Figure 3.9.

Production rate of O_3 (P) = $d[O_3]/ dt$

Since two O_3 molecules are produced per O_2 molecule photolyzed, we have

$JO_2 = P/ 2* [O_2]$

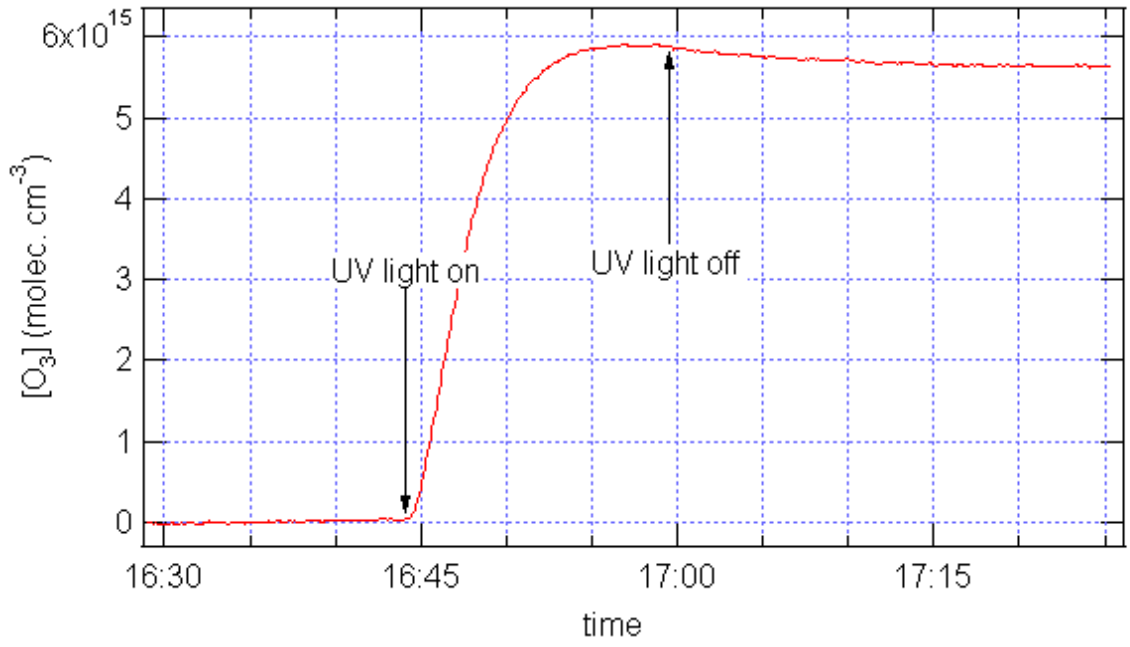

Figure 3.9: Evolution of of O_3 formation as a function of time at 100mb of O_2 with Puritec lamp.

For the O_3 concentration measurements, we took into account inhomogeneities in the spatial distribution of O_3 concentration in the cell by monitoring O_3 concentration at two different positions using two pairs of quartz windows, one close to the lamp emission area and one in the center of the reactor as shown in Figure 3.8 The measured concentration of O_3 was found to be independent of the irradiation spot, which implies that O_3 concentration was effectively homogeneous in the reactor.

The rate of formation of O_3 is dependent on the partial pressure and nature of the third body [Sehested et al. 1998], therefore O_3 formation was also monitored in O_2/CO_2 mixture to simulate the routine experimental setup. Indeed O_3 formation quantum yields were similar between the O_2 and O_2/CO_2 mixture under our experimental setup. The JO_2 was measured at different O_2 pressures of relevance to different experiments and results are shown in Table 3.2.

Table 3.2: Effect of pressure on the photolysis rates for O_3 formation using Puritech lamp.

P *(mb)*	O_2 (molecule cm^{-3})	equilibrium O_3 (molecule cm^{-3})	Production rate of O_3 (molecule cm^{-3} s^{-1})	$J(O_2)$ (s^{-1})
100	2.4×10^{18}	6.5×10^{15}	2.1×10^{13}	4.1×10^{-6}
(92)[a]	2.2×10^{18}	4.9×10^{15}	1.7×10^{13}	3.9×10^{-6}
150	3.7×10^{18}	1.1×10^{16}	3.1×10^{13}	4.0×10^{-6}
250	6.1×10^{18}	2.1×10^{16}	5.2×10^{13}	4.3×10^{-6}

a = in this measurement CO_2 was used additionally (O_2/CO_2 ~10) to simulate the experimental conditions.

3.5.2 Time profile for O_3 dissociation

In order to measure JO_3, ozone was filled into the same reaction cell and dissociation of O_3 was monitored as a function of time. The O_3 concentration decreases rapidly after irradiating the with UV light as shown in Figure 3.10. The formation of nascent O_3 was neglected in the initial stage of irradiation because rate constant for the O_3 photo dissociation is much higher ($k = 1.5 \times 10^{-2}$ molecules cm^{-3} s^{-1}) in comparison to O_3 formation ($k = 6.0 \times 10^{-34}$ molecules cm^{-3} s^{-1}).

Loss rate of O_3 $(L) = d[O_3]/ dt$

Since the oxygen atom from ozone photolysis immediately destroy another O_3 molecule, JO_3 is calculated as

$JO_3 = L(O_3)/ 2* [O_3]$

In the JO_3 measurements, the photolysis cell was evacuated to 10^{-6}mb at the end using a turbo molecular pump to measure the background signal.

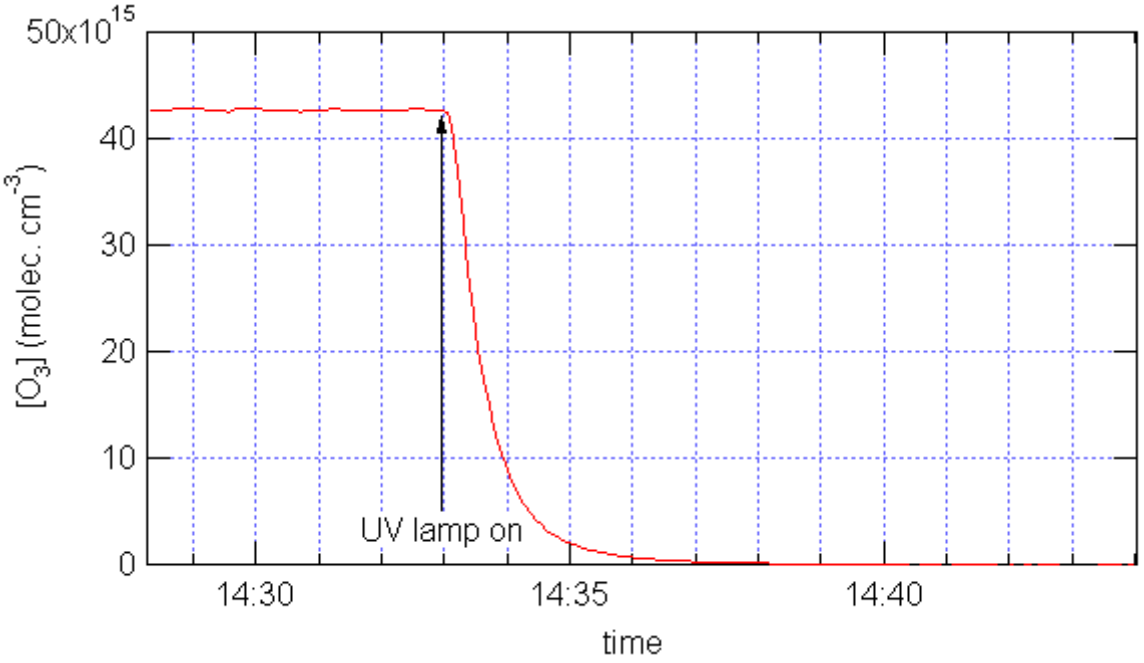

Figure 3.10: Time profile of O_3 destruction at 1.6 ± 0.2 mb of O_3 and 46 ± 1 mb of CO_2 in the cell with Puritech lamp.

Table 3.3: Photolysis rates for O_3 destruction using Puritech lamp.

CO_2 (molecule cm^{-3})	O_3 (molecule cm^{-3})	Loss rate of O_3 (molecule cm^{-3} s^{-1})	$J(O_3)$ (s^{-1})
1.09×10^{17}	4.17×10^{16}	8.2×10^{14}	9.78×10^{-3}
1.13×10^{18}	4.33×10^{16}	9.18×10^{14}	1.06×10^{-2}
1.11×10^{18}	4.27×10^{16}	9.15×10^{14}	1.07×10^{-2}

3.6 CO_2 extraction method

To extract CO_2 from ambient air samples, air samples were processed through a CO_2 extraction system (Figure 3.14) which basically consists of a cold trap immersed in liquid nitrogen attached to a vacuum manifold, using a rotary vane vacuum pump (Duo 2.5, Pfeiffer, Germany). The flow rate of 40 cm^3 min^{-1} was maintained by a mass flow controller (GFC Analyt G91130k, Germany) in front of the extraction system. Under these conditions the

pressure in the extraction system is ~ 100mb. Before the first extraction of the day, approximately 60 cm^3 of air was processed through the system and wasted directly to the vacuum pump to flush the line. In a typical extraction, CO_2 was condensed in the spiral cold trap at liquid nitrogen temperature. When the necessary amount of air (~ 0.5 L) had been processed, the system was pumped to high vacuum (5x 10^{-7} mb) with a turbo molecular pump (TSH 071E, DCU, Pfeiffer, Germany) for 2-3 minutes. The pump valve was then closed and the trap warmed manually with the heat gun adjusted at about 250°C. The CO_2 sample was transferred to a vial containing P_2O_5 at 77K and kept in contact with drying agent for ~20 minutes. The dry CO_2 samples were then transferred to a calibrated volume to measure the amount of CO_2 recovered. The samples were stored in clean and dry glass vials (~ $1cm^3$) for analysis on the dual inlet mass spectrometer. The complete setup for CO_2 extraction and CeO_2 exchange is shown in Figure 3.11.

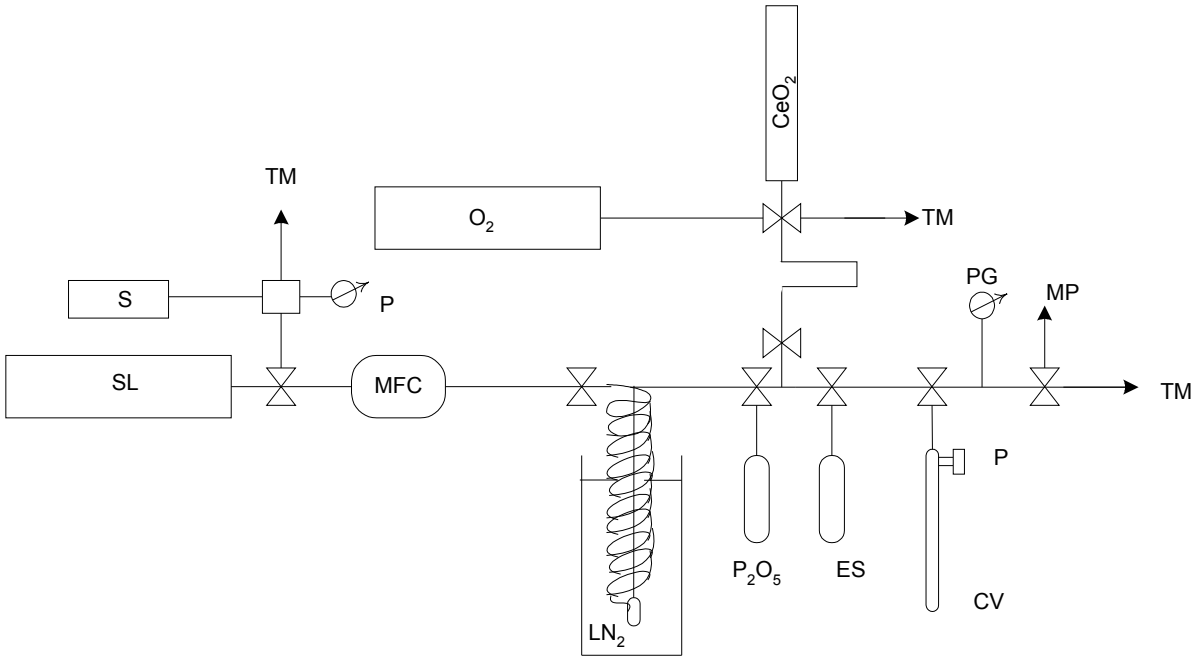

Figure 3.11: CO_2 extraction line and CeO_2 exchange system. SL= Schauinsland air; this air cylinder was used as a reference gas to monitor the extraction efficiency and stability of results, MFC = mass flow controller, P_2O_5 = vial with P_2O_5 as drying agent, ES= ethanol slurry at 203K, CV= calibrated volume, P = pressure sensor, PG = pirani guage, MP = membrane pump, TM = turbo molecular pump, CeO_2 = cerium oxide exchange reactor operated at 850 °C, O_2 = oxygen gas cylinder to refresh CeO_2 after 10-12 samples, S= stratospheric air samples.

In our initial approach for cryogenic extraction of CO_2 at 77K we tested two traps made from Duran glass (D50 Schott, Germany) and Quartz glass (HLQ210, Heraeus, Germany). In order

to increase the trapping efficiency, and to increase the cold surface area a spiral trap was built with a borosilicate fiber thimble installed at the base of the outlet tubing to ensure that no CO_2 crystals escape with the flow of air.

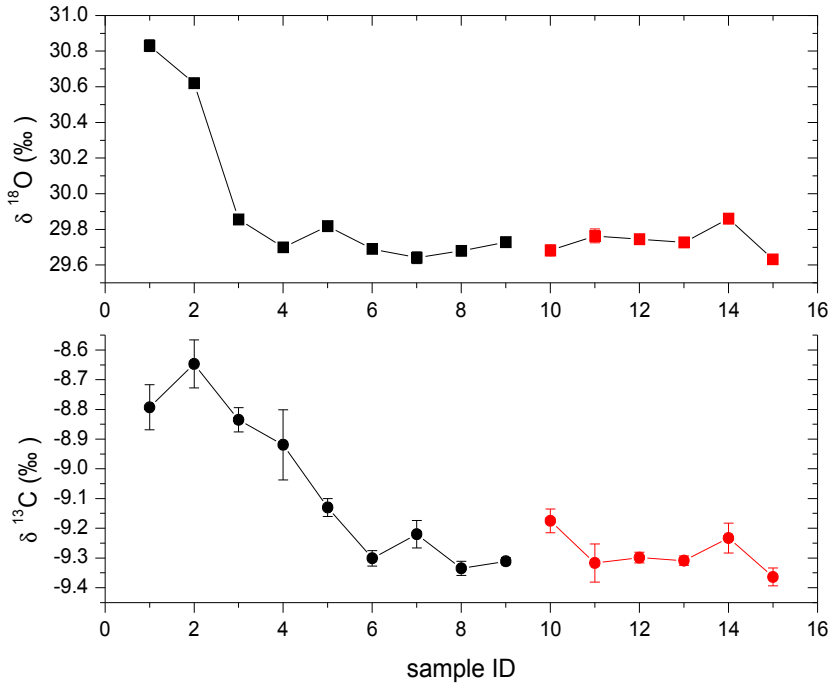

Figure 3.12: Variations in CO_2 isotopic composition extracted cryogenically (77K) with the glass trap.

It can be observed that after 6-7 extractions stable results are achieved Figure 3.12) and (Figure 3.13). Therefore the system was routinely conditioned with the reference air before extracting stratospheric samples. The need for conditioning could be due to impurities on the glass surface which are removed after some extractions. It has been noticed earlier during CO_2 extraction using automated CO_2 extractions for isotope ratio mass measurements [Werner et al.2001] that ~30 freeze-release cycles are required to achieve stable results when a quartz trap is used for CO_2 condensing.

The statistical information of more than 75 extractions of CO_2 from Schauinsland air (cylinder A) is summarized in Table 3.4. The data indicated that a quartz trap is more suitable for CO_2 extraction from atmospheric air samples. High accuracy and precision is required for these samples as an error of 0.1 ‰ in $\delta\,^{13}C$ translates into an error of 1.5‰ in $\delta\,^{17}O$ which is well above the precision of dual inlet mass spectrometer. As an internal quality check for CO_2 extraction we always used Schauinsland air before stratospheric sample.

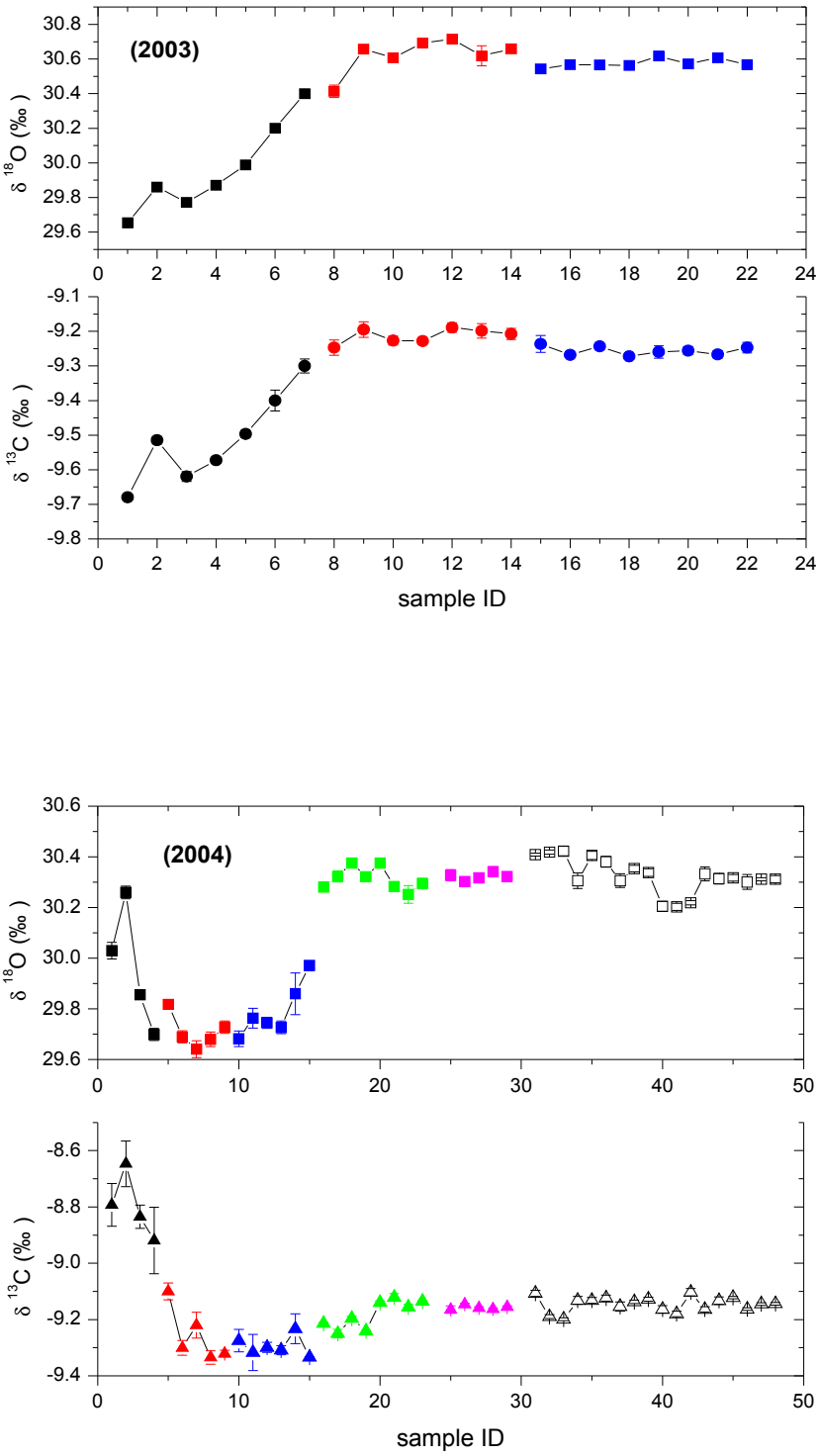

Figure 3.13: Long term variations (2003 – 2004) in CO_2 isotopic composition extracted cryogenically(77K) using quartz trap.

It can be observed that after 6-7 extractions stable results are achieved (Figure 3.13 and Figure 3.12). Therefore the system was routinely conditioned with the reference air before extracting stratospheric samples. The need for conditioning could be due to impurities on the glass surface which are removed after some extractions. It has been noticed earlier during CO_2 extraction using automated CO_2 extractions for isotope ratio mass measurements [Werner et al.2001] that ~30 freeze-release cycles are required to achieve stable results when a quartz trap is used for CO_2 condensing.

The statistical information of more than 75 extractions of CO_2 from Schauinsland air (cylinder A) is summarized in Table 3.4. The data indicated that a quartz trap is more suitable for CO_2 extraction from atmospheric air samples. High accuracy and precision is required for these samples as an error of 0.1 ‰ in $\delta^{13}C$ translates into an error of 1.5‰ in $\delta^{17}O$ which is well above the precision of dual inlet mass spectrometer. As an internal quality check for CO_2 extraction we always used Schauinsland air before stratospheric sample.

Table 3.4: Long term fluctuation in the CO_2 isotopic composition extracted cryogenically from Schauinsland air (cylinder A denoted as S) with different traps.

	n	$\delta^{13}C$ ***(‰)***	$\delta^{18}O$ ***(‰)***
Glass trap	10	-9.28 $\pm$ 0.06	29.71 $\pm$ 0.07
Quartz trap (2003)	13	-9.23 $\pm$ 0.03	30.60 $\pm$ 0.05
Quartz trap (2004)	33	-9.16 $\pm$ 0.03	30.32 $\pm$ 0.05

As complete removal of water vapor is critical to high precision measurements, two methods were tested for the removal of water from CO_2, namely P_2O_5 as drying agent and cryogenic separation with an ethanol slurry at 203K.

Table 3.5: Comparison of CO_2 isotopic compositions, separated cryogenically in a glass trap and dehydrated using either an ethanol slurry at 203K or P_2O_5.

SID	***Quantity***	***Ethanol slurry***		***SID***	***Quantity***	***P_2O_5***	
	(μ *moles)*	$\delta^{13}C$ (‰)	$\delta^{18}O$ (‰)		(μ *moles)*	$\delta^{13}C$ (‰)	$\delta^{18}O$ (‰)
S1	70.27	-9.36	30.05	S10	62.09	-9.36	29.87
S2	71.16	-9.34	29.74	S11	66.96	-9.45	30.04
S3	70.05	-9.35	29.83	S12	65.19	-9.47	30.01
S4	69.61	-9.43	30.11	S13	64.86	-9.42	29.88
S5	64.64	-9.17	30.20	S15	70.38	-9.52	30.03
S6	62.76	-9.29	30.35	S16	69.61	-9.44	29.94
S7	64.08	-9.30	30.16	S17	67.84	-9.33	30.29
S8	67.40	-9.29	30.26	S18	67.40	-9.34	30.42
S14	68.21	-9.28	30.36	S21	67.95	-9.32	30.45
S19	71.82	-9.36	30.34	S22	69.06	-9.31	30.43
S20	72.37	-9.37	30.32	S25	66.74	-9.35	30.48
S23	73.59	-9.35	30.25	S26	66.74	-9.37	30.37
S24	72.92	-9.34	30.26	S27	69.89	-9.38	30.37
Average		-9.33	30.17			-9.38	30.20
SD		0.06	0.19			0.06	0.23

The data shown in Table 3.5 indicate that both methods produce acceptable results ($\delta^{13}C$ = -9.3 ± 0.06 ‰ and $\delta^{18}O$ = 30.2 + 0.2 ‰). We chose to use P_2O_5 as a dehydrating agent because it is less time consuming and cost effective. But care must be taken not to leave the CO_2 sample too long in P_2O_5 vials: Two samples left accidentally overnight in P_2O_5 showed 0.3 ‰ depletion in $\delta^{13}C$ and 0.6 ‰ depletion in $\delta^{18}O$.

3.7 N_2O correction

During cryogenic extraction of CO_2, also N_2O is trapped, since it has similar condensation point and thus separation is not possible during the cryogenic extraction and both CO_2 and contaminating N_2O are introduced to the IRMS. Unfortunately, N_2O and its isotopologues have the same molecular mass as CO_2, and both gases contribute to measured signals at m/z

44, 45, 46. Since the molecular isotope ratios are very different, a correction for N_2O must be applied to dual-inlet measurements of CO_2 isotopes. This correction is a function of the relative amount of N_2O in the sample, its stable isotopic composition (the variance of which is assumed negligible), and the ionization efficiency of N_2O relative to CO_2 in the IRMS, which changes with the filament age and may be specific to each machine [Sirignano et al. 2004, Gosh and Brand 2004]. Therefore a calibration was carried out by mixing varying amounts of N_2O in CO_2. It is based on the fact that due to the production of the fragment NO^+ in the ion source, the mass spectrum of N_2O exhibits a relatively large mass 30 peak (Table 3.6), while mass 30 is a minor isotopic peak (stemming from $^{12}C^{18}O^+$) for CO_2. The possibility of using this peak was noted by Moore [1974] and recently measurements of the NO^+ fragment have actually been used to examine the intramolecular distribution of ^{15}N in N_2O, since it is mainly the central nitrogen atom of N_2O that is retained in the NO^+ fragment upon fragmentation [Brenninkmeijer and Röckmann, 1999].

The $^{45}\delta_n$ and $^{46}\delta_n$ values of pure N_2O relative to standard CO_2 were measured by introducing N_2O at the sample side and standard CO_2 at the standard side of the double inlet system of mass spectrometer. We obtained experimentally $^{45}\delta_n$ = - 354‰ and $^{46}\delta_n$ = - 490‰ which agrees well with the theoretically derived values [Mook and van der Hoek 1983] and experimentally measured values [Friedli and Siegenthaler 1988]. The subscripts 'n' and 'm' with raw delta 45 and 46 denote pure N_2O and CO_2-N_2O mixtures.

Table 3.6: Typical mass spectra of CO_2 and N_2O normalized to mass 44 intensity.

Mass	***CO_2***		***N_2O***	
	Ion	Peak height	Ion	Peak height
12	$^{12}C^+$	0.025		
14			$^{14}N^+$	0.043
16	$^{16}O^+$	0.060	$^{16}O^+$	0.017
28	$^{12}C^{16}O^+$	0.061	$^{14}N_2^+$	0.066
30	$^{12}C^{18}O^+$	4×10^{-5}	$^{14}N^{16}O^+$	0.197
44	$^{12}C^{16}O_2^+$	1	$^{14}N_2{}^{16}O^+$	1

Furthermore, N_2O-CO_2 mixtures were prepared by adding 2.65, 3.0, 3.92, 5.19, 7.28 μ moles of N_2O to 4.665 mmoles of CO_2 to obtain CO_2/N_2O ratios of 641, 898, 1190, 1555 and 1760.

N_2O measurement based on the same principle were carried out by other researchers too [Moore 1974, Friedli and Siegenthaler 1988].

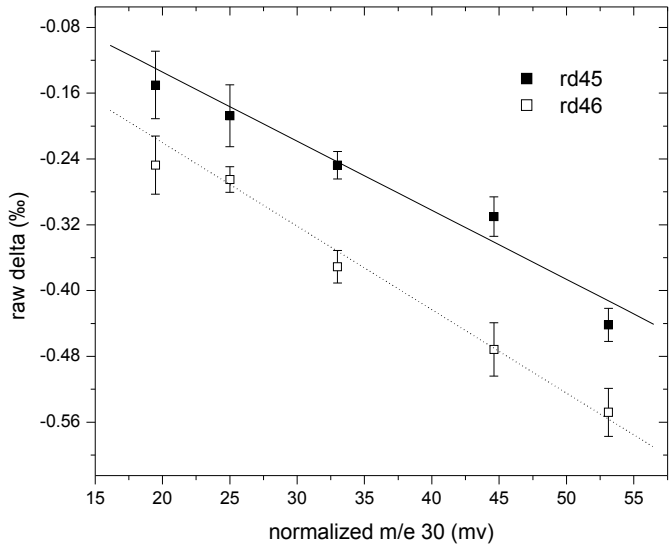

Figure 3.14: Mass ratio 45/44 and 46/44 expressed as raw delta for N_2O- CO_2 mixtures measured against the pure CO_2. The amount of N_2O was varied between 2-7 μ moles to get CO_2/N_2O ratios from 641 to 1760 at maximum. $rd^{45}\delta_{CO2} = 0.0075 * {}^{45}\delta_m$ and $rd^{46}\delta_{CO2} = 0.0106 * {}^{46}\delta_m$

For measurements in the mass spectrometer, the CO_2 standard and CO_2-N_2O mixture were adjusted to the same signal height at mass 44 and signal at m/z 30 are measured after the isotope measurements with the "interfering mass" routine of the commercial software.

The difference between peak intensities at m/z 30 between the sample and the CO2 reference gas $^{30}I = {}^{30}I_{sample} - {}^{30}I_{std}$ were then used to derive a N_2O correction for $^{45}\delta$ and $^{46}\delta$ of stratospheric CO_2 samples. Here I_{sample} and I_{std} denotes signal intensity for sample and standard. For this we plotted $^{45}\delta_m$ and $^{46}\delta_m$ for various N_2O-CO_2 mixtures against corresponding $^{30}I_n$ and used this correlation to correct the stratospheric CO_2 samples according to their $^{30}I_n$ values as shown below:

$rd^{45}\delta_{CO2} = rd^{45}\delta_{measured} + 0.0075 * {}^{30}I$

$rd^{46}\delta_{CO2} = rd^{46}\delta_{measured} + 0.0106 * {}^{30}I$

These corrections were also applied to the CO_2 samples in those experiments where N_2 and N_2O were used additionally in the O_2-CO_2 mixture to study the effect of other gases on the CO_2 and O_3 isotope exchange via $O(^1D)$.

4 Photochemical Equilibrium between Carbon Dioxide and Ozone

The main goal of the work presented in this thesis was the investigation of the isotope exchange process between ozone and carbon dioxide via $O(^1D)$. To study this process in detail, a large number of long-term experiments were carried out using photolysis in laboratory reactor system described in section 4.2. The main goal was to characterize the photochemical isotope equilibrium between O_2 and CO_2, which is mediated via formation of O_3 and isotope exchange with $O(^1D)$ from ozone photolysis. The isotope equilibrium point could be precisely characterized by using CO_2 and O_2 gases of various isotopic composition in three isotope space. The experiments were carried out with different CO_2 gases of natural and artificial isotopic compositions (CO_2 enriched either in ^{17}O or ^{18}O) in a bath gas of O_2 or O_3.

Note that in the CO_2-O_3 experiments, the ozone is effectively photolyzed to O_2 in a few minutes, so except for those few minutes all experiments are basically CO_2-O_2 exchange experiments.

The mechanism for the $O(^1D)$-CO_2 interaction can be generally described as shown in Figure 4.1. Ozone is produced by the reaction of $O + O_2$ in the presence of a third body. It is important to note that $O(^3P)$ is in a very fast isotope equilibrium with O_2, i.e. isotope exchange is about three orders of magnitude faster than O_3 formation. Thus the principal source of $O(^3P)$ is irrelevant (in the laboratory experiments it is O_2 photolysis at 184 nm)

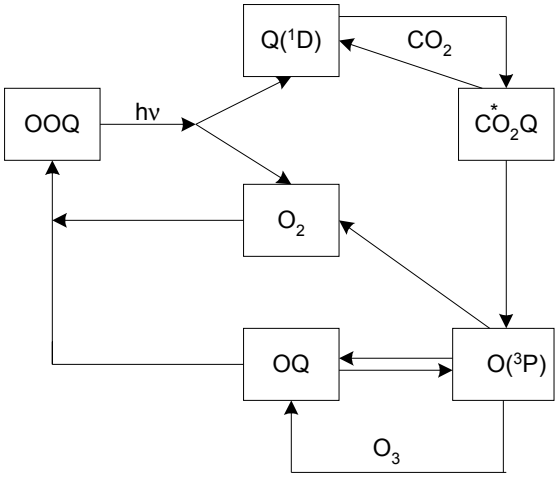

Figure 4.1: Schematic diagram showing the principal chemical pathways for exchange of oxygen between O_2 and CO_2 reservoirs. Here Q = ^{17}O or ^{18}O. Not all possible isotopic reaction combinations are shown.

The O_3 molecule after absorbing light of wavelength < 310 nm produces $O(^1D)$, which can either react with CO_2 to form a short lived CO^*_3 complex or can be simply quenched to $O(^3P)$. Isotope exchange with CO_2 can occur either on the singlet or triplet surface. The $O(^3P)$ thus produced, reacts again with O_2 molecules to produce new O_3 molecules. This way O atoms are recycled several times between O_3 and CO_2. In order to clarify the exchange mechanism we have used letter "Q" to denote heavy isotope of oxygen which can be ^{17}O or ^{18}O.

4.1.1 Blank experiments

To test the possibility of fractionation induced by processes other than photochemical isotope exchange (e.g. fractionation during sample extraction, impurities or wall effects), two types of blank experiments were performed.

(i) Pure CO_2 (~100 μmole) was kept in the reactor for 30 min and extracted back. The results indicated negligible fractionation from sample handling.

(ii) CO_2 and O_2 were kept in the reactor for short (30 min) as well as long times (64 h) without operating the lamp.

Data indicated a negligible fractionation for oxygen ($\ln\delta^{17}O$ = -0.059 ‰, $\ln\delta^{18}O$ = 0.029 ‰) and a small fractionation for CO_2 ($\ln\delta^{17}O$ = 0.356 ‰ and $\ln\delta^{18}O$ = -0.119 ‰). It is important to note that no additional correction is required to correct for this artifact wit the analytical system employed because ^{13}C is actually determined after extraction and ^{17}O of CO_2 samples is calculated using the cerium oxide equilibration method, i.e. two measurements of the isotopic composition, before and after exchange. Therefore, no assumptions have to be made about stability of the isotopic composition of CO_2 and the small changes indicated by the blank experiments are directly accounted for by the analytical procedure.

4.1.2 Temporal evolution of CO_2 and O_3 isotopic exchange

A typical example of the time evolution of an isotope exchange experiment is shown in Figure 4.2, where a mixture of CO_2 (62 ± 1μ mole) and O_2 (800 ± 10 μ mole) in a small reactor (250mL) was irradiated with a mercury pen ray lamp for various time intervals. CO_2 gets isotopically enriched, whereas O_2 gets depleted. It is evident from Figure 4.2 that the extent of enrichment in CO_2 increases exponentially (fit parameters are discussed in sec.5.3) and attains a plateau after some time. No significant change in CO_2 isotopic composition is observed when the mixture is exposed to even longer irradiation times.

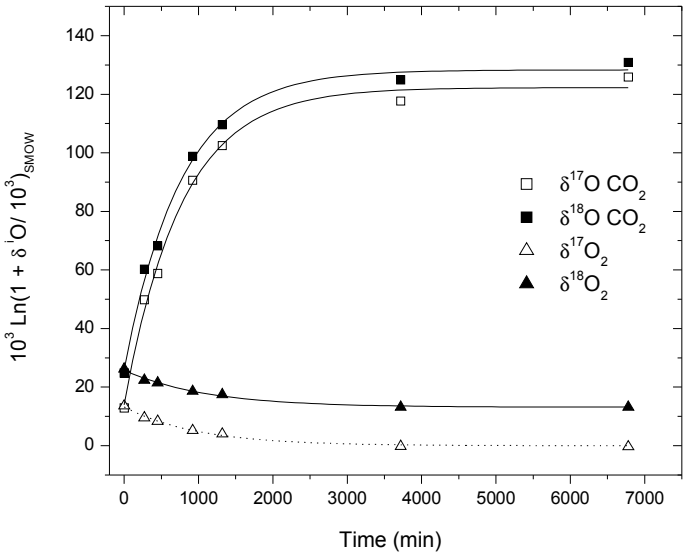

Figure 4.2: Oxygen isotope enrichment in CO_2 as a function of time at constant ratio of CO_2 and O_2 (~ 12 $\pm$ 1). $^iO = {}^{17}O$ or ^{18}O in the ordinate. The lines indicates exponential fit to the isotopic data

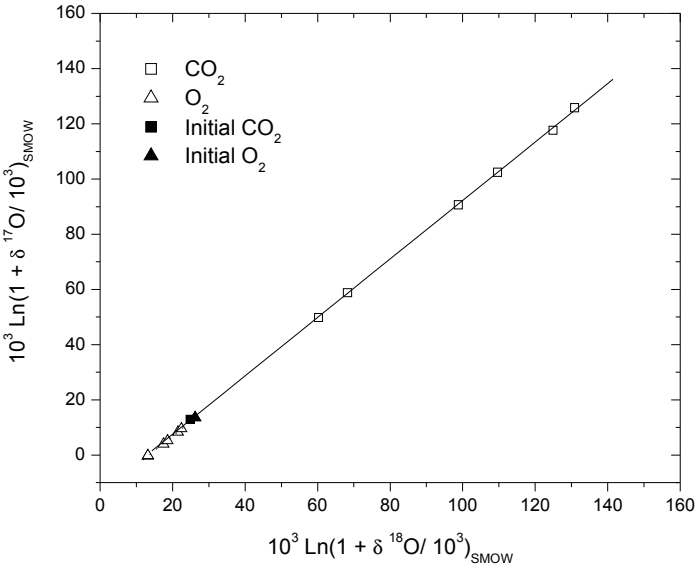

Figure 4.3: Three isotope plot showing the enrichment in the CO_2 reservoir and corresponding isotopic depletion of O_2 reservoir. The O_2-CO_2 reaction carried out at room temperature with Oriel Hg-pen ray lamp.

It has to be noted that the enrichment in CO_2 is presented on the VSMOW scale. The enrichment in CO_2 isotopic composition is accompanied by a corresponding isotopic depletion in O_2 reservoir as shown inFigure 4.2. As the total mass is conserved, the depletion in the large O_2 reservoir is small (~ 14‰) than the enrichment in the CO_2 reservoir. On a conventional three isotope plot the corresponding changes in the system are depicted in Figure 4.3 . The enrichment in CO_2 and corresponding depletion in O_2 define a slope of 1.01 ± 0.01 in a three isotope plot.

4.2 Photo chemical equilibrium between CO_2 and O_3

Three different types of CO_2 gases were used in photochemical equilibrium experiments between CO_2 and O_3 as shown in Table 4.1. CO_2 I is the mass dependently fractionated laboratory CO_2 standard gas ($\delta^{17}O = 0.516\delta^{18}O$) whereas the other two CO_2 gases are enriched in heavier isotopes (see sec. 3.3 about CO_2 production from O_2) in a mass independent fashion ($\delta^{17}O \neq 0.516\delta^{18}O$). The reason for this approach is that the photochemical isotope equilibrium point can be determined in a "triangulation" method.

Experiments were conducted with CO_2 in the range of 0.07 to 0.17 mmole and O_3 (expressed in terms of O_2 equivalent) in the range of 0.8 to 2.8 mmole. The CO_2-O_3 mixture were irradiated with the Oriel Hg-pen ray lamp from 20 minutes up to ~ 5days in a 2.2L reactor. Notice that initial O_3 is destroyed photochemically with UV light in ~ 3 minutes, leading to mass independently fractionated O_2 reservoir for further reaction. The enrichments in CO_2 after reaction with O_3 are shown in a three isotope plot (Figure 4.4).

Table 4.1: Initial isotopic composition of the CO_2 gases employed for the experiments and the average O_3 isotopic composition used to determine the photochemical equilibrium point in set I experiments.

	Initial Isotopic composition	
	$\delta\,^{17}O_{SMOW}$ (‰)	$\delta\,^{18}O_{SMOW}$ (‰)
CO_2 I	12.97 ± 0.06	25.14 ± 0.03
CO_2 II	103.58 ± 0.06	36.26 ± 0.03
CO_2 III	21 ± 0.06	173.16 ± 0.03
Average initial O_3	78 ± 3	101 ± 3

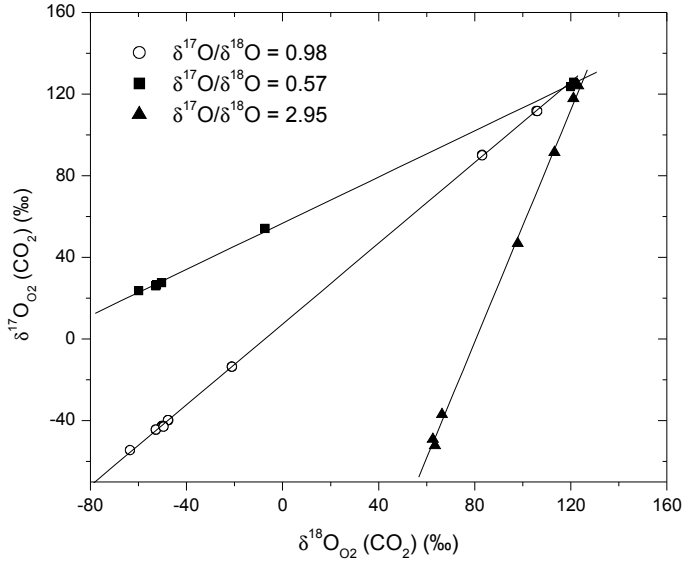

Figure 4.4: Three isotope plot of the triangulation experiments to determine the photochemical isotope equilibrium point using three different CO_2 gases. Delta values are expressed relative to O_2. The CO_2- O_3 mixture was irradiated with Hg-pen ray lamp at room temperature. Three isotope slopes for various CO_2 gases are also shown in the figure.

Irrespective of the initial CO_2 isotopic composition, the isotopic composition of the CO_2 approaches a common point at long irradiation times. This is the point at which the entire system depicted in Figure 4.1 i.e. O_2, O_3, $O(^3P)$, $O(^1D)$ and O_3 are in isotopic equilibrium. Under these specific experimental conditions, the CO_2 at equilibrium point has $\delta^{17}O_{O2}$ (CO_2) = 130 $\pm$ 0.2‰ and $\delta^{18}O_{O2}$ (CO_2) = 126 $\pm$ 0.2‰ as derived from the intersection of the fit lines. To show the inherent photochemical isotope equilibrium between CO_2 and O_2 the values shown are the delta values of CO_2 vs O_2 and not versus SMOW.

In the second set of experiments, again three different CO_2 gases were used but ozone was replaced by mass dependently fractionated oxygen as shown in Table 4.2. The amount of CO_2 varied between 0.04 to 18 mmole and O_2 ranged from 0.4 to 170 mmole. These experiments were also carried out in the 2.2L reactor. The mixture was irradiated from 60 minutes to ~ 6 days but in some of the long time experiments the Puritech lamp was used instead of Oriel lamp. The time required to achieve photochemical equilibrium was longer (e-folding time ~ 2100 min) due to higher pressure employed in CO_2-O_2 mixture. Therefore the lines are extrapolated to the photochemical equilibrium point.

Table 4.2: Initial isotopic composition of various CO_2 gases and O_2 isotopic composition used to determine the photochemical equilibrium point in set II experiment.

	Initial Isotopic composition	
	$\delta\ ^{17}O_{SMOW}$ (‰)	$\delta\ ^{18}O_{SMOW}$ (‰)
CO_2 I	12.97 ± 0 .06	25.14 ± 0.03
CO_2 II	102.12 ± 0.06	51.63 ± 0.03
CO_2 III	21 ± 0.06	174.29 ± 0.03
oxygen	3.79 ± 0.03	7.39 ± 0.02

In this experiment individual slopes in the three isotope plot are different, since the isotopic composition of the starting oxygen reservoir in set I experiment (i.e. ozone) is totally different, and thus the position of the various CO_2 gases relative to O_2 in the three isotope plot is different too. For example the slope for the ^{18}O enriched CO_2 slope changes from +3 to -3 because in set I experiments the initial $\delta^{18}O$ of this CO_2 is lower than the photochemical equilibrium point, whereas in set II it is higher than the photochemical isotope equilibrium point. However, the photochemical equilibrium point itself is similar to the set I results and in this experiment we find equal enrichment in both isotopes ($\delta^{17}O_{O2}$ (CO_2) =130.97 ± 0.4‰ and $\delta^{18}O_{O2}$ (CO_2) = 130.8 ± 0.4‰) as shown in Figure 4.5. The slight difference of the photochemical equilibrium points between the two sets of experiments is likely due to 1) the difference in total pressure in the reactor and 2) the difference photolysis lamp employed. (The effect of pressure and lamp types are discussed in detail in chapter 5).

It is quite clear from Figure 4.4 and Figure 4.5 that it is not sufficient to exclusively discuss slopes in three isotope plots in relation to the exchange mechanism, since they are obviously very much dependent on the isotopic composition of the starting gases. This is also the case when data are presented on SMOW scale, and it should be kept in mind when comparing slopes data from different experimental series. Our experiments with artificially enriched gases makes this point very clear.

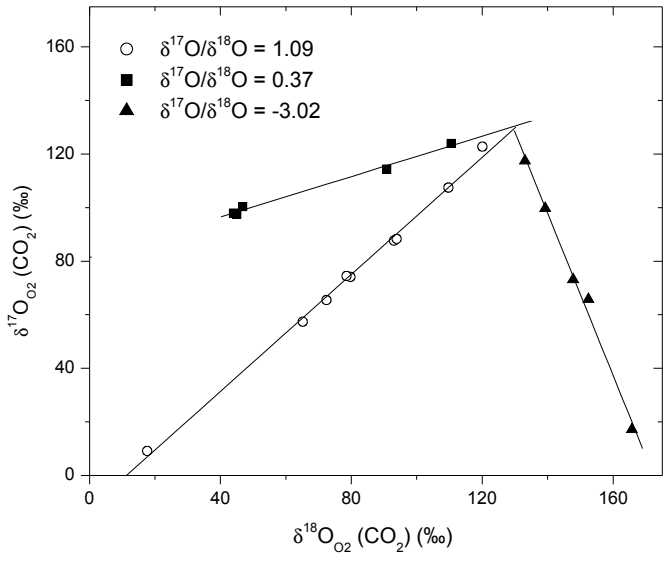

Figure 4.5: Three isotope plot of triangulation experiments to determine the photochemical isotope equilibrium using three different CO_2 gases. The CO_2-O_2 mixture was irradiated with Hg-pen ray lamp at room temperature.

Importantly, our experimental results show that the photochemical isotope equilibrium is an inherent property of the isotope exchange system. By studying this equilibrium point, we can gain more relevant insight about the exchange process than by studying slopes which are obviously dependent on the initial isotopic compositions of the reactants.

4.3 Discussion

One of the important features of the experiment is the observed anomalous fractionation pattern. When a mixture of mass dependent CO_2 and oxygen is irradiated with Hg-pen ray lamp, the CO_2 gets isotopically enriched with time. The resultant CO_2 has isotopic composition quite distinct from the initial CO_2 and evolve towards equilibrium value with a slope of 1.01 ± 0.01 as shown in Figure 4.3. The oxygen reservoir gets depleted isotopically with time and the resultant oxygen also has a slope of 1.01 ± 0.01.

This exchange mechanism can be explained by the fact that photolysis of O_2 at wavelength of 184 nm produces $O(^3P)$ that leads to the formation of O_3 in a three body reaction from O_2. The $O(^1D)$ are produced from the photolysis of O_3 at wavelength of 253 nm. The quantum yield of $O(^1D)$ is 0.92 ± 0.04 at 253.7 nm [Cobos et al. 1983, Takahashi et al. 2002], and every photon absorbed, leads to one $O(^1D)$ atom and one $OO(^1\Delta)$ molecule. The primary fate of O

(^1D) is quenching after collision with surrounding molecules. As the rate constant for the reaction of $O(^1D)$ with CO_2 ($k = 1.1 \times 10^{-10}$) is ~3 times higher in comparison to O_2 ($k = 4 \times 10^{-11}$), a significant fraction of $O(^1D)$ react with CO_2 to form CO_3^* at 300K, although the O_2 reservoir is larger. The CO_3^* formed dissociates back to CO_2 and $O(^3P)$ but its isotopic signatures are different from the original CO_2. The new CO_2 thus formed mixes with the initial CO_2 pool so the CO_2 isotopic composition is a mixture of anomalous CO_2 formed via CO^*_3 and the initial mass dependent CO_2. This process continues until the isotope equilibrium is reached i.e., the CO_2 before and after isotope exchange with $O(^1D)$ does no longer differ in isotopic composition. The formation of CO during reaction of $O(^1D)$ with CO_2 has been ruled out by many investigators [Sedlacek et al. 1989 and references therein].

Note that quenching of $O(^1D)$ with O_2 and $OO(^1\Delta)$ in general is temperature dependent (Table 7.1). The reaction of $O(^1D)$ with O_3 ($k = 1.2 \times 10^{-10}$) destroy odd oxygen and leads to the termination of isotope exchange cycle, where O atoms are exchanged between CO_2 and O_2. Nonetheless, the concentration of O_3 is ~2 orders of magnitude less than that of CO_2, this channel is slow. On the other hand $OO(^1\Delta)$ quenching ($k = 1.54 \times 10^{-18}$) at 300K is 3 orders of magnitude lower than its reaction with O_3 ($k = 3.8 \times 10^{-15}$), but O_3 concentration is ~3 orders of magnitude less than other species (CO_2 and O_2). So the two processes are of similar magnitude and $OO(^1\Delta)$ will contribute to the O_3 dissociation. Due to the slow quenching channel, the life time of $OO(^1\Delta)$ is also much longer in comparison to $O(^1D)$ as shown in Table 4.3.

The $O(^3P)$ formed in the system can either react with O_3, forming two oxygen molecule($k = 8.3 \times 10^{-15}$) or it can recombine with O_2, reforming O_3 ($k = 6 \times 10^{-34}$). The first reaction again destroys odd oxygen and ends the photochemical isotope exchange chain. Nevertheless, the isotope exchange reaction with O_2 molecules ($k = 2.9 \times 10^{-12}$) is three orders of magnitude faster than reaction of $O(^3P)$ with O_3 to form two oxygen molecules. The secondary O_3 formed in the reaction mixture will have higher enrichment ($\delta^{17}O = 170 \pm 10‰$, $\delta^{18}O = 210 \pm 10$ ‰ based on our model calculations) due to the strong isotope effect in the formation of O_3 [Mauersberger et al. 1999, Janssen et al. 2001].

Table 4.3: Concentration of various species at photochemical equilibrium and their life times (τ_1) obtained using numerical simulations.

Species	***Concentration (molecule cm^{-3})***	τ_1 ***(s)***
O_3	3.7×10^{14}	42.6
$O(^1D)$	1.6×10^{5}	9.4×10^{-8}
$OO(^1\Delta)$	9.1×10^{11}	4.4
$O(^3P)$	1.1×10^{11}	0.33
O_2	2.2×10^{17}	-
CO_2	1.7×10^{16}	-

The secondary O_3 thus produced leads to further enrichment in CO_2 via the above mentioned procedure. This way the O atoms are cycled several times between CO_2 and O_2 reservoir leading to continuous enrichment in CO_2 and depletion in O_2. When the irradiation time is long enough, an isotopic equilibrium is established at steady state between CO_2 and $O(^1D)$ derived from O_3 and no further enrichment in CO_2 isotopic composition is observed after this point.

The anomalous CO_2 at photochemical equilibrium in the set I experiment has $\delta^{17}O_{O2}$ (CO_2) = 130 $\pm$ 0.2‰ and $\delta^{18}O_{O2}$ (CO_2) = 126 $\pm$ 0.2‰ as shown in Figure 4.4. Similarly in Set II experiment, CO_2 at photochemical equilibrium has $\delta^{17}O_{O2}$ (CO_2) = 131 $\pm$ 0.4‰ and $\delta^{18}O_{O2}$ (CO_2) = 131 $\pm$ 0.4‰ as shown in Figure 4.5. Given the slight differences in reaction conditions and light source employed, the data clearly indicate that CO_2 isotopic composition at photochemical equilibrium is independent of the initial oxygen reservoir and initial CO_2 isotopic composition. In set I experiments we have mass independent O_2 available for secondary O_3 formation because almost all of the O_3 in set I is converted to O_2 after ~ 3 minutes of photolysis ($JO_3 = 2 \times 10^{-2}$). In set II experiments, the initial oxygen is mass dependent, leading to O_3 formation from a normal oxygen reservoir available. This situation is closer to the atmospheric conditions where O_3 is formed from mass dependently fractionated oxygen.

In the experiments above we have established the isotopic composition of CO_2 relative to O_2 at photochemical isotope equilibrium. We have also demonstrated that this photochemical equilibrium point is the inherent property of the exchange process which provides the

underlying information to obtain three-isotope slopes. Here we use the obtained information about the equilibrium point to calculate three-isotope slopes, which then only depend on the initial CO_2 and O_2 isotopic compositions. We start with the isotope equilibrium point from CO_2-O_2 exchange experiments which we denote by ^{17}X and ^{18}X:

$^{17}X = \delta^{17}O_{O2}\,(CO_2)$

$^{18}X = \delta^{18}O_{O2}\,(CO_2)$

From the measurements ^{17}X and ^{18}X have been determined to be 131‰.

In terms of VSMOW, final CO_2 is given by

$$\delta_{O2f}CO_{2f} = \frac{RCO_{2f} - RO_{2f}}{RO_{2f}} * 1000 = \frac{\frac{RCO_{2f}}{R_{SMOW}} - \frac{RO_{2f}}{R_{SMOW}}}{\frac{RO_{2f}}{R_{SMOW}}} * 1000 = \frac{\delta_{SMOW}CO_{2f} - \delta_{SMOW}O_{2f}}{1 + \delta_{SMOW}O_{2f}/1000} \quad (4.1)$$

Using the definition of ${}^nX$, this can be rearranged to relate final O_2 to CO_2 and X, with δ (delta) values defined on the SMOW scale:

$${}^n\delta_{SMOW}O_{2f} = ({}^n\delta_{SMOW}CO_{2f} - {}^nX)/(1 + {}^nX/1000) \quad (4.2)$$

for n = ^{17}O or ^{18}O. Using square brackets to denote molecular abundances, conservation of mass requires that

$$[CO_2]^n\delta CO_2 + [O_2]^n\delta O_2 = constant\,. \quad (4.3)$$

When relative amounts ρ (rho) = $[O_2]/[CO_2]$ are introduced, one can express this also as

$${}^n\delta CO_2 + \rho\,{}^n\delta O_2 = constant\,,$$

which in particular implies a relation between initial (*ini*) and final (*f*) delta values:

$${}^n\delta(ini\,CO_2) + \rho\,{}^n\delta(ini\,O_2) = {}^n\delta(f\,CO_2) + \rho\,{}^n\delta(f\,O_2) \quad (4.4)$$

We need to define ${}^n\delta(fCO_2)$ in terms of knowns i.e X, ρ, ${}^n\delta(ini\ CO_2)$, ${}^n\delta(ini\ O_2)$. Therefore we use equation (4.2) to substitute $\delta(fO_2)$ in equation (4.4), which gives

$${}^n\delta(f\,CO_2) = {}^nX + \frac{(1 + {}^nX/1000) * \{{}^n\delta(ini\,CO_2) + \rho\,{}^n\delta(ini\,O_2) - {}^nX\}}{1 + {}^nX/1000 + \rho}$$

This now allows to determine the CO_2 slope in the three isotope plot, that is defined as

$$slope = \frac{{}^{17}\delta(f\,CO_2) - {}^{17}\delta(ini\,CO_2)}{{}^{18}\delta(f\,CO_2) - {}^{18}\delta(ini\,CO_2)}\,. \quad (4.5)$$

Therefore, we finally obtain:

$$slope = \frac{{}^{17}X + \frac{(1+{}^{17}X/1000)*\{{}^{17}\delta(ini\,CO_2)+\rho\,{}^{17}\delta(ini\,O_2)-{}^{17}X\}}{1+{}^{17}X/1000+\rho} - {}^{17}\delta(ini\,CO_2)}{{}^{18}X + \frac{(1+{}^{18}X/1000)*\{{}^{18}\delta(ini\,CO_2)+\rho\,{}^{18}\delta(ini\,O_2)-{}^{18}X\}}{1+{}^{18}X/1000+\rho} - {}^{18}\delta(ini\,CO_2)} \qquad (4.6)$$

This expresses the slope in terms of the initial reactants and the fractionation values ${}^{17}X$ and ${}^{18}X$ between final CO_2 and O_2.

Using the prediction from the photochemical equilibrium point inherent in equation (4.6) the observed slopes for various experimental set ups can be reproduced fairly well. This is shown in Table 4.4 .

Table 4.4: Comparison of calculated CO_2 slopes with experiments carried out at room temperature.

amount (mmole)		***Initial CO_2***		***Initial O_2/O_3***		***CO_2 slope***	
CO_2	O_2 or O_3	$\delta^{17}O$	$\delta^{18}O$	$\delta^{17}O$	$\delta^{18}O$	Experiment	Calculated
0.08	1.04[a]	12.97	25.14	76.6	99.4	0.96 ± 0.003	0.95
0.14	1.28[a]	103.6	36.26	77.1	101.7	0.54 ± 0.006	0.56
0.08	1.44[a]	21.00	173.7	79.9	103.3	2.99 ± 0.06	2.97
0.06	0.89	12.97	25.14	3.7	7.3	1.04 ± 0.007	1.07
0.06	0.87	102.1	51.63	3.7	7.3	0.42 ± 0.03	0.37
0.06	0.76	21.09	174.29	3.7	7.3	-3.44 ± 0.02	-3.30

a: ozone is expressed as oxygen equivalents.

The photochemical equilibrium point equation (4.6) was also used to simulate previous studies. The calculated slopes agrees well with the previous measurements of CO_2 enrichments observed during the isotope exchange reaction between CO_2 and O_2 [Johnston et al. 2000] and exchange reaction between CO_2 and O_3 [Wen and Thiemens, 1993] as shown in Table 4.5. However our calculation method based on photochemical equilibrium point could not reproduce the finding of Chakraborty and Bhattacharya [2003].

Table 4.5: Application of photochemical equilibrium method to previous studies on the isotope exchange reaction between CO_2 and O_3.

	Initial CO_2		***Initial O_2 or O_3***		***CO_2 slope***	
	$\delta^{17}O$	$\delta^{18}O$	$\delta^{17}O$	$\delta^{18}O$	Experiment	Calculated
(Johnston et al. 2000)[a]	5.7	11	8.3	16	0.96	0.98
(W and T 1993)[b]	1.27	5.27	22.9	44.4	0.99	0.94
(C and B 2003)[c]	20.4	39.3	106	125	1.8	1.00
	2.2	4.1	106	125	1.5	0.93
	-5.6	-10.9	106	125	1.3	0.91

a: experiments with mass dependently fractionated CO_2 and O_2 at room temperature using Oriel lamp.

b: Wen and Thiemens 1993, experiments with mass independently fractionated CO_2 and mass dependently fractionated O_3 at room temperature using Hg lamp.

c: Chakraborty and Bhattacharya 2003, experiments with mass dependently fractionated CO_2 and mass independently fractionated O_3 at room temperature using Hg resonance lamp.

Because of its general applicability, we can also apply equation (4.6) to the stratosphere, using isotopic compositions of tropospheric CO_2 and O_2. Using photochemical equilibrium results for CO_2-O_2 system we obtained $\delta^{17}O$-$\delta^{18}O$ slope of ~ 1.07 for stratospheric CO_2 as shown in Figure 4.6. Briefly, implication of our photochemical equilibrium point to the atmospheric conditions does not reproduce the stratospheric $\delta^{17}O$/ $\delta^{18}O$ slope of 1.7. This results clearly indicate that in order to understand the atmospheric data as well as to get a complete insight into the exchange mechanism, other parameters need to be addressed which may include temperature, pressure and photolysis wavelength. Furthermore, isotopic fractionation in the quenching of $O(^1D)$ with other gases(e.g. N_2 which constitute ~78% of the atmosphere) may alter the isotopic composition of $O(^1D)$ that is available for reaction with CO_2. These parameters are investigated in the next chapter.

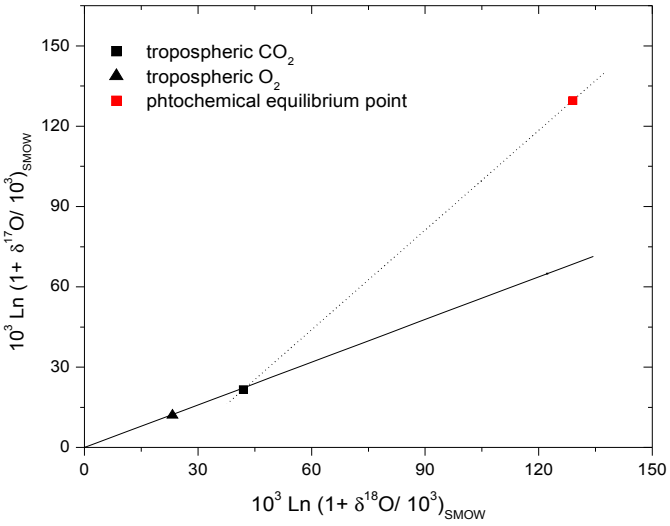

Figure 4.6: Extrapolation of photochemical equilibrium point obtained at room temperature to atmospheric CO_2 and O_2. Solid line indicates terrestrial mass dependent fractionation line with $\delta^{17}O/\delta^{18}O$ ~0.52 , dashed line is extrapolation for stratospheric CO_2 with $\delta^{17}O/\delta^{18}O$ ~1.07.

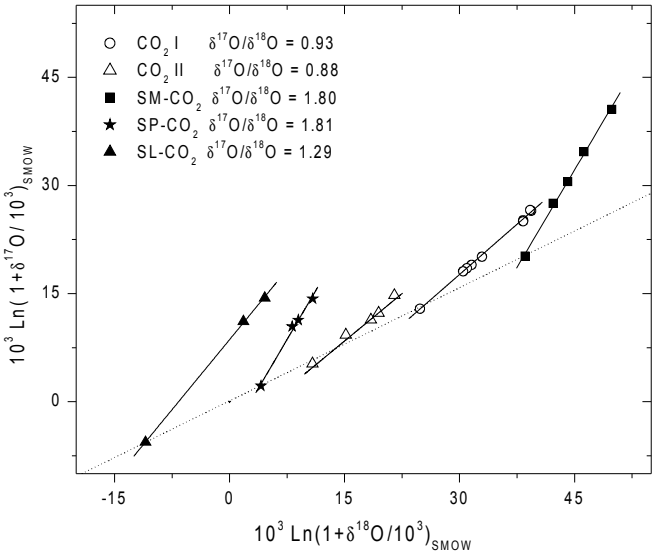

Figure 4.7: Comparison of anomalous CO_2 development after interaction with $O(^1D)$ in O_3/CO_2 mixture (~ 8 ratio) with other investigations. Open symbols denotes present work and closed symbols denotes the work from Chakraborty and Bhattacharya [2003].

Due to the significant differences in the calculated slopes based on photochemical equilibrium

method and findings of Chakraborty and Bhattacharya [2003], we also tried to reproduce some of their experiments using two mass dependently fractionated laboratory standard CO_2 reference gases and O_3 produced with commercial O_3 generator. We adopted this approach because the anomalous CO_2 evolution from mass dependent CO_2 seems to be independent of initial O_3 in the light of our findings and previous laboratory results [Wen and Thiemens, 1993]. We used O_3/CO_2 ratio of 12 (in terms of O_2 equivalents) and irradiated the mixture with Oriel Hg-pen ray lamp for short interval ranging from 10 -35 minutes.

In the Figure 4.7. we have plotted their data points with O_3/CO_2 ratio ~ 8 and short irradiation times < 70 minutes on the 1000 Ln(1+δ^{i}O/1000) scale along with our results for two mass dependent CO_2 to enable the comparison on the same scale

It can be seen from Figure 4.7 that difference in $\delta^{18}O$ between CO_2 I and CO_2 II (our two lab standard CO_2 gases shown with open symbols) is ~14‰ and these two CO_2 evolve with slopes of 0.93 and 0.88 i.e. the slope increases by ~ 5% as we move from the light to the heavy CO_2. The relative difference in $\delta^{18}O$ of SP-CO_2 and SL-CO_2 is also ~15‰ but these two CO_2 evolve with quite different slopes of 1.81 and 1.29. This 28% increase in slope just by changing isotopic composition of initial CO_2 and using same O_3 could not be reproduced in our laboratory.

5 Temperature and Pressure Dependence of the Isotope Exchange Reaction

To date, all experimental studies of isotope exchange between O_3 and CO_2 via $O(^1D)$ have been carried out at room temperature only. In this chapter we report the temperature dependence (200K< T< 310K) of the enrichment in CO_2 at photochemical equilibrium. Additionally, experiments were conducted over a range of pressures between 60 and1000mb to investigate the effect of pressure on the exchange reaction as well as the effect of O2/CO2 ratios in the gas mixture. In order to study the effect of photolysis wavelength on the CO_2 and $O(^1D)$ isotope exchange reaction, some experiments conducted using a broad band light source,

5.1 Temperature effect

5.1.1 Blank experiments

Like the previous experiments at room temperature, blank experiments were carried out at low temperature as well to determine the error due to the handling and extraction procedure

(i) Mixtures of CO_2 and O_2 with similar ratios as used for the experiment were left in the reactor for ~2 hrs, extracted and analyzed isotopically.

(ii) Pure CO_2 (60 $\pm$ 10 μmoles) was left in the reactor at 200K and 248K with UV illumination for 72h.

The data indicated no significant fractionation during the extraction of CO_2 from the CO_2-O_2 mixture from the low temperature reactor exposed for short time to low temperatures. However, when CO_2 alone was irradiated for long times at low temperatures, data indicated a -0.15‰ and -0.2‰ change in $\delta^{13}C$ and $\delta^{18}O$ with prolonged irradiation time. Nevertheless, it should be kept in mind that the samples are completely characterized isotopically after the photolysis experiments and thus possible contaminating CO_2 is then also in photochemical isotope equilibrium.

5.1.2 Low temperature experiments with the Oriel lamp

Low temperature experiments were carried out at 200 $\pm$ 2K and 250 $\pm$ 2K (bath temperature, see discussion on actual reaction temperature below) to investigate the temperature dependence of isotope exchange between CO_2 and O_3. In these experiment the O_3/CO_2 ratio was kept constant 18 $\pm$ 2. As described in the experimental section, for the low temperature experiments the reactor was modified to fit into the cryostat. In order to account for the

change in geometry and to compare results at different temperatures, experiments at room temperature were also conducted with the same setup as used for low temperature experiments.

We present the data as enrichments in CO_2 vs O_2 i.e. $\delta^{17}O_{O2}$ (CO_2) and $\delta^{18}O_{O2}$ (CO_2) to characterize the photochemical equilibrium fractionation. This also facilitates comparison of the results between the CO_2-O_2 and CO_2-O_3 experiments. The results from first set of experiments carried out with the Oriel Hg-pen ray lamp are presented in Figure 5.1 which shows the complete measurement series in a three isotope plot. It is evident that the equilibrium enrichment decreases at low temperature. Maximum enrichment in CO_2 ($\delta^{17}O$ =135.2‰ and $\delta^{18}O$ =125.2‰) was observed at room temperature and minimum enrichment $\delta^{17}O$ =117‰ and $\delta^{18}O$ =96 ‰ in CO_2 was observed at 200 ± 2K. The figure also shows that the three-isotope slopes increase at low temperature. This is due to the fact that the temperature effect is larger for $\delta^{18}O$ than for $\delta^{17}O$.

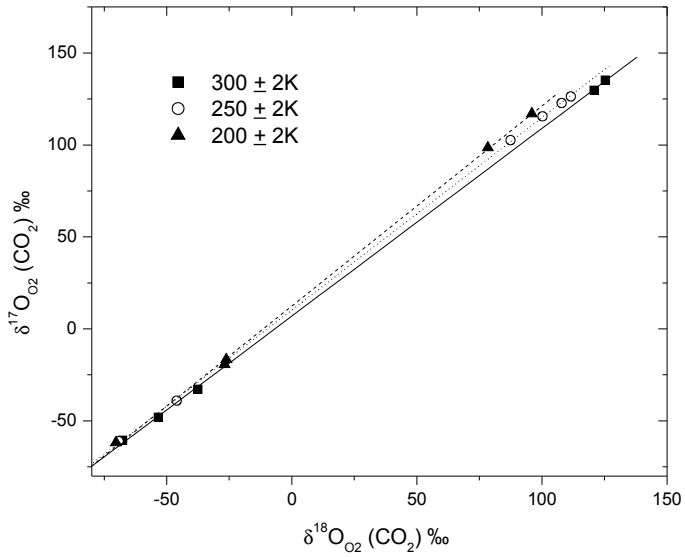

Figure 5.1: Effect of temperature on the enrichment in CO_2 in O_3/ CO_2 mixture (18 ± 2, P ~ 60-80 mb) irradiated with the Oriel pen ray lamp.

5.1.3 Low temperature experiments with the Puritech lamp

The Puritech lamp was employed for low temperature photochemical equilibrium "triangulation" experiments and all further room temperature photochemical isotopic

equilibrium experimentation, because it was observed during our photochemical equilibrium experiments at room temperature, that the Oriel lamp had a rather short life time. Moreover, the time required to reach photochemical equilibrium was ~ 3 times faster with the Puritech lamp as indicated by the decay constants (e-folding time) in Table 5.1. In order to avoid any ambiguity in the triangulation experiments, the effect of temperature on the CO_2- $O(^1D)$ isotope exchange experiments was monitored with the Puritech lamp too. In these experiments O_3/CO_2 ratio (18 $\pm$ 2 in terms of oxygen equivalents) was also kept constant and experiments were performed at room temperature and at 220K. The intensity of the Puritech lamp was ~3 times higher than the Oriel lamp, therefore, temperature in the finger as well on the reactor surface was monitored carefully. In the room temperature experiments the flow rate of nitrogen through the finger was ~ 60 $cm^3\ s^{-1}$ but still the temperature was quite high (312K) due to highly energetic UV photons and IR radiations. In the experiments conducted at low temperature (200K bath temperature, 220K gas temperature) the finger was kept cold by flushing with cold N_2 and further increasing the flow rate (~ 120 $cm^3\ s^{-1}$). The measurements show a similar temperature effect as obtained with the Oriel lamp i.e., higher enrichment at higher temperature as shown in Table 5.1.

Table 5.1: Effect of temperature and lamp type on the final enrichment in CO_2 in a mixture containing CO_2 and O_3 initially

Lamp	***Temperature (K)[a]***	***Ratio (O_3/CO_2)[b]***	***(CO_2 enrichment)[c]***			***(Time constant)[e]***	
			^{17}O (‰)	^{18}O (‰)	slope	^{17}O (min)	^{18}O (min)
Oriel	200	18.2 $\pm$ 0.6	113.9	95.9	(1.18)[d]	216 $\pm$ 16	201 $\pm$ 18
Oriel	250	19.2 $\pm$ 0.8	126.3	111.5	1.13	420 $\pm$ 30	431 $\pm$ 35
Oriel	300	20.1 $\pm$ 0.5	135.2	125.2	1.08	850 $\pm$ 24	845 $\pm$ 28
Puritech	220	16.8 $\pm$ 0.5	122.1	104.1	1.17	109 $\pm$ 11	113 $\pm$ 15
Puritech	310	16.5 $\pm$ 0.5	136.6	129.5	1.05	263 $\pm$ 20	256 $\pm$ 24

a: temperature is inferred from gas pressure. b: O_3 is expressed as O_2 equivalents; c: enrichment in CO_2 at photochemical equilibrium expressed versus O_2; d: error on the slope is <0.01; e: e-folding time.

The temperature dependence of the isotope equilibrium point in the exchange reaction between CO_2 and O_3 is shown in Figure 5.2. Overall the enrichment in CO_2 increases with temperature from 200 to 310K by 0.19‰ /K for ^{17}O and 0.28‰ /K for ^{18}O. The temperature dependency is stronger for ^{18}O compared to ^{17}O, which is in qualitative agreement with the

enrichment in the precursor molecule O_3. Also for O_3 formation, the temperature dependence for ^{18}O is stronger in comparison to ^{17}O as will be discussed in the discussion section.

Our data of CO_2 at photochemical equilibrium indicated that the decrease in CO_2 enrichment at lower temperatures is accompanied by a corresponding increase in slope. This is illustrated in Figure 5.3 where the three-isotope slope is plotted as a function of temperature. Data revealed an increase in the slope values by 0.00114/K or 0.114 for 100K decrease in temperature.

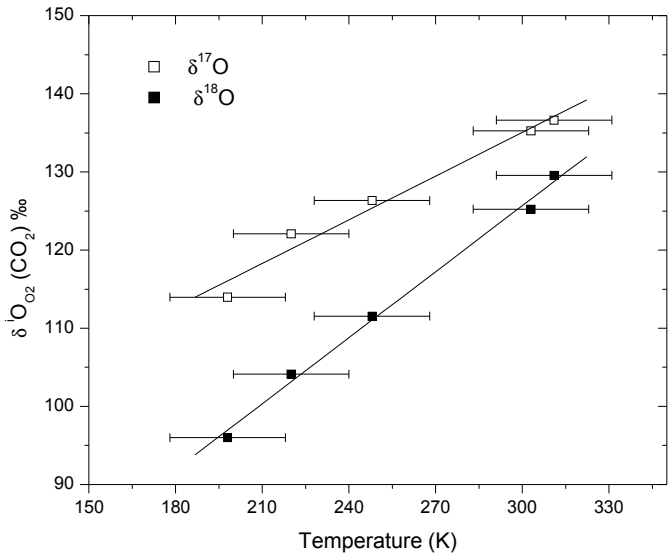

Figure 5.2: Enrichment in CO_2 at photochemical equilibrium as a function of temperature. The large error bars on the temperature are due to uncertainty of the reaction temperature for exchange reaction. Here ^{i}O: ^{17}O or ^{18}O.

Additionally with the Puritech lamp, the time evolution of the exchange process was monitored with high temporal resolution over the initial 60 minutes. Measurements showed that the O_3 exchange process proceeds faster at low temperatures, i.e. initially the enrichments in CO_2 is higher at low temperature in comparison to the room temperature experiments (Figure 5.4) . This is due to more ozone formation at low temperature, leading to faster isotope exchange. However, the enrichment in CO_2 at the photochemical equilibrium point was higher at higher temperature because enrichment in O_3 increases with temperature.

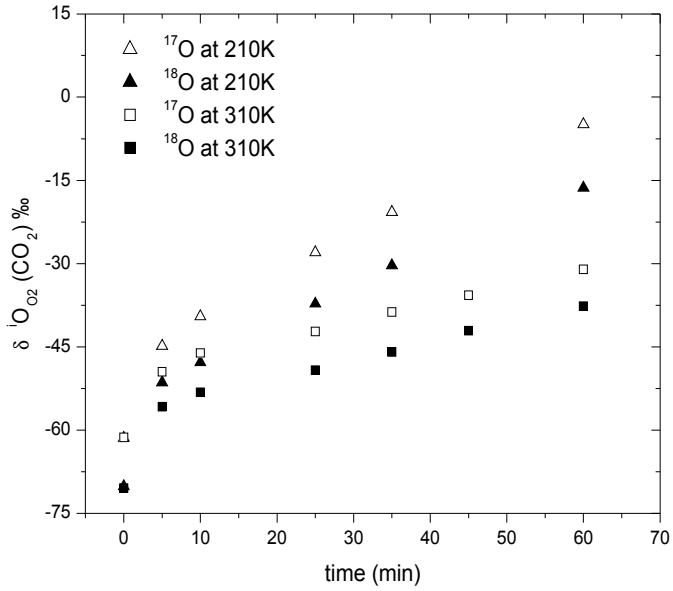

Figure 5.4: Effect of temperature on the initial enrichment in CO_2 in O_3/ CO_2 mixture (16 ± 1, P ~ 60 mb) irradiated with the Puritech lamp.

temperature for exchange reaction

5.2 Photochemical equilibrium (triangulation experiments) at low temperature

In order to simulate the conditions of relevance to the stratosphere, further experiments were conducted using triangulation method with O_2-CO_2 mixture (O_2/CO_2 = 550 ± 20) at a pressure of 250 ± 10mb and temperature of 220 ± 2 K (gas temperature only). The experimental approach is the same as that previously used to demonstrate that the CO_2 isotopic composition at photochemical equilibrium is independent of the initial CO_2 used. In these experiments O_3 was also collected through a specially designed cold trap (see sec.3.4) at the triple point of nitrogen (63K). This excludes artifacts from possible fractionation due to incomplete trapping of ozone [Krankowsky et al. 2003]. The isotopic composition of all three components, i.e CO_2, O_2 and O_3 was determined in this particular experiment in order to get a comprehensive view of the exchange mechanism. The amount of O_3 collected was 26 ± 3 μ moles. The isotopic composition of the different CO_2 gases and the O_2 used to measure the photochemical equilibrium at low temperature (220 ± 2K) using the triangulation approach are given in Table 5.2.

Table 5.2: Initial isotopic composition of various gases used to determine the photochemical equilibrium point at low temperature with the triangulation method (220 ± 2K).

	Initial Isotopic composition	
	$\delta\ ^{17}O_{SMOW}$ (‰)	$\delta\ ^{18}O_{SMOW}$ (‰)
CO_2 I	12.97 ± 0 .06	25.14 ± 0.03
CO_2 II	101.32 ± 0.06	53.94 ± 0.03
CO_2 III	20.24 ± 0.06	165.73 ± 0.03
oxygen	13.59 ± 0.03	26.21 ± 0.02

The CO_2 at photochemical equilibrium has $\delta^{17}O$ =116‰ and $\delta^{18}O$ =102‰ which is 14‰ less in ^{17}O and 26‰ less in ^{18}O than the photochemical equilibrium point determined at room temperature with O_2-CO_2 mixture using the triangulation approach. These findings are in qualitative agreement with the previous experiments conducted with O_3 and CO_2 mixture, which also indicated lower enrichment at lower temperature Figure 5.1 and Figure 5.2. The CO_2 at photochemical equilibrium in CO_2-O_3 mixture (P =60 ± 10mb, O_2/CO_2 = 18 ± 2) irradiated with the Puritech lamp at 220 ± 2K (gas temperature) has $\delta^{17}O$ =122‰ and $\delta^{18}O$ =104‰ which is 5‰ less in ^{17}O and 2‰ less in ^{18}O than the triangulation experiment conducted with CO_2-O_2 mixture at pressure of 250 ± 10mb and O_2/CO_2 = 550 ± 20. The small discrepancy in final equilibrium values are due to pressure and ratio effect. It will be discussed in next section that total pressure and O_2/CO_2 ratios in the reactor also determine the enrichment in CO_2 at photochemical equilibrium.

The CO_2 at photochemical equilibrium is enriched in comparison to the total O_3 at photochemical equilibrium as shown in Figure 5.5. For these experiments, the intramolecular oxygen isotope distribution of ozone at photochemical equilibrium was also measured by tunable diode laser absorption spectroscopic technique [Tuzson, 2005] which can distinguish the symmetric and asymmetric isotopomers. These measurements showed that asymmetric ozone has a higher enrichment ($\delta^{17}O$ =131 ‰ and $\delta^{18}O$ =135 ‰) in comparison to total O_3 ($\delta^{17}O$ =89 ‰ and $\delta^{18}O$ =90 ‰), both measured with respect to final O_2. This implies that heavy isotope enrichment is almost exclusively concentrated in the terminal atoms of O_3. The combination of both results yields important information about the exchange process through the CO_3^* intermediate. The line connecting asymmetric O_3 and equilibrium CO_2 has a normal mass dependent relationship with $\delta^{17}O/\ \delta^{18}O \sim 0.51$.

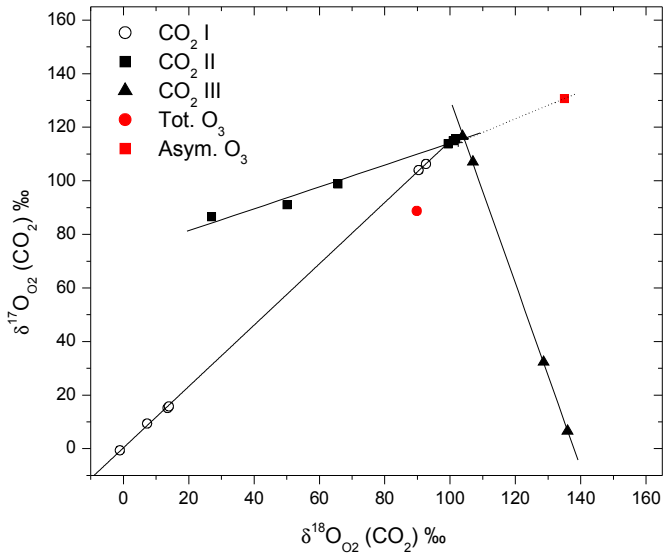

Figure 5.5: Photochemical equilibrium point of CO_2 at 220 ± 2K using CO_2/O_2 = 500 + 20. The mixture was irradiated with the Puritech lamp.

Table 5.3: Comparison of three-isotope slopes of various CO_2 gases used to measure the photochemical equilibrium point at low temperature (220 ± 2K) and at room temperature (300 ± 2K).

	Slopes	
	(220 ± 2K)[a]	(300 ± 2K)[b]
CO_2 I	1.14 ± 0 .006	1.04 ± 0.007
CO_2 II	0.41 ± 0.03	0.42 ± 0.03
CO_2 III	-3.63 ± 0.03	-3.44 ± 0.02

a: initial O_2 used ($\delta^{17}O$ =13.6 ‰ and $\delta^{18}O$ =26.2 ‰) vs SMOW. The errors in temperature indicates uncertainty in the gas temperature only.

b: initial O_2 used ($\delta^{17}O$ =3.7 ‰ and $\delta^{18}O$ =7.36 ‰) vs SMOW. The errors in temperature indicates uncertainty in the gas temperature only.

These measurements showed that the CO_2 slopes at two different temperatures using triangulation method are slightly different (Table 5.3). Since the temperature effect goes approximately in the the direction of the three-isotope slope for CO_2 II, there is almost no effect on the slope. The three-isotope slope for CO_2 III, however is almost perpendicular to the temperature shift, thus temperature has a large effect on the slope there. Similarly for CO_2 I the significant increase in slope is due to strong temperature effects for ^{18}O than ^{17}O.

5.3 Enrichment in CO_2 as a function of pressure and O_2/CO_2 ratio

Several series of experiments were carried out with different O_2/CO_2 ratios and at various pressures to assess the effect of ratio and pressure on the enrichment in CO_2. These experiments were conducted in a small reactor at room temperature using the Puritech lamp. In these experiments the time of illumination was sufficiently long (~ 6 days) so that the system was in photochemical and isotope equilibrium. In order to quantify the effect of pressure or O_2/CO_2 ratio on the time constants of the exchange process and enrichment in CO_2, an exponential fit was applied to each data series.

$\delta = \delta_{eq} - (\delta_{eq} - \delta_0) \exp((-t)/t_e)$

Here δ_{eq} is the equilibrium enrichment in CO_2 and t_e is the e-folding time of the reaction. δ_0 = is the initial ^{17}O or ^{18}O isotopic composition of CO_2 and t is the reaction time.

The results obtained are summarized in Table 5.4. There do, however, appear to be the real differences regarding the lamp intensity. It is evident from the e-folding times of experiment 115 and 116 that the Puritech lamp is ~ 3 times faster than the Oriel lamp.

Table 5.4: Summery of the enrichment in CO_2 and e-folding times (t_e) obtained at various O_2/CO_2 ratios and pressures with different lamps at room temperature.

Exp. No	***Ratios*** O_2/CO_2	***Tot. Pr.*** ***(mb)***	$(^{17}O)^g$		$(^{18}O)^g$	
			δ (‰)	t_e	δ(‰)	t_e
(115-SR)[a]	12	80	131 ± 2	824 ± 48	122 ± 2	825 ± 46
(116-SR)[b]	12	80	138 ± 1	269 ± 12	133 ± 1	266 ± 14
(117-SR)[b]	31	190	138 ± 3	244 ± 29	136 ± 3	258 ± 29
(118-SR)[b]	36	81	144 ± 1	289 ± 18	140 ± 2	287 ± 40
(130-SR)[b]	100	580	117 ± 2	343 ± 16	127 ± 2	376 ± 20
(131-SR)[b]	190	1000	109 ± 1	488 ± 36	123 ± 2	498 ± 48
(132-SR)[b]	700	520	122 ± 3	257 ± 51	129 ± 2	246 ± 38
(136-SR)[c]	22	990	84 ± 2	860 ± 73	87 ± 2	881 ± 76
(137-SR)[d]	62	270	130 ± 2	857 ± 77	131 ± 2	855 ± 109
(123-MR)[e]	84	270	46 ± 3	257 ± 54	48 ± 4	248 ± 60
(135-NR)[f]	44	280	118 ± 11	1400 ± 261	106 ± 8	1370 ± 213

a: experiment with the Oriel Hg pen- ray lamp in a small reactor ($250cm^3$).

b: experiments with the Puritech lamp in small reactor.

c: experiments with CO_2-O_2 and N_2 in small reactor using the Puritech lamp.

d: experiments with CO_2-O_2 and N_2O in the reaction mixture in small reactor using the Puritech lamp.

e: experiments with the Puritech lamp in a medium reactor (510cm^3) especially designed to fit in the cryostat.

f : experiments with Sb-lamp in a specially designed longer reactor (450cm^3).

g: isotopic compositions of CO_2 are expressed with respect to O_2.

If we plot the enrichment in CO_2 as a function of pressure, the data clearly show an inverse relationship between equilibrium enrichment in CO_2 and total pressure. The enrichment decreases by 0.04‰ /mb for ^{17}O and 0.02‰ /mb for ^{18}O and indeed there is a crossover point between ^{17}O and ^{18}O enrichments. Enrichments below 200mb are higher for ^{17}O whereas at pressure above 400mb the enrichments for ^{18}O are higher as shown in Figure 5.6. Additionally, data indicated that magnitude of enrichment in CO_2 also depends on the O_2/CO_2 ratios. The maximum enrichment ($\delta^{17}O$ =144‰ and $\delta^{18}O$ =140‰) was observed at 80mb with O_2/CO_2 ratio of 31 and it decreases by ~ 8‰ at a ratio of 12 ($\delta^{17}O$ =138‰ and $\delta^{18}O$ =133‰). This indicates that the enrichment decreases at photochemical equilibrium with increase in O_2/CO_2 ratio.

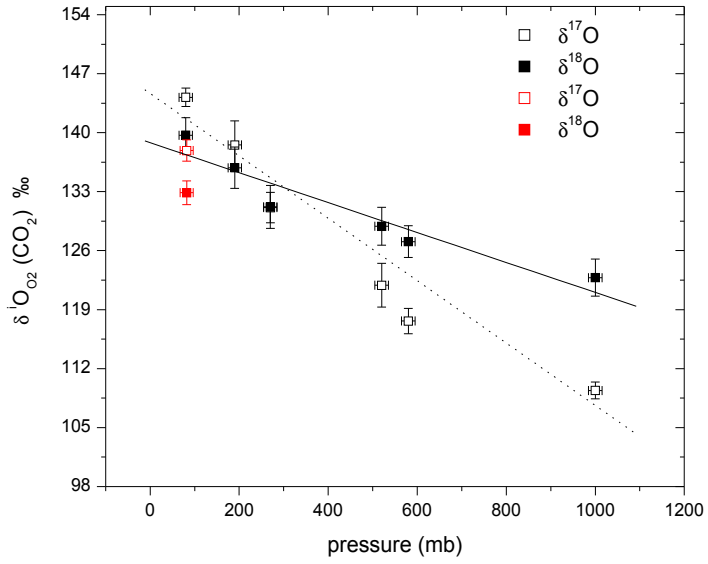

Figure 5.6: Effect of pressure on the enrichment in CO_2 in the CO_2-O_2 mixture irradiated with the Puritech lamp at room temperature. The enrichments are equilibrium values obtained from the exponential fit. For comparison, modeled asymmetric O_3 is also given. Here $^iO = ^{17}O$ or ^{18}O.

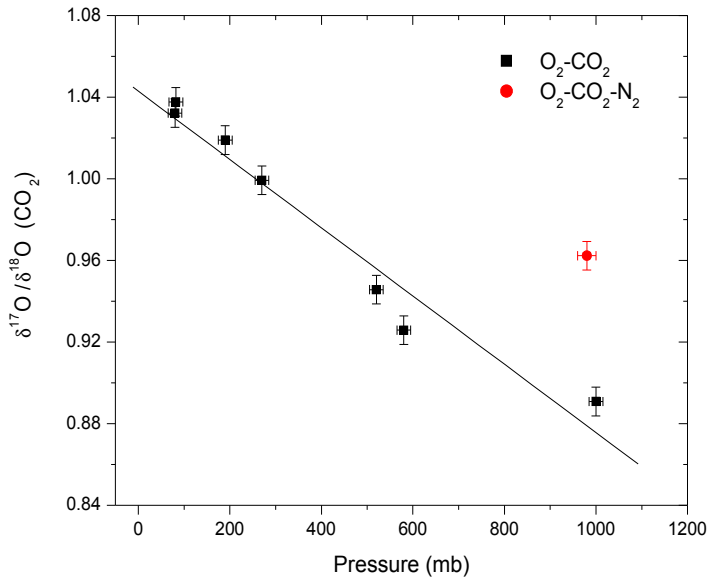

Figure 5.7: Effect of pressure on the slope of CO_2 in O_2-CO_2 mixture irradiated with the the Puritech lamp.

A plot of the three-isotope slopes CO_2 versus pressure presented in Figure 5.7 shows that the slope of CO_2 ($\delta^{17}O/\delta^{18}O$) decreases by 0.0167 with every 100mb rise in pressure as shown in However the experiment with O_2-CO_2-N_2 has a significantly higher slope in comparison to the O_2-CO_2 mixture at the same pressure. Nonetheless, the CO_2 at photochemical equilibrium showed much less enrichment in O_2-CO_2-N_2 mixture. The effect of other gases on the photochemical equilibrium is presented in detail in the next section.

5.4 Effect of other gases on the CO_2-O_3 isotope exchange

5.4.1 Effect of N_2

Although our experimental data cover the pressure and temperature range of relevance to the stratosphere, the main constituent N_2 present in the atmosphere is missing in these experiments. In order to address this issue we conducted some experiments at room temperature with O_2/CO_2 ratio of ~22 (leading to ~ 170mb pressure) and adding up N_2 to a total pressure of ~1 bar in the reactor. At photochemical equilibrium CO_2 is much less enriched ($\delta^{17}O$ = 85‰ and $\delta^{18}O$ = 89‰) as shown in Figure 5.8.

These results can be understood quantitatively if we take into account the fact that enrichment in O_3 is pressure dependent and at 1 bar pressure the enrichment decreases significantly. Nevertheless. if we compare this experiment with experiment 131 where total pressure is 1bar

and O_2/CO_2 ratio is 190 the CO_2 at photochemical equilibrium has $\delta^{17}O$ =144‰ and $\delta^{18}O$ = 141‰. This indicates that quenching with N_2 may be different in comparison to O_2 because O_3 formation rates are similar for N_2 and O_2 and also the enrichments in O_3 are unaffected by bath gases [Güenther et al. 2000].

The O_3 produced during these exchange reaction had a slope 0.96 $\pm$ 0.04 (Table 5.5). Additionally, higher pressure with N_2 leads to an increased time for the system to reach the steady state as can be judged from the ~1.7 times higher e-folding times (t_e for ^{17}O = 860 $\pm$ 73 min and t_e for ^{18}O = 881$\pm$ 76 min) in comparison to exp 131 (t_e for ^{17}O = 488 $\pm$ 36 min and t_e for ^{18}O = 498 $\pm$ 48 min). This can be explained because the total amount of O_3 available for O (^1D) formation is higher in experiment 131 than in experiment 136.

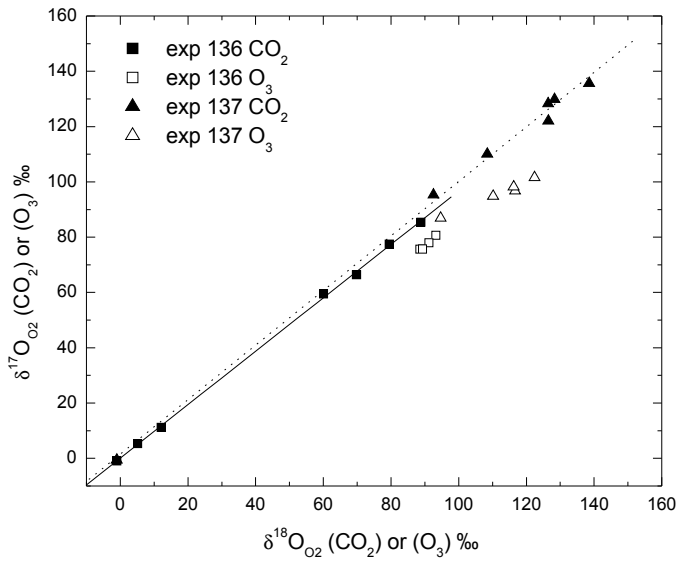

Figure 5.8: Enrichment in CO_2 under various experimental setups. Exp. 136, CO_2 -O_2 -N_2 mixture irradiated with the Puritech lamp. Exp. 137, CO_2-O_2 -N_2O mixture irradiated with the Puritech lamp.

5.4.2 Effect of N_2O

Some experiments were conducted at room temperature by adding various amounts of N_2O to the O_2-CO_2 mixture (0.01- 29 μmoles) keeping pressure and O_2/CO_2 ratios nearly constant (P ~ 270 mb, O_2/CO_2 ~ 65 $\pm$ 5). The N_2O was added in these experiments because N_2O photolysis not only yields O(^1D) in the stratosphere but O(^1D) also react with N_2O to produce

NO. The role of NO in the catalytic destruction of O_3 by the NO_x family is well known phenomenon [Brasseur and Solomon1986] and could affect the results.

The CO_2 at photochemical equilibrium had $\delta^{17}O$ =136‰ and $\delta^{18}O$ = 139‰. The enrichment in CO_2 in this setup defines $\delta^{17}O/\ \delta^{18}O = 0.98 \pm 0.03$ (Table 5.5). Thus, the final equilibrium point does not seem to be much affected by the presence of N_2O/NO_x. Nevertheless, a notable exception in the experiments with N_2O is that O_3 collected showed a mass dependent relationship. The amount of O_3 collected was much less (~2.5 μ moles), probably due to reaction of O_3 with NO_x but still all five O_3 data points clearly define this relation ($\delta^{17}O = 0.5\delta^{18}O$) as shown in Figure 5.8. On the other hand, the overall enrichment of O_3 is not very much affected, and thus also not the enrichment in CO_2.

Table 5.5: Effect of wavelength and other constituents present in the mixture (N_2 and N_2O) on the isotope exchange reaction between CO_2 and O_3.

Exp. No.	***Components***	***Ratio*** ***(O_2/CO_2)***	***Pressure*** ***(mb)***	***CO_2*** ($\delta^{17}O/\ \delta^{18}O$)	***O_3*** ($\delta^{17}O/\ \delta^{18}O$)
135	$(O_2\text{-}CO_2)^a$	44 ± 1	270 ± 5	1.11 ± 0.01	-
136	$(O_2\text{-}CO_2\text{-}N_2)^b$	22 ± 1	980 ± 10	0.96 ± 0.01	0.96 + 0.04
137	$(O_2\text{-}CO_2\text{-}N_2O)^b$	65 ± 5	270 ± 5	0.98 ± 0.03	0.51 ± 0.05

a: experiments conducted with Sb- broad band lamp.

b: experiments conducted with the Puritech lamp (line source).

A notable exception in the experiments with N_2O is that O_3 collected showed a mass dependent relationship, although the O_3 collected was much less (~2.5 μ moles) but still all five O_3 data points clearly define this relation ($\delta^{17}O = 0.5\delta^{18}O$) as shown in Figure 5.8.

5.5 Effect of photolysis wavelength

To get some information about the role of wavelength for the isotope exchange process, experiments were carried out with 1kW antimony lamp (Heraeus, Hanau) that had already been used to investigate the effect of wavelength for the N_2O photolysis [Röckmann et al. 2001, Kaiser et al. 2002]. The lamp features a continuous emission spectrum from 200-300 nm. The O_2-CO_2 mixture (P~ 270 mb, O_2/CO_2 ~45) was irradiated from 15 minutes to a maximum of about 48 hours. Longer irradiation times were avoided due to excessive heating of the Sb-lamp. Although steady state was not achieved in these experiments, the results still

indicate a higher three isotope slope towards photochemical equilibrium $\delta^{17}O = 1.11 \pm 0.007\delta^{18}O$ as shown in Figure 5.9 The exponential fit to the data predict $\delta^{17}O$ =118‰ and $\delta^{18}O$ = 106‰ at photochemical equilibrium. If we compare these findings with experiment 117 where pressure and ratios (P ~ 190mb, O_2/CO_2 ~ 36) are comparable, the CO_2 at photochemical equilibrium shows higher enrichment $\delta^{17}O$ =138‰ and $\delta^{18}O$ = 136‰ with a slope of 1.018 ± 0.01 in a three isotope-plot. Our data clearly indicates significant increase (~ 9%) in slope using the broad band light source.

We note here that reaction proceed very slowly (~ 6 times slower) in comparison to the Puritech lamp used in exp 117. The enrichments and e-folding times with total pressures and O_2/CO_2 ratios for these series of experiments are summarized in Table 5.4.

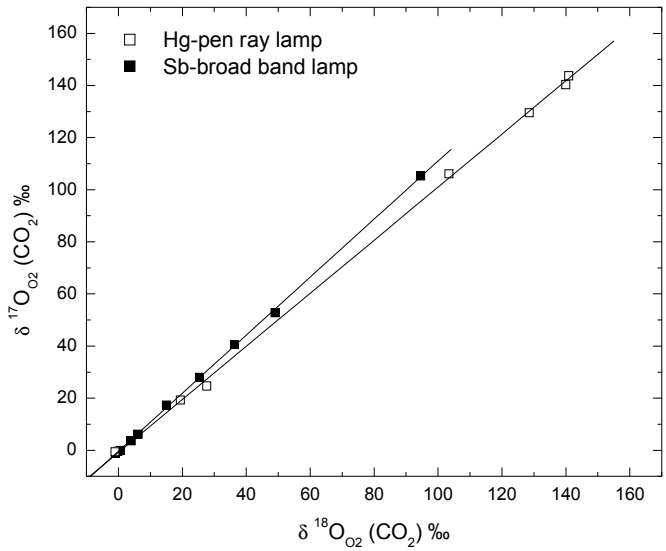

Figure 5.9: The enrichment in CO_2 using the Puritech lamp (photolysis with a line source) and a Sb-lamp (broad band photolysis).

5.6 Discussion

The effect of temperature on the CO_2 and O_3 isotopic exchange via $O(^1D)$ is investigated for the first time. The measurements showed that at lower temperature, the transfer of heavy oxygen to CO_2 is higher initially (Figure 5.4) , which is due to more O_3 amount available for $O(^1D)$ production as O_3 formation/dissociation is also temperature dependent. Our model predicts following concentrations of O_3 and $O(^1D)$ with the Puritech lamp for a typical O_2-CO_2 experiment with P ~ 70mb, O_2/CO_2 ~18 at two different temperatures (Table 5.6).

Table 5.6: Concentrations of O_3 and $O(^1D)$ obtained with numeric simulations for two different temperature of relevance to the experiments.

Temperature *(K)*	***O_2*** *(molecule.cm^{-3})*	***O_3*** *(molecule.cm^{-3})*	***$O(^1D)$*** *(molecule.cm^{-3})*
310 ± 15	1.47 x 10^{18}	6.32 x 10^{15}	8.31 x 10^{5}
220 ± 15	1.47 x 10^{18}	1.53 x 10^{16}	1.87 x 10^{6}

Importantly, our data sets with O_3/CO_2 of 18 ± 2 (O_3 expressed as oxygen equivalents) clearly indicate that enrichments at photochemical equilibrium decreases towards low temperature by -0.19‰ /K for ^{17}O and -0.28‰ /K with a concomitant increase in $\delta^{17}O/\ \delta^{18}O$ slopes (0.00114/K in the range of 200-310K) as shown in Figure 5.2 and Figure 5.3. Since the enrichment is transferred from asymmetric O_3 to CO_2, it is interesting to look at the temperature variations in the precursor molecule. In fact, lower enrichment in total O_3 at low temperature have already been reported [Morton et al., 1999]. The comparison of CO_2 enrichments at photochemical and isotope equilibrium at different temperature with the asymmetric O_3 calculated using model equation indicates at least qualitative agreement up till 250K but at higher temperatures (300-320K) the model predicts reverse trend and also higher enrichment in asymmetric O_3 but the enrichments observed in CO_2 are consistently lower (Figure 5.10).

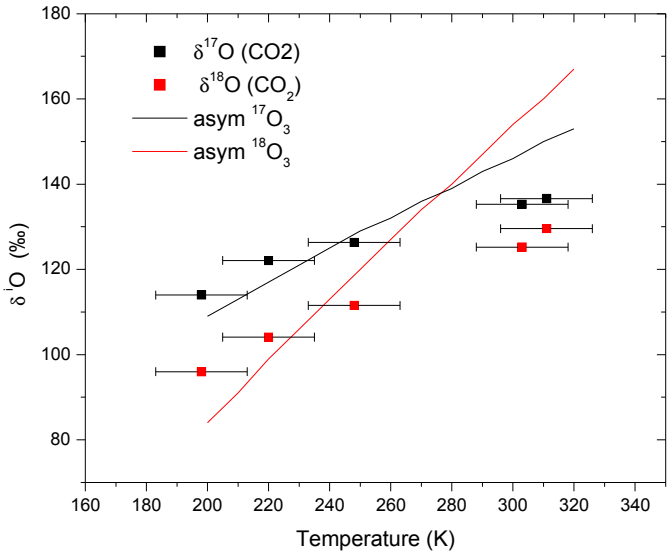

Figure 5.10: Effect of temperature on the enrichment in CO_2 at photochemical equilibrium and modeled values for asymmetric O_3 which is the source for the transfer of anomaly to CO_2.

The temperature dependence for the rate coefficients of $^{18}O_3$ formation has been well documented in the range 230-350K [Janssen et al. 2000], however the effect of temperature on the rate coefficients for $^{17}O_3$ formation is not known to date and they are derived based on certain assumptions [C. Janssen, personal communication]. The discrepancy between asymmetric O_3 and CO_2 could also be due to bias in assigning the temperature as we have used average gas temperature (deduced from pressure change in the reactor) and the actual reaction temperature for the O_3 formation could be different. This topic is dealt with detail in the chapter 7. The enrichments in CO_2 observed at 220 $\pm$ 15K and 200 $\pm$ 15K are slightly higher than asymmetric O_3. The most plausible reason to answer this dilemma leads to the postulations that in addition to temperature dependence of O_3 formation, photolysis fractionation could also be temperature dependent. To date no measurements are are available for the temperature dependent photolysis fractionation in O_3. Additionally the isotope exchange reaction of $O(^1D)$ with CO_2 could also be temperature dependent which may lead to even higher enrichments in CO_2. However, it has to be noted, that these are the first measurements of the enrichment in CO_2 as a function of temperature in the $CO_2 + O_3$ isotope exchange reactions via $O(^1D)$.

In view of the importance of the stratospheric CO_2 anomaly we adopted the photochemical and isotope equilibrium approach at low temperature also. The data reveal that CO_2 at

photochemical equilibrium (Figure 5.7) is more enriched than the total O_3. A simple look at this figure may lead to invoke the proposition that an additional enrichment in CO_2 may be the result of some fractionation in CO^*_3 complex or the $O(^1D)$ produced from this O_3 has higher enrichment. Wen and Thiemens [1993, Fig. 4] concluded from their experiments with anomalous CO_2 and mass dependently fractionated O_3 using a Hg-pen ray lamp for photolysis that additional isotope effects are caused by processes in CO^*_3 intermediate. In an attempt to model their laboratory results, Johnston et al. [2000] also attributed additional fractionation to CO^*_3 intermediate. Note that both the groups reported $\delta^{17}O/\ \delta^{18}O \sim 1$ in photolysis experiments starting with CO_2 and O_3 or O_2 in the lab frame at room temperature.

The important aspect of our measurements lies in the fact that we conducted these experiments at low temperatures and identified the contribution of asymmetric O_3 to the photolysis process for the first time. Calculations predicts that $O(^1D)$ is produced from the terminal O atoms during O_3 photolysis [Sheppard and Walker, 1983]. If this is the case our measurements clearly indicates that no additional mass independent fractionation is involved in the CO^*_3 intermediate because isotopic composition of asymmetric O_3 and CO_2 at photochemical equilibrium intersects with a well defined relation $\delta^{17}O = 0.5\delta^{18}O$. On the other hand, CO_2 at photochemical equilibrium has $\delta^{17}O$ =116‰ and $\delta^{18}O$ =102‰ in our low temperature experiments defining a relation $\delta^{17}O = 1.14\delta^{18}O$ which cannot reproduce stratospheric CO_2 observations [Lämmerzahl et al. 2002].

In order to get an insight about CO_2- O_3 isotopic exchange system as a function of pressure, enrichment in CO_2 were measured at different pressures and O_2/CO_2 ratios. The data indicate an inverse pressure dependence i.e. -0.04‰ /mb for ^{17}O and -0.02‰ /mb for ^{18}O in the pressure range of 80 to 1000mb. The pressure dependency of the enrichment in asymmetric O_3 derived from the model equation reproduce very well the equilibrium enrichment in CO_2 for ^{17}O as shown in Figure 5.11. However, compared to CO_2 the enrichments in ^{18}O of the asymmetric O_3 derived from the simple rate coefficients equation are higher for low pressure (pressure < 300mb) and lower at 1 bar pressure. Additionally, it predicts exactly an opposite $\delta^{17}O$ and $\delta^{18}O$ relation in the asymmetric O_3 in comparison to what has been observed in the CO_2 at photochemical and isotope equilibrium points. Note that the pressure dependency of the individual rate coefficients for asymmetric O_3 is not available but has been calculated based on informations available on two rate coefficients ($^{18}O + {}^{16}O^{16}O = {}^{18}O^{16}O^{16}O$, $^{16}O + {}^{18}O^{18}O = {}^{16}O^{18}O^{18}O$) and from the total enrichments of O_3 [Günther et al.1999, Morton et al.

1990]. Further information about asymmetric O_3 will soon become available [B. Tuzson and C. Janssen, personal communication] so that this question may be answered soon.

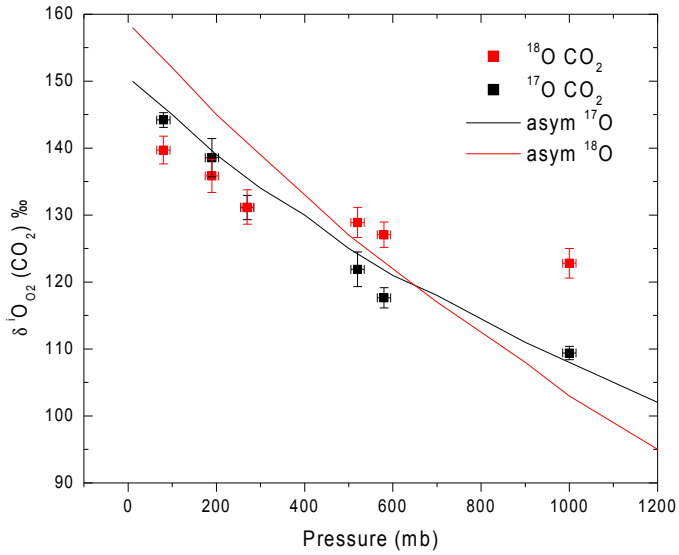

Figure 5.11: Effect of pressure on the enrichment in CO_2 at photochemical equilibrium and modeled values for asymmetric O_3 which is the source for the transfer of anomaly to CO_2.

Some additional experiments were conducted to study the effect of O_2/CO_2 ratio on the isotope exchange process by keeping the pressure constant. the data indicate higher enrichments in CO_2 at photochemical equilibrium with increasing ratio as shown in Figure 5.6 and Table 5.7.

We know from our low temperature "triangulation" photochemical equilibrium experiments that asymmetric O_3 has higher enrichments than CO_2 and thus $O(^1D)$ as $O(^1D)$ is most likely derived from asymmetric O_3 [Shepard and Walker, 1983]. Additionally our model predicts higher enrichments for $O(^1D)$ when collisional fractionation is included in the reaction scheme (for details see 7.3). The most reasonable argument about the low enrichment in $O(^1D)$ at photochemical equilibrium could be the possible contribution of $O(^1D)$ from less enriched CO_2 via non quenching exchange and thus diluting the enrichment in $O(^1D)$ at higher concentrations of CO_2 as in our experiment 116 where concentration of O_3/CO_2 at photochemical equilibrium is ~3 times higher in comparison to experiment 118. These

findings may indicate isotope exchange between CO_2 and $O(^1D)$ on a singlet surface as observed during recent cross molecular beam experiments [Perri et al. 2004].

Table 5.7: Enrichment in CO_2 at photochemical equilibrium at different O_2/CO_2 ratios. The mixture was irradiated with the Puritech lamp.

Exp. No.	***CO_2 (μmoles)***	***O_2 (μmoles)***	***Ratio***	***Pressure (mb)***	***$(\delta\ ^{17}O)^a$*** (‰)	***$(\delta\ ^{18}O)_a$*** (‰)
116	65.5	814	12	81 $\pm$ 2	138	(133
118	24.5	883	36	82 $\pm$ 2	144	141

a : enrichments in CO_2 are versus oxygen

In order to grasp some additional information about the nature of $O(^1D)$ quenching in the CO_2 and O_3 isotope exchange reaction and to address other processes of relevance in $O(^1D)$ production, additional experiments with N_2 and N_2O in the reaction mixtures were conducted. Our data with N_2 indicates the pressure effects associated with O_3 formation [Morton et al., 1999] as O_3 at photochemical equilibrium had lower enrichment ($\delta^{17}O$ = 76‰ and $\delta^{18}O$ = 89‰). Hence, CO_2 at photochemical equilibrium also showed lower enrichment ($\delta^{17}O$ = 85‰ and $\delta^{18}O$ = 89‰). However, if we compare this experiment with experiment 131 with total pressure of 1bar with O_2, data revealed 22‰ less enrichment in $\delta^{17}O$ and 31‰ in $\delta^{18}O$ in the CO_2 at photochemical equilibrium. Thus the pressure effect in the experiments with N_2 is much more pronounced than when only oxygen is present. One possibility to explain this observation is that collisional quenching of $^{18}O(^1D)$ with N_2 is stronger thus leaving the $O(^1D)$ reservoir enriched in ^{17}O to react with CO_2. This effect is quite evident in Figure 5.7 where slope ($\delta^{17}O/\ \delta^{18}O$) of CO_2 is plotted against pressure. We also suspected the presence of NO_x in the reaction mixture, which could affect the O_3 isotopic composition. However this could be dismissed because the primary fate of $O(^1D)$ is quenching with N_2 as is evident from higher rate coefficient.

$O(^1D) + N_2 \rightarrow O(^3P) + N_2$ $\quad [k = 2.7 \times 10^{-11}\ cm^3.molec^{-1}.s^{-1}]$ (R5.1)

$O(^1D) + N_2 \rightarrow N_2O$ $\quad [k = 2.68 \times 10^{-37} cm^6.molec^{-2}.s^{-1}]$ (R5.2)

The second reaction being slower and owing to less number density of excited oxygen atoms ($O(^1D) \sim 2.02 \times 10^6$ molec.cm^{-3}) leads to negligible contribution ($N_2O \sim 1.37 \times 10^{-11}$ molec. cm^{-3}, the precursor of NO). Secondly no indications for NO_x was found in the reaction mixture as m/z 30 was measured in each CO_2 sample (for details see sec. 3.7).

Additionally, as $O(^1D)$ is quenched effectively at higher pressure with bath gases, the time

required for the photochemical equilibrium becomes longer (e-folding time = 870 ± 60 min) as shown in the time constant of the various exponential fits of the chemical kinetics data in Table 5.7.

In experiments where N_2O is used additionally (exp 137), most of the N_2O is destroyed by photolysis with UV light (λ ~182 nm)

$N_2O + h\nu \rightarrow N_2 + O(^1D)$ (R5.3)

$N_2O + O(^1D) \rightarrow N_2 + O_2$ [$k = 4.9 \times 10^{-11}$ molec.cm^{-3}.s^{-1}] (R5.4)

$N_2O + O(^1D) \rightarrow NO + NO$ [$k = 6.7 \times 10^{-11}$ molec.cm^{-3}.s^{-1}] (R5.5)

Reaction (R5.3) accounts for ~ 90% of photochemical N_2O destruction. The other 10% loss of N_2O is via (R5.4) and (R5.5). About 40% of the $N_2O + O(^1D)$ reaction proceed via (R5.4) and about 60% proceeds via (R5.5) [Minschwaner et al.1993, Cantrell et al. 1994].

The reaction (R5.5) leads to NO concentrations of 2.5×10^{12} molec.cm^{-3} which is quite significant and it reacts with odd oxygen species [Brasseurs and Solomon et al. 1986]

$NO + O_3 \rightarrow NO_2 + O_2$ (R5.6)

$NO_2 + O \rightarrow NO + O_2$ (R5.7)

Examination of the data reveals that O_3 shows a three-isotope slope of about 0.5 in these experiments as shown in Figure 5.8. These results support some of the O_3 observations made in Pasadena with high NO_x concentrations [Johnston and Thiemens 1997]. Their four data points define a three isotope slope ($\delta^{17}O/\delta^{18}O$) of 0.54 for O_3 collected in this area. However, the O_3 samples at Pasadena showed much less enrichments ($\delta^{17}O = 66 \pm 6$ and $\delta^{18}O = 86 \pm 6$) than ours ($\delta^{17}O = 106 \pm 6$ and $\delta^{18}O = 140 \pm 6$). Nevertheless, these higher enrichments in our lab experiments are due to lower pressure (270mb) as the enrichment in O_3 is pressure dependent [Morton et al., 1990] and secondly due to additional fractionation in UV photolysis of O_3 [Wen and Thiemens, 1991, Bhattacharya et al., 2002] which favors further enrichment in left over O_3. Although O_3 is destroyed photochemically by NO_x reactions, the data indicate that it do not affect the CO_2 slope significantly (0.98 ± 0.03) except that CO_2 at photochemical equilibrium is 10‰ less enriched in ^{17}O and 15‰ less enriched in ^{18}O in comparison to normal O_2-CO_2 photolysis experiments at comparable pressure and ratio (exp. 117 with $O_2/CO_2 = 31$ and P = 200mb).

The experiments with Sb-lamp resulted in a slope of 1.11 ± 0.01. Although the photochemical equilibrium was not achieved in these experiments but we can infer from the

available data that broad band light source significantly affects the enrichment in CO_2 towards photochemical equilibrium. It also indicates that in the atmosphere the photolysis fractionation at the $\lambda < 310$ nm may lead to additional enrichments. Overall, our measurements at different temperatures and pressures show that low temperature, pressure and the photolysis wavelength all contribute to the observed enrichment [Lämmerzahl et al. 2002] in the stratospheric CO_2.

6 Stratospheric Carbon Dioxide

The anomalous oxygen isotope enrichment in stratospheric CO_2 has been investigated in several studies [e.g. Thiemens et al.1995, Zipf and Erdmann 1994, Lämmerzahl et al. 2002, Boering et al., 2004]. Nevertheless, the number of data points is still limited due to the difficulties in performing high precision $\delta^{17}O$ measurements on stratospheric CO_2 samples. During the present study, further stratospheric air samples became available from a balloon-borne cryogenic multi sampling system [Schmidt et al. 1987] and an automated whole air sampler mounted on the high altitude aircraft Geophysica, during the EUPLEX (European Polar Leewave Experiment) campaign. Details of sampling date, altitude, longitude and latitude along with potential temperature of the samples presented below are given in Appendix I.

6.1 Long term stability of the extraction system

CO_2 was cryogenically separated from the air samples and analyzed immediately after extraction using the extraction system described in chapter 3. After extraction, measurement of the oxygen isotope anomaly was carried out by two independent measurements on the CO_2 before and after complete oxygen isotope exchange with CeO_2 (see section 3.1). Due to isobaric interferences between CO_2 and N_2O for m/z 44,45,46, a N_2O correction was applied to the stratospheric air samples (as well as to laboratory reference air) based on the N_2O concentration that was also measured on those samples. The reproducibility of the entire system includes extraction, measurement and isotope exchange procedures. Since many improvements were made to our analytical system over the years during these measurements, here we discuss in detail the long term variations in CO_2 extraction from various air samples used as internal quality control in our lab.

As pointed out in the experimental section, before CO_2 extraction from stratospheric air samples some conditioning of the extraction trap was required and the results presented below are from representative samples after the system had achieved the required reproducibility. Measurement results for pure CO_2 samples from our laboratory reference gas cylinder and CO_2 extracted from Schauinsland air (cylinder 2) after exchange with CeO_2 are given in Table 6.1. The delta values are presented on a linearized log natural scale and the anomaly is calculated as

$$\Delta^{17}O = 1000\mathrm{Ln}(1 + \delta^{17}O/1000) - 0.516 * 1000\mathrm{Ln}(1 + \delta^{18}O/1000)$$

The data indicate a standard deviation of ±0.2‰ in $\Delta^{17}O$ for pure CO_2 and ±0.4‰ for CO_2

extracted from Schauinsland air samples, both measured using the CeO_2 exchange method.

Table 6.1: Long-term stability of the isotope results for working standard CO_2 and CO_2 extracted from Schauinsland air (cylinder B, i.e.,SLB) after exchange withCeO_2 method.

Sample	***Working standard CO_2***			***Sample***	***CO_2 extracted from air samples***		
No.	$(\delta^{17}O)^a$	$(\delta^{18}O)^a$	$\Delta^{17}O$	***No.***	$(\delta^{17}O)^a$	$(\delta^{18}O)^a$	$\Delta^{17}O$
46	12.47	24.83	-0.34	SLB-2	18.80	35.25	0.61
52	12.51	24.88	-0.32	SLB-3	18.73	35.19	0.57
57	12.54	24.82	-0.26	SLB-4	18.84	35.23	0.66
59	12.42	24.83	-0.39	SLB-5	18.53	34.76	0.59
62	12.51	24.79	-0.27	SLB-7	18.36	35.17	0.14
65	12.87	25.06	-0.06	SLB-9	18.03	35.28	-0.17
69	12.52	24.84	-0.29	SLB-11	18.49	34.85	0.51
71	12.53	24.86	-0.30	SLB-14	17.78	34.82	-0.20
79	13.01	24.83	0.20	SLB-15	17.81	35.02	-0.25
Average	12.59	24.86	-0.22	Average	18.37	35.06	0.27
SD	0.20	0.07	0.18	SD	0.41	0.20	0.39

a: delta values are presented as $1000Ln(1+\delta^{i}O/1000)$, here ^{i}O denotes ^{17}O or ^{18}O.

6.2 Evaluation of data quality

Despite the stability of the extraction system described above, the raw data reveal considerable differences between individual sets of samples, e.g., some balloon samples that had been sub-sampled from their original containers in 1999 and subsequently stored in 2L volume stainless steel flasks appear to have a significant systematic positive $\Delta^{17}O$ offset, and other samples from a more recent balloon flight revealed a smaller negative offset. Those $\Delta^{17}O$ offsets do not occur for individual samples, but for the entire data series. This includes in particular also the near-tropopause samples, which can easily be identified by their tropospheric N_2O values. Of course, an oxygen isotope anomaly at the tropopause is unrealistic and those deviations are thought to be artifacts arising most likely from sample storage or from the analytical procedure (although stability tests shown above indicate the absence of large systematic effects in extraction and analysis for our reference air sample). Nevertheless, the samples within individual data series look reasonable and therefore we have developed a correction method in which the apparent isotope anomaly at the tropopause for

each data series is subtracted from each point in the data series. This is realized by correlating measured $\delta^{17}O$ and $\delta^{18}O$ data versus the logarithm of the remaining N_2O fraction in the sample (i.e., $\ln(N_2O/N_2O_0)$; N_2O is the observed N_2O concentration and N_2O_0 the tropospheric entry value). For this, time and age corrected N_2O concentrations are used (Kaiser et al., manuscript in preparation). At $\ln(N_2O/N_2O_0)=1$ the correlation then yields the $\delta^{17}O$ and $\delta^{18}O$ isotopic composition of tropospheric CO_2 that is implied by each individual data series. Those intercepts are then adjusted to a common value which is taken as the intercept of the highest quality data series of stratospheric CO_2 presently available [Lämmerzahl et al. 2002] and the mass dependent fractionation line $\delta^{17}O = 0.52\ \delta^{18}O$. The result of this correction is that the individual data series have common $\delta^{17}O$ and $\delta^{18}O$ entry values near the tropopause, which are consistently determined for each data series by the $\delta^{17}O - \ln(N_2O/N_2O_0)$ and $\delta^{18}O - \ln(N_2O/N_2O_0)$ correlations of the entire data series. Thus this correction puts the results of the different data series on a common scale and removes the apparent offsets between them. Nevertheless, we note that this correction also removes possible natural variability, which is expected to be minor, though.

6.3 Stratospheric CO_2 samples

The stratospheric CO_2 samples are plotted on a linearized log natural scale in Figure 6.1. The data from Lämmerzahl et al. [2002] are also included in the figure to facilitate the comparison with previous measurements.

The stratospheric CO_2 samples obtained with the balloon samplers are divided into two sets as they were subject to two different correction procedures as described above: Samples from one balloon flight at high northern latitudes in 2003 (67 $\pm$1°N, 26 $\pm$ 1°E, balloon 40) and a mix of samples from various latitudes (5 tropical, 1 mid-latitude, 1 polar) that had been stored in electro-polished 2L flasks for the past 5 years (flasks). The aircraft samples obtained with the Geophyscia whole air sampler above northern Europe cover a smaller altitude range than the balloon samples (8 to 20 km), but larger latitude (65.6 to 80ºN) and longitude (9.1 to 48.8ºE) bands.

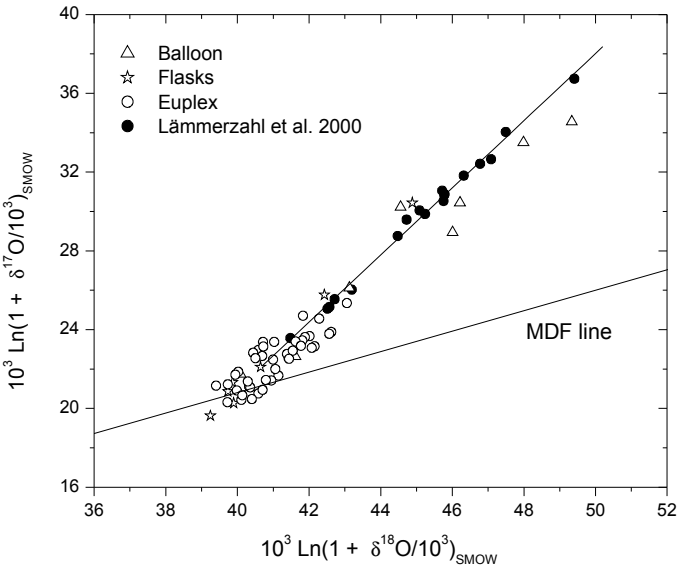

Figure 6.1: Stratospheric CO_2 samples obtained using balloon gondola(Balloon) and (Flasks) and whole air sampler mounted on Geophysica during EUPLEX-03 campaign. Data form Lämmerzahl et al. [2002] is included for comparison.

Figure 6.1 shows a good general agreement between the corrected data and the reference correlation from Lämmerzahl et al. [2002]. It is evident that the scatter in the present measurements is larger, which we attribute to the higher experimental error and partly sample alteration effects. A single correlation through the balloon samples yields a three-isotope slope of 1.5, i.e., less than the 1.7 reported by Lämmerzahl et al. [2002], but this may also be attributed to the large scatter. We note, however, that some of the highest enrichment samples collected during this flight were affected by a mesospheric intrusion. This may have an effect on the CO_2 isotope composition and could be a natural cause for the lower slope observed. However, this cannot be decided based on the samples presented here.

The aircraft samples show only smaller isotope enrichments because the samples were taken near the tropopause. These samples bridge the gap between the balloon samples from Lämmerzahl et al. [2002], which were all collected at higher altitudes, and the tropopause. The isotope data display a relatively high degree of scatter and a three-isotope slope of 1.2. This is much lower than the reported value of 1.7. The discrepancy could be due to several reasons. One of them is sample alteration in the canisters, as CO_2 was extracted about 2 years after sampling. As the sample canisters were received just before the campaign, and were used

the first time for air sampling in the EUPLEX project and could not follow a complete conditioning. However, they were thoroughly evacuated to 10^{-6} mb before sampling. Also, no leak was observed in canisters, i.e., after the long storage time the pressure in the flasks was not altered significantly. A second reason is natural variability. Near-tropopause samples are effected by mixing with tropospheric air, and the isotopic composition of CO_2 follows a clear seasonal cycle. Thus admixture from seasonally varying tropospheric CO_2 could contribute to the variability seen in the data and may also lead to a lower slope.

Nevertheless, since the Geophysica samples connect the balloon samples well with the inferred value of tropospheric CO_2 and given the over all size of scatter all fall close to the three-isotope line inferred from Figure 6.1, we conclude that the new data support the findings of Lämmerzahl et al. [2002]. This is further supported by comparing the results also to the high altitude aircraft results from Boering et al. [2004] (Figure 6.2). It is clear that the EUPLEX data extend the Lämmerzahl et al. [2002] data better than the measurements from Boering et al. [2004]. Note, however, that this is expected since the correction algorithm for our data has brought the two data sets to a common scale. However, we also note that the apparent scatter in the three-isotope plot seems to be less for the EUPLEX measurements in comparison to the results of Boering et al. [2004].

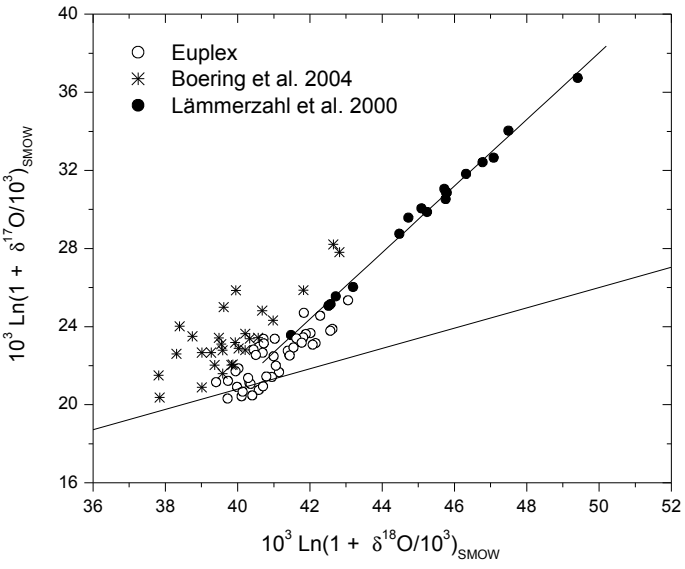

Figure 6.2: Comparison of low altitude samples obtained during Euplex-03 campaign with high altitude air craft data from Boering et al. [2004]. Data from Lämmerzahl et al. [2002] is included for comparison.

6.4 Discussion

The laboratory experiments help to understand the evolution of the CO_2 isotopic composition in the stratosphere. In the troposphere the isotopic composition of CO_2 is mainly determined by isotope exchange with water in leaf and soils [Ciais et al. 1997] and therefore, it has a normal mass dependent signature ($\delta^{17}O = 0.5\ \delta^{18}O$). As the air enters the stratosphere, the heavy isotope content increases with altitude due to the interaction of CO_2 with O_3 via $O(^1D)$. This way the isotope anomaly initially present in O_3 is transferred to CO_2. The enrichment increases further with residence time in the stratosphere and tends to drive the CO_2 towards photochemical equilibrium as has been demonstrated in the laboratory experiments in section 4. Therefore, the observed isotopic composition of CO_2 in the stratosphere represents the "photochemical age" of the CO_2 after it has entered the stratosphere. This may be used in photochemical models to investigate the coupling of transport and chemistry in the stratosphere, since the chemical interaction with O_3 leaves an isotope signature in CO_2 that is integrated over the entire journey of CO_2 through the stratosphere.

Our data indicated an increase in $\Delta\ ^{17}O_{CO2}$ with altitude. However, these measurements show a high degree of variability in $\Delta\ ^{17}O_{CO2}$. This is surprising given the very tight correlation as published by [Lämmerzahl et al. 2002] but those samples were generally obtained at higher altitudes, i.e., well within the stratosphere. Significant variability near the tropopause was also found by Boering et al. [2004]. This $\Delta\ ^{17}O_{CO2}$ variability could be due to the mixing of older air parcels with tropospheric air having low anomaly. Nevertheless, given the considerable scatter in our data also for the balloon samples, at the moment it also cannot be excluded that the scatter is an artifact, produced for example by alteration of the samples in the sample canisters.

As the $\Delta^{17}O_{CO2}$ derives from isotope exchange with O_3 via $O(^1D)$ the magnitude of anomaly can be used as an index of the degree of isotope exchange with $O(^1D)$. Older air will undergo more isotope exchange and will have a higher anomaly. Now that a large number of $\Delta^{17}O_{CO2}$ data are available, it will be interesting to compare $\Delta^{17}O_{CO2}$ to the age of air throughout the stratosphere. This will potentially enable to establish a link between photochemical age and actual age in the stratosphere, and thus provide a new parameter that connects stratospheric transport and chemistry. Furthermore, in regions where tracers like N_2O and CH_4 lose their dynamic range because they have been depleted to very low concentrations, the application of $\Delta^{17}O_{CO2}$ can be a useful tool to study the transport process as it has no sink in the stratosphere

[Alexander et al. 2001].

We have shown in section 6.5 that enrichment in CO_2 at photochemical equilibrium is closely related to asymmetric O_3 with $\delta^{17}O = 0.5\ \delta^{18}O$, therefore, it would be very interesting to have simultaneous measurements of asymmetric O_3 and CO_2 in the atmosphere. Assuming that asymmetric ozone and CO_2 at isotopic equilibrium are indeed related by a slope 0.5 line in the three-isotope plot, this will enable to determine the CO_2 equilibrium enrichment point in the atmosphere from the intersect of the three-isotope slope of stratospheric CO_2 and a slope 0.5 line through asymmetric ozone. Given the information that is now available about the equilibrium point from laboratory measurements, this can provide information about whether other processes in the atmosphere will affect the isotopic composition of stratospheric CO_2. From the measurements presented in this thesis, in particular on temperature, pressure and wavelength dependence of the exchange process, we have significantly advanced the understanding about the exchange process.

7 Photochemical Box Model

7.1 General description

In order to evaluate the laboratory experiments and to gain insight into the molecular level details of the isotope exchange mechanism between CO_2 and O_3 via $O(^1D)$, a photochemical box model was developed using FACSIMILE, a commercial software package designed for time evolution problems as they typically appear in chemical kinetics [Malleson et al. 1990]. The basic reaction scheme was adapted from Johnston et al. [2000] and is given in Table 7.1. There are twelve chemical reactions in the scheme but consideration of the isotopic species expands this list of reactions to a total number of 85. To simplify notation, Q represents ^{18}O and P represents ^{17}O. Multiply substituted species (such as OQP or CQP) were not included, to keep the number of reactions less and the model simple. The fact that not all possible isotopomers are considered introduces an offset in the calculated delta values. Heavy isotopes that would originally form multiply substituted molecules must end up as a singly substituted species in the model, because mass is conserved in the integration. In the model relative oxygen isotopic abundances (O = 0.99761, Q = 0.0020048, and P = 0.00038091) were used to calculate delta values [Hoefs 1997] , the offset due to neglect of the multiply substituted species is about 2 - 4 ‰. For some of the utilized reactor geometries, the photolysis rates of O_2 and O_3 ($J(O_2)$ and $J(O_3)$) have been determined experimentally (see section 3) For individual ozone formation channels a set of rate coefficients was derived from results of recent symmetry resolved isotope measurements [Tuzson 2005]. Their temperature and pressure dependencies were assumed in agreement with existing data on isotopologue and isotopomer enrichments and rate coefficients [Janssen et al. 2005, Morton 1990, Güenther 2000]. This approach was necessary, because the pressure and temperature dependence of individual rate coefficients is not known with enough precision. The temperature dependence of the isotope exchange reaction between O_2 and O was incorporated in the model [Anderson et al. 1985, Fleurat Lessard et al. 2003]. Due to the crucial role of the ozone isotopic composition, a detailed description of the derivation is presented in the next section.

For the reaction rate constants of isotopically substituted species, equal branching ratios are assumed for cases where two different isotopic products may derive from one reactant (e.g. R2b and R2c) since no information is available. The branching ratio between isoelectronic exchange and quenching for the $O(^1D)$ and CO_2 reaction were taken from the recent crossed molecular beam experiments [Perri et al. 2004]. The branching ratio for the photolysis of O_3

to the singlet and triplet products was assigned according to the recommendations of Atkinson et al. [1996] and DeMore et al. [1997]. According to theoretical predictions [Sheppard and Walker 1983], $O(^1D)$ is assumed to exclusively derive from the ozone end atoms. Isotope effects in these reactions are not known. In bimolecular reactions of excited species where no information about isotope fractionation is available, the isotope effects were assumed to be dependent on molecular collision frequencies that scale with the inverse square root of the reduced masses.

Table 7.1: Reaction scheme included in the one box model.

Reaction no.	***Reaction***	***Rate coefficient***
	O_2 photolysis	
R1a	$OO + h\nu \rightarrow O + O$	$k1a = 4.0 \times 10^{-6}$
R1b	$OQ + h\nu \rightarrow O + Q$	k1a
R1c	$OP + h\nu \rightarrow O + P$	k1a
	O_3 photolysis: singlet products	
R2a	$OOO + h\nu \rightarrow O(^1D) + OO(^1\Delta)$	$k2a = 0.9\ (1.0 \times 10^{-2})$
R2b	$OOQ + h\nu \rightarrow O(^1D) + OQ(^1\Delta)$	k2a /2
R2c	$OOQ + h\nu \rightarrow Q(^1D) + OO(^1\Delta)$	k2a /2
R2d	$OQO + h\nu \rightarrow O(^1D) + OQ(^1\Delta)$	k2a
R2e	$OOP + h\nu \rightarrow O(^1D) + OP(^1\Delta)$	k2a /2
R2f	$OOP + h\nu \rightarrow P(^1D) + OO(^1\Delta)$	k2a /2
R2g	$OPO + h\nu \rightarrow O(^1D) + OP(^1\Delta)$	k2a
	O_3 photolysis: triplet products	
R3a	$OOO + h\nu \rightarrow O(^3P) + OO$	$k3a = 0.1\ (1.0 \times 10^{-2})$
R3b	$OOQ + h\nu \rightarrow O(^3P) + OQ$	k3a /2
R3c	$OOQ + h\nu \rightarrow Q(^3P) + OO$	k3a /2
R3d	$OQO + h\nu \rightarrow O(^3P) + OQ$	k3a
R3e	$OOP + h\nu \rightarrow O(^3P) + OP$	k3a /2
R3f	$OOP + h\nu \rightarrow P(^3P) + OO$	k3a /2
R3g	$OPO + h\nu \rightarrow O(^3P) + OP$	k3a
	O_3 formation	
R4a	$O + OO + M \rightarrow OOO + M$	$k4a = 6.0 \times 10^{-34}(T/300)^{-2.5}$
R4b	$O + OQ + M \rightarrow OOO + M$	$(k4a /2)*(F4b)^a$
R4c	$O + OQ + M \rightarrow OOO + M$	$(k4a /2)*(F4c)^a$

Reaction no.	***Reaction***	***Rate coefficient***
R4d	$Q + OO + M \rightarrow OOO + M$	$(k4a)*(F4d)^a$
R4e	$O + OP + M \rightarrow OOO + M$	$(k4a/2)*(F4e)^a$
R4f	$O + OP + M \rightarrow OOO + M$	$(k4a/2)*(F4f)^a$
R4g	$P + OO + M \rightarrow OOO + M$	$(k4a)*(F4g)^a$
	O_3 decomposition	
R5a	$OOO + O \rightarrow OO + OO$	$k5a = 8.0 \times 10^{-12} \exp(-2060/T)$
R5b	$OOO + O(^1D) \rightarrow OO + O + O$	$k5b = 1.2 \times 10^{-10}$
R5c	$OOO + O(^1D) \rightarrow OO + OO$	k5b
R5d	$OOO + OO(^1\Delta) \rightarrow OO + OO + O$	$k5d = 3.8 \times 10^{-15}$
R5e	$OOO + Q \rightarrow OO + OQ$	k5a
R5f	$OOO + Q(^1D) \rightarrow OO + O + Q$	k5b
R5g	$OOO + Q(^1D) \rightarrow OO + OQ$	k5b
R5h	$OOO + OQ(^1\Delta) \rightarrow OO + OO + Q$	k5d /2
R5i	$OOO + OQ(^1\Delta) \rightarrow OO + OQ + O$	k5d /2
R5j	$OOO + P \rightarrow OO + OP$	k5a
R5k	$OOO + P(^1D) \rightarrow OO + O + P$	k5b
R5l	$OOO + P(^1D) \rightarrow OO + OP$	k5b
R5m	$OOO + OP(^1\Delta) \rightarrow OO + OO + P$	k5d /2
R5n	$OOO + OP(^1\Delta) \rightarrow OO + OP + O$	k5d /2
R5o	$OOQ + O \rightarrow OO + OQ$	k5a
R5p	$OOQ + O(^1D) \rightarrow OO + Q + O$	k5b /2
R5q	$OOQ + O(^1D) \rightarrow OQ + OO + O$	k5b /2
R5r	$OOQ + O(^1D) \rightarrow OQ + OQ$	k5b
R5s	$OOQ + OO(^1\Delta) \rightarrow OO + OQ + O$	k5d
R5t	$OOP + O \rightarrow OO + OP$	k5a
R5u	$OOP + O(^1D) \rightarrow OO + P + O$	k5b /2
R5v	$OOP + O(^1D) \rightarrow OP + OO + O$	k5b /2
R5w	$OOP + O(^1D) \rightarrow O + OP$	k5b
R5x	$OOP + OO(^1\Delta) \rightarrow OO + OP + O$	k5d

Reaction no.	*Reaction*	*Rate coefficient*
R5y	$OQO + O \rightarrow OQ + OO$	k5a
R5z	$OQO + O(^1D) \rightarrow OQ + O + O$	k5b
R5aa	$OQO + O(^1D) \rightarrow OQ + OO$	k5b
R5bb	$OQO + OO(^1\Delta) \rightarrow OQ + OO + O$	k5d
R5cc	$OPO + O \rightarrow OP + OO$	k5a
R5dd	$OPO + O(^1D) \rightarrow OP + O + O$	k5b
R5ee	$OPO + O(^1D) \rightarrow OP + OO$	k5b
R5ff	$OPO + OO(^1\Delta) \rightarrow OP + OO + O$	k5d
	$O(^1D)$ quenching	
R6a	$O(^1D) + OO \rightarrow O + OO$	$k6a = 3.2 \times 10^{-11} \exp(67/T)$
R6b	$Q(^1D) + OO \rightarrow Q + OO$	k6a /2
R6c	$Q(^1D) + OO \rightarrow O + OQ$	k6a /2
R6d	$P(^1D) + OO \rightarrow P + OO$	k6a /2
R6f	$P(^1D) + OO \rightarrow O + OP$	k6a /2
	$OO(^1\Delta)$ quenching	
R7a	$OO(^1\Delta) + M \rightarrow OO + M$	$k7a = 3.0 \times 10^{-18} \exp(-200/T)$
R7b	$OQ(^1\Delta) + M \rightarrow OQ + M$	k7a
R7c	$OP(^1\Delta) + M \rightarrow OP + M$	k7a
	CO_3^* formation	
R8a	$O(^1D) + COO \rightarrow COOO$	$k8a = 1.1 \times 10^{-10}$
R8b	$Q(^1D) + COO \rightarrow COOQ$	k8a
R8c	$O(^1D) + COQ \rightarrow COOQ$	k8a
R8d	$P(^1D) + COO \rightarrow COOP$	k8a
R8e	$O(^1D) + COP \rightarrow COOP$	k8a
	CO_3^* decomposition (quenching)	
R9a	$COOO \rightarrow COO + O$	$k9a = 0.84x (1.1 \times 10^{10})$
R9b	$COOQ \rightarrow COO + Q$	k9a /3
R9c	$COOQ \rightarrow COQ + O$	k9a 2/3
R9d	$COOP \rightarrow COO + P$	k9a /3
R9e	$COOP \rightarrow COP + O$	k9a 2/3
	CO_3^* decomposition (isoelectronic)	
R10a	$COOO \rightarrow COO + O(^1D)$	$k10a = 0.16x (1.1 \times 10^{10})$

Reaction no.	*Reaction*	*Rate coefficient*
R10b	$COOQ \rightarrow COO + Q(^1D)$	k10a /3
R10c	$COOQ \rightarrow COQ + O(^1D)$	k10a 2/3
R10d	$COOP \rightarrow COO + P(^1D)$	k9a /3
R10e	$COOP \rightarrow COP + O(^1D)$	k9a 2/3
	Isotope exchange	
R11a	$Q + OO \rightarrow O + OQ$	$k11a = 2.9 \times 10^{-12}(300/T)$
R11b	$O + OQ \rightarrow Q + OQ$	k11a /kqex
R11c	$P + OO \rightarrow O + OP$	k11a
R11d	$O + OP \rightarrow P + OO$	k11a /kpex

*kqex = 1.9456*exp(31.782K/T) [1-9.3 x 10^{-6}(T/K) + 1.97 x10-8(T/K)^2] [Janssen 2005]*

*kpex = ((kqex/2-1)*0.52+1)*2*

a: photolysis fractionation factors are presented in Table 7.3.

7.2 Modeling of ozone rate coefficients

Ozone formation has a strong temperature and a linear pressure dependence. Similarly, different channels for isotopic reactions have pressure and temperature dependencies that may slightly deviate from standard O +O_2 recombination reaction. These additional temperature and pressure dependencies for most of the required individual rate coefficients, are unknown, however. Recently, the room temperature fractionation factors for the relevant isotope channels were determined for the first time [Tuzson 2005]. To date, pressure and temperature dependence of only $^{18}O + {}^{16}O_2$ (R4d) has been measured [Günther 1999, Janssen 2003]. The missing information may be inferred from the additional information about rate coefficients on O+Q2 [Güenther 1999, Janssen 2003] and the overall pressure and temperature dependencies of isotopologue enrichments [Morton 1990, Janssen 2003)]

Accordingly, no pressure and temperature dependency is expected for the reactions leading to symmetric product molecules (R4c, R4f). The slow rate Q+OO (and presumably P+OO) have a strong temperature dependence [Janssen et al. 2003], but no pressure dependence [Günther 1999], while the fast rates O+OQ = OOQ and O+OP = OOP presumably show a pressure dependence, as the reaction Q+QO = QQO does [Günther 1999].

Assuming a small isotope effect in the visible light decomposition of ozone, which has not yet been directly investigated by experiments [Brenninkmeijer et al. 2003], but may well be between 0 (Morton et al.1990) up to 19 ‰ [Chakraborty & Bhattacharya 2003] for ^{18}O, the following rate coefficients are obtained from the pressure and temperature dependencies of the

total enrichments (Figure 7.1a, b).

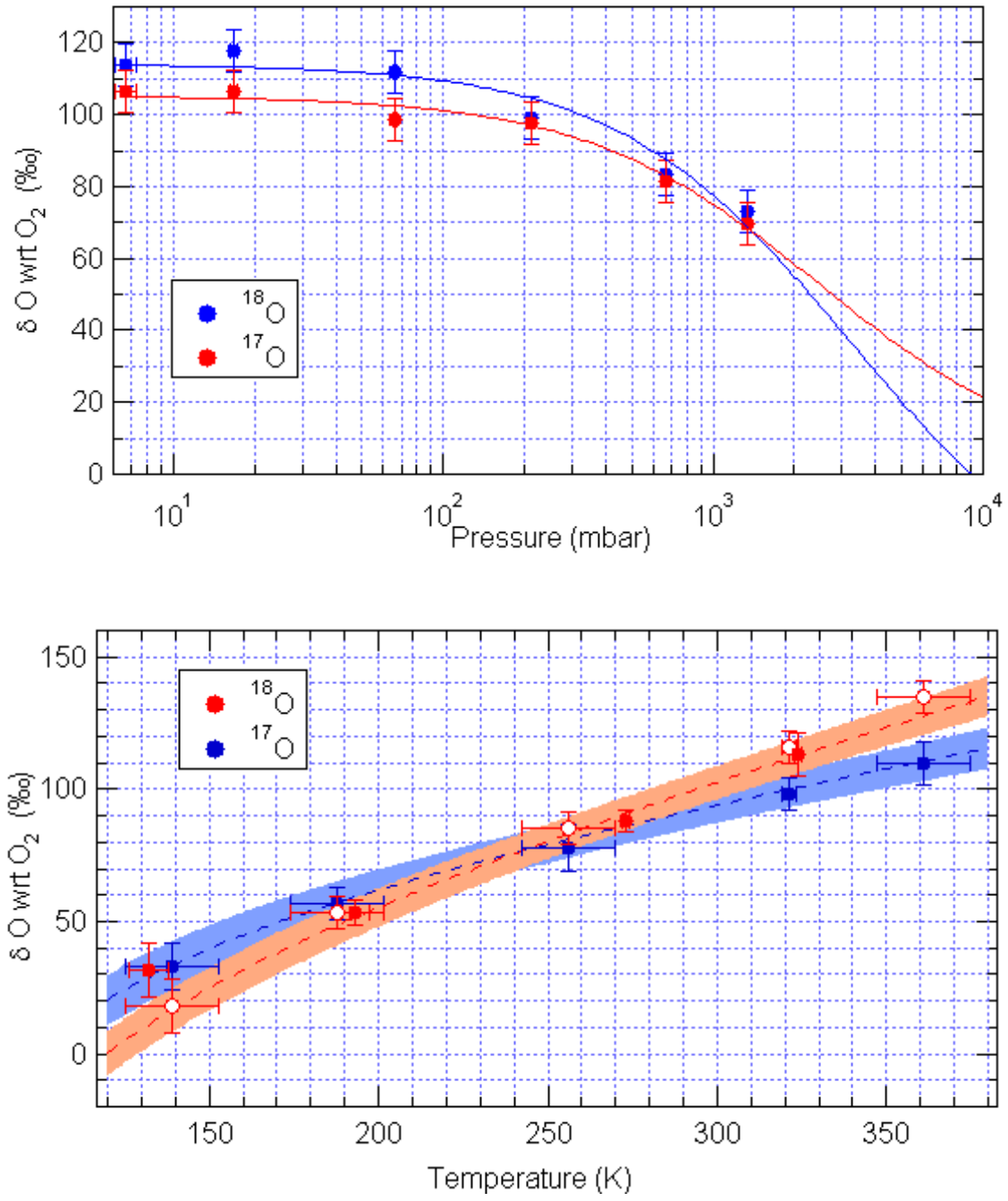

Figure 7.1: Isotopic composition of O_3 as a function of pressure (a) and temperature (b). Original data were corrected by 10‰ for ^{18}O and 5‰ for ^{17}O. The correction is due to the isotope fractionation in the visible light photodissociation of O_3. Temperature open symbols [Janssen 2003], closed [Morton 1990], pressure [Morton 1990]. Line shows best fit to the data. Shaded areas indicates errors of the fit.

Table 7.2: Fractionation factors in ozone formation rate coefficients derived from previous studies and those used in the model to get best agreement with the CO_2 and O_3 isotope exchange experiments.

Model label	***Reaction***	***Derived***	***Model***
F4b	O+OQ →OOQ	1+0.466/(1+p/(3200 mbar))	1+0.466/(1+p/(3200 mbar))
F4c	O+QO →OQO	1.010	1.007
F4d	Q+OO →OOQ	0.920+ 0.0011 (T-300K)	0.920+ 0.0011 (T-300K)
F4e	O+OQ →OOP	1+0.307/(1+p/(2600 mbar))	1+0.307/(1+p/(2600 mbar))
F4f	O+PO →OPO	1.005	1.00364
F4g	P+OO →OOP	1.025+0.00065 (T/K-300)	1.035+0.0005(T/K-300)

Two sets of rate coefficients were finally used in the simulations(Table 7.2). The first one was derived from Fits to the available experimental data [Morton 1990, Janssen et al 2003, Tuzson 2005]. In the second set the temperature dependence of R4g was assumed to be weaker within the given error limits of the reference data and less enrichments in symmetric isotopomers (R4c,R4f). This leads to much better agreement with the experimental results and it is with in the error limits of these rate coefficients (shaded region in Figure 7.1).. The obtained pressure dependence of the rate coefficients agrees with earlier data [Günther 1999, Morton 1990] and is the same for both rate coefficient sets.

7.3 Simulation of lab experiments

In the initial approach to simulate our experimental data, the model parameters were fixed to the low temperature equilibrium point measurements as for this experiment we had isotopic informations about both total O_3 and asymmetric O_3. The specific numerical values for the O_3 photolysis fractionation factors were chosen purely on the basis to reproduce observed O_3 equilibrium isotopic compositions that agree well with the experimental results (Table 7.3). This was achieved by iterative model fits to the data with different parameters to provide the best match with the experimental values. The fractionation factors introduced in the ozone photolysis lead to $O(^1D)$ that is isotopically lighter in heavier isotopes in a mass dependent fashion.

Table 7.3: Fractionation factors for the ozone photolysis with Hg pen ray lamp at two different temperatures to simulate the experimental data.

O_3 isotopomer	***Program label***	***Fractionation factor***	
		250K	300K
$^{16}O^{16}O^{18}O$	FO_3a_OOQ	0.984	0.965
$^{16}O^{18}O^{16}O$	FO_3s_OQO	1.030	1.030
$^{16}O^{16}O^{17}O$	FO_3a_OOP	0.992	0.979
$^{16}O^{17}O^{16}O$	FO_3s_OPO	1.015	1.015

As explained in chapter 5, there is a temperature gradient between the center of the spherical reactor (up to 320 K inside the finger, where the Hg pen ray lamp is placed) and the outside wall (198K) in contact with the thermostat liquid. In order to assess the average gas temperature during the low temperature experiments, the pressure change in the reactor was determined upon irradiation of the reaction mixture. The observed pressure change in the reactor indicates an average gas temperature of about 220K. As irradiation is most intense close to the light source and ozone concentrations are high compared to room temperature experiments, the actual reaction region will be hotter. Therefore, we used a temperature of 250K for the simulation of the low temperature experiments.

The model was initialized with 5.2 m moles of O_2 and 10 μ moles of CO_2 in anticipation of comparing the model calculation with the experimental data.

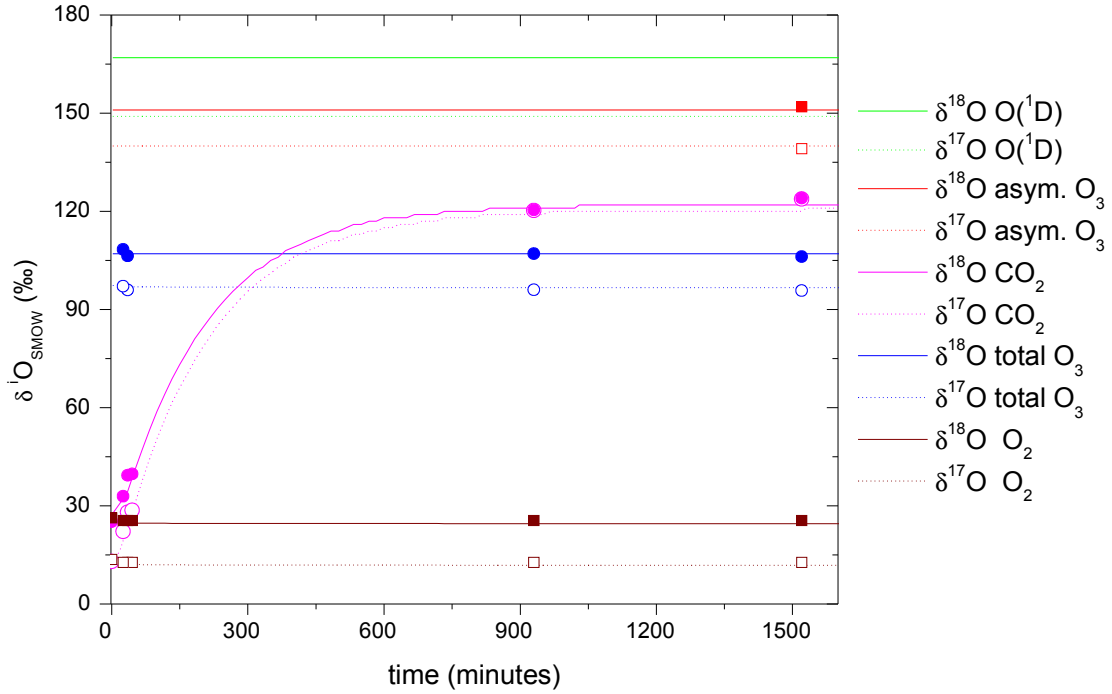

Figure 7.2: Modeled time evolution of the isotopic compositions of various species in CO_2-O_2 mixture, irradiated with UV lamp and comparison with experimental values. The lines are modeled results. Solid and open symbols with similar colors show the experimental values.

It is evident from Figure 7.2 that the enrichment in CO_2 increases with time but the isotopic composition of O_3 and O_2 do not change significantly because of the large O_2 reservoir. The numerical simulations showed a very good agreement with the experimental values of various species in the reaction mixture.

The inclusion of mass dependent collisional fractionation in the rate constants increased the $O(^1D)$ isotopic composition by a factor of 1.4 and 1. 2 in ^{18}O and ^{17}O as shown in Figure 7.3. However, the equilibrium O_3 and CO_2 isotopic composition showed an increase of only 4 and 6.6‰ in ^{18}O and 2 and 3.3‰ in ^{17}O which is comparably a small change. The simulated isotope equilibrium points for all three CO_2 were in agreement with the experimentally determined values.

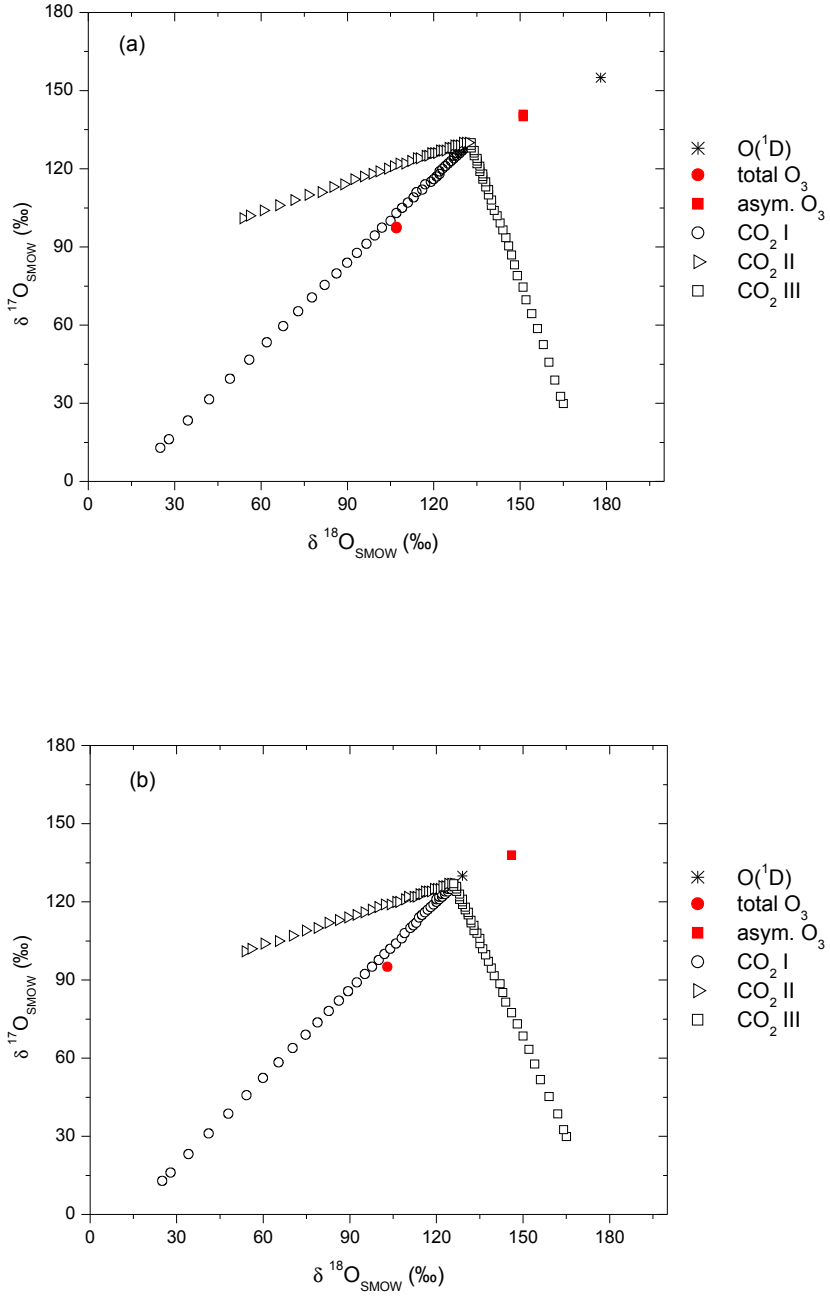

Figure 7.3: Numerical simulations of low temperature equilibrium points with three CO_2 gases of different isotopic composition. Simulations with (a) and without (b) mass dependent collisional fractionation in the respective rate coefficients.

7 Photochemical Box Model

To continue the model development for the CO_2 equilibrium point determination at room temperature with both O_2 and O_3 as initial oxygen reservoirs, the same reaction scheme and modified O_3 photolysis fractionation factors were used at a reaction temperature of 300K. In the room temperature experiments O_2/CO_2 ratios were low (9-12) and a large reactor (2.2L) was used in these experiments. The numerical simulations showed a good agreement with the experimentally measured slopes of various CO_2 in the CO_2-O_3 and CO_2-O_2 setups as shown in Table 7.4.

Table 7.4: Comparison of simulated CO_2 slopes at 300 ± 10K with experiments carried out at room temperature.

amount (mmole)		***Initial CO_2***		***Initial O_2 or O_3***		***CO_2 slope***	
CO_2	O_2 or O_3	$\delta^{17}O$	$\delta^{18}O$	$\delta^{17}O$	$\delta^{18}O$	Experiment	Simulated
0.08	1.04[a]	12.97	25.14	76.6	99.4	0.96 ± 0.003	0.95 ± 0.01
0.14	1.28[a]	103.6	36.26	77.1	101.7	0.54 ± 0.006	0.57 ± 0.00
0.08	1.44[a]	21.00	173.7	79.9	103.3	2.99 ± 0.06	2.78 ± 0.20
0.06	0.89	12.97	25.14	3.7	7.3	1.04 ± 0.007	1.08 ± 0.03
0.06	0.87	102.1	51.63	3.7	7.3	0.42 ± 0.03	0.43 ± 0.02
0.06	0.76	21.09	174.29	3.7	7.3	-3.44 ± 0.02	- 4.05 ± 0.26

a: ozone is expressed as oxygen equivalents.

Comparison between model simulation and experimental values indicate a good agreement for the photochemical equilibrium point as well as for the respective slopes except for the ^{18}O enriched CO_2 slope in O_2 mixture (line 6 in Table 7.4) because error associated with ^{18}O enriched CO_2 simulated slope is quite high.

The model was then used to simulate other experiments where CO_2 (0.036 mmol) , O_2 (1.1 mmol) and N_2 (10.9 mmol) were used initially to determine the effect of quenching of $O(^1D)$ with both N_2 and O_2. The simulated CO_2 equilibrium point agrees for the ^{18}O but it is 11 ‰ higher in ^{17}O than the experimentally determined value ($\delta^{17}O$ =100‰ and $\delta^{18}O$ =117‰ values are versus SMOW). Similarly, the O_3 isotopic composition was not in good agreement with the measured O_3 values. However, this discrepancy could be due to our assumption about the temperature and pressure dependency of the ^{17}O rate coefficients in the ozone formation. In our present reaction scheme we did not include any reaction of $O(^1D)$ with N_2 to produce N_2O and further NO_x chemistry. Nonetheless, the presence of NO_x was dismissed because no

indication of NO_x were found in the reaction mixture measured with mass spectrometer.
In order to understand the stratospheric observations, the same ratios of CO_2, O_2 and N_2 under reduced pressure (30mb) and temperature (220K) conditions were used to simulate the photochemical equilibrium point. We used 220K for the simulation based on the observation of stratospheric O_3 of Krankowsky et al. [2000]. These authors inferred an O_3 formation temperature (190-250K) based on the enrichments observed in stratospheric O_3. The CO_2 slope increased by ~17% (from 1.06 to 1.27) in comparison to the standard conditions accompanied by a slight decrease of the CO_2 enrichment at photochemical equilibrium Figure 7.4.

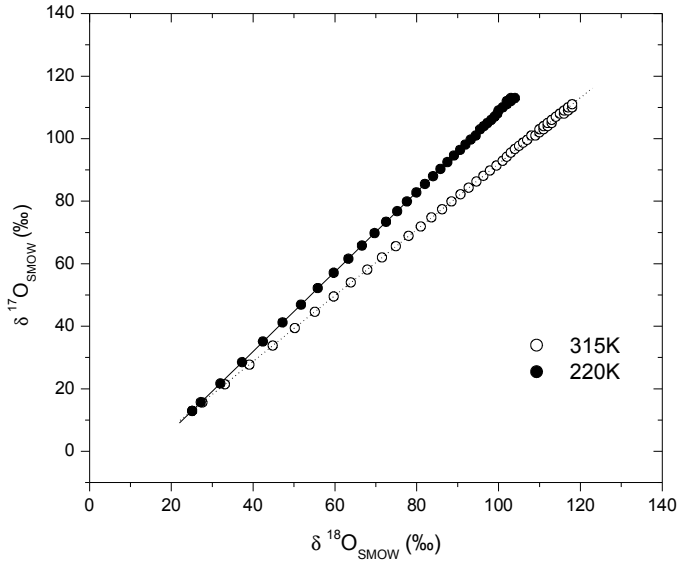

Figure 7.4: Simulation of lab experiment with CO_2-O_2-N_2 mixture at 315K (inferred from pressure change in reactor) and at 220K with simultaneous decrease in pressure.

7.4 Implications of laboratory results to stratospheric CO_2

We performed model runs in order to understand, the stratospheric CO_2 with $\delta^{17}O/\delta^{18}O = 1.7$, because slope of the $\delta^{17}O$- $\delta^{18}O$ relationship and photochemical equilibrium point were the crucial model output for comparison with experimental data. The numerical simulations with these reaction coordinates i.e. with initial tropospheric CO_2 and O_2 isotopic composition and at two temperature 300K and 220K produced stratospheric CO_2 with a slope of 1.04 and 1.49 as shown in Figure 7.5. We used 300K for model simulations to compare these results with

our room temperature photochemical equilibrium point.

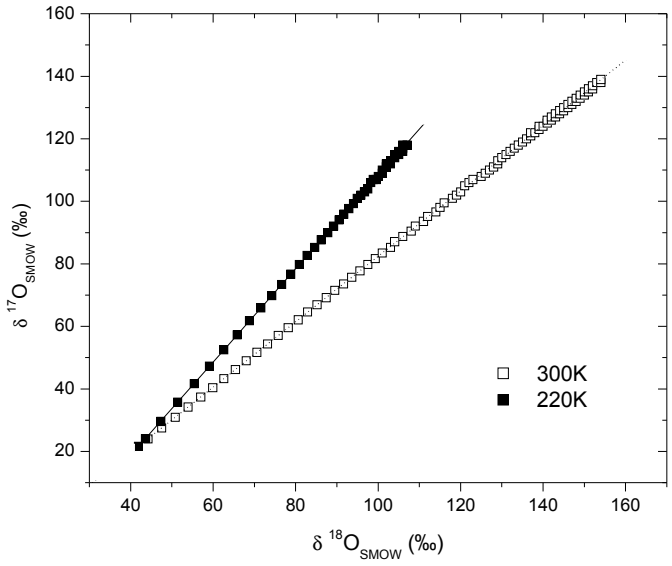

Figure 7.5: Numeric simulations of CO_2 and O_3 isotope exchange between tropospheric CO_2 and O_2 at two temperatures.

7.5 Model sensitivity test

The sensitivity of the model towards the branching ratio of O_3 photolysis to $O(^1D)$ and $O(^3P)$ was checked. Increasing the quantum yield of the singlet channel to 100 % or decreasing to 80% did not effect the model calculated isotopic compositions. Similarly varying the concentration (100 or 80%) of the triplet channel exchange of $O(^1D)$ with CO_2 did not affect the equilibrium isotopic values in our standard model (low temperature experimental setup, $O_2/CO_2 = 550 \pm 20$, P 250 + 10mb). However, in other experiments at room temperatures where O_2/CO_2 ratio was low (9-12), CO_2 at photochemical equilibrium showed ~ 4‰ higher ^{18}O. The model showed higher sensitivity to the temperature and pressure dependence of rate coefficients for asymmetric and symmetric O_3 formation.

The fractionation factors derived for low temperature experiment were also employed to simulate room temperature experiments but it leads to slightly higher enrichments in CO_2 as shown in Table 7.5. The photolysis fractionation in O_3 dissociation affects the $O(^1D)$ isotopic composition which ultimately changes the isotopic composition of CO_2 at photochemical

equilibrium.

Table 7.5: Effect of photolysis fractionation (α_{ph}) on the CO_2 enrichment at photochemical equilibrium point. Experimental values are also given for comparison.

	CO_2-O_3 system			***CO_2-O_2 system***		
	$\delta^{17}O$ (‰)	$\delta^{18}O$ (‰)	slope	$\delta^{17}O$ (‰)	$\delta^{18}O$ (‰)	slope
Experimental values	207	228	0.98	132	135	1.09
(α_{ph} at 300K)[a]	205	228	0.95	131	134	1.08
(α_{ph} at 250K)[b]	212	241	0.92	137	146	1.03
(α_{ph} at 250K)[c]	212	244	0.91	137	149	1.01

a: simulations with photolysis fractionation assumed for 300K and CO_2+ $O(^1D)$ isotope exchange reaction assumed to be 84% on triplet surface and 16% on singlet surface.

b: simulations with photolysis fractionation assumed for 250K and CO_2+ $O(^1D)$ isotope exchange reaction assumed to be 84% on triplet surface and 16% on singlet surface.

c: simulations with photolysis fractionation assumed for 250K and CO_2+ $O(^1D)$ isotope exchange reaction assumed to be 100% on triplet surface.

7.6 Discussion

The low temperature experiments were used as the basis for the model development for two reasons: firstly we have information about the enrichment in the asymmetric isotopmer of O_3, which is considered to be the true source of heavy atoms transfer to other atmospheric species [Shepard and Walker 1983] . Secondly, in this particular set up the oxygen reservoir is large in comparison to CO_2 (O_2/CO_2 = 500) which does not affect the O_3 isotopic composition. It has been pointed out by Janssen [2005] that O_3 isotopic composition is determined by the O_2 reservoir in a closed system due to the mass balance constrains. Under these experimental conditions there is too little CO_2 to wash out the isotopic enrichment in O_3 as can bee seen from Figure 7.2 therefore the O_3 isotopic composition remains unaltered during the experiment. This situation is close to the real atmosphere where O_2 is the principal reservoir and CO_2 is the minor reservoir. Photo dissociation of O_3 produces $O(^1D)$ that is lighter in comparison to asymmetric O_3 by 15.5 ‰ in ^{18}O and 7.3 ‰ in ^{17}O in the absence of any collisional fractionation in reaction rates. Therefore CO_2 at photochemical equilibrium has the same isotopic composition ($\delta^{17}O$ =127 ‰ and $\delta^{18}O$ =126 ‰ yielding $\delta^{17}O/\delta^{18}O$ = 1.13) as $O(^1D)$ in this scenario. On the other hand, if mass dependent collisional fractionation is included in the reaction scheme, $O(^1D)$ becomes heavier by 13‰ in $\delta^{17}O$ and 23.7‰ in $\delta^{18}O$

than the asymmetric O_3 from which it is formed. In this situation the quenching of $O(^1D)$ to O (^3P) mainly after collision with O_2 leads to an enrichment of the heavy oxygen atoms in the remaining $O(^1D)$ compared to the initial asymmetric O_3 and secondly the collision frequency of $O(^1D)$ with CO_2 is smaller for isotopically substituted $O(^1D)$ and CO_2. Both effects depend on the reduced masses of $O(^1D)$ and its reaction partner and thus nearly cancel out

The dissociative reaction of O_3 with $OO(^1\Delta)$ (R5d) is important in the laboratory experiment because half of the ozone is destroyed through this channel. This, however, is not the case in atmosphere where dissociation of the O_3 almost exclusively occurs through photolysis $\lambda < 310$ nm [Brasseur and Solomon 1986, Brasseur et al. 1999]. However, the reactions of $O(^1D)$ with O_3 (R5b and R5c) only contribute less than 3% to ozone destruction, because its concentration is kept low due to quenching by bath gases.

Table 7.6: Concentration of various species at photochemical equilibrium and their total life times (τ_1) inferred from numerical simulations. Life time (τ_2) with respect to primary channel of dissociation is also given for comparison.

Species	***Concentration (molecule cm^{-3})***	τ_1 ***(s)***	τ_2 ***(s)***
O_3	6.94×10^{16}	52.8	[a]100
$O(^1D)$	2.28×10^{6}	3.71×10^{-9}	[b]3.85×10^{-9}
$OO(^1\Delta)$	2.28×10^{12}	3.68×10^{-3}	[c]3.79×10^{-3}

a: against photolysis (R2 and R3)

b: against reaction with O_2 (R6)

c: against reaction with M (R7)

Additionally in our low temperature experiments, $O(^1D)$ and $OO(^1\Delta)$ are produced at higher photon energies than they are typically produced in the atmosphere. Details of the upper electronic potential surface may therefore be important for photo dissociation at the threshold ($\lambda < 310$nm), but may be of not much significance at the high kinetic energies in this system. It may thus be possible that the branching ratio for photo dissociation of OOQ into $O(^1D)$ and $Q(^1D)$ product channels may show a significant isotope effect in the atmosphere, but not in the laboratory system. For the barrier free $O + O_2$ system large isotope effects at the threshold have been found [Fleurat Lessard 2003].

Due to the zero activation energy reported for the reaction of $O(^1D)$ with CO_2 [De More and

Dede 1970] and because of the highly kinetic $O(^1D)$ present in our experimental setup, no strong temperature dependence of the isotope effect in this reaction is expected. However, our low temperature photochemical equilibrium experiments show some temperature dependency for the exchange reaction. In the present model, temperature and pressure dependencies for various channels of O_3 isotopomer and isotopologue formation [Janssen et al. 2003, Güenther et al.1999] have been included for the first time, along with the recent observation for temperature dependence of isotope exchange reactions [Janseen 2005]. We employed additional fractionation (15-30‰) in the photolysis of O_3. This leads to very good agreement with the measured photochemical equilibrium point. In fact, the observed enrichments in CO_2 at different temperatures and pressures seems to be the direct result of O_3 enrichments. The discrepancy observed for high pressure experiment (exp 136 where N_2-O_2-CO_2 was used) could be due to relatively large uncertainty in the O_3 enrichment at atmospheric pressure where only one data point [Morton et al. 1990] determines the fit values for the overall O_3 enrichments. Therefore, more precise values for enrichment in O_3 at these pressure are mandatory. Moreover, contribution of asymmetric O_3 to the overall enrichment is required for the interpretations of these measurements.

We believe that the experimental evidence and numeric simulations accumulated so far are sufficient to invoke the influence of temperature and photon energy on the stratospheric CO_2 enrichments. Unfortunately, no data is available about the photolysis fractionation in O_3 at different wavelengths and temperature, since fractionation factors may vary in the region of vibrational structures around the maximum in the O_3 absorption spectrum. Our experiments with Hg-pen ray lamp and Sb-broad band lamp in CO_2-O_2 mixture however, clearly show that in addition to O_3 isotopic composition, the temperature and wavelength of ozone photolysis are important parameters which influence the stratospheric CO_2 slope in a three isotope plot.

However, our experimental data as well as numeric simulations were not able to predict the $\delta^{17}O$- $\delta^{18}O$ relationship of 1.7 for stratospheric CO_2 at room temperature using line source. These findings are in contradiction to the measurements of Chakraborty and Bhattacharya [2003] who claim to reproduce stratospheric CO_2 slope even at room temperature.To investigate this discrepancy, we employed our model to simulate their experiments. They used three different CO_2 gases (SM-CO_2, SP-CO_2, SL-CO_2) and O_3 (with averge isotopic composition of $\delta^{17}O$ = 106 ‰ $\delta^{18}O$= 125‰) with O_3/CO_2 ratio of 8 to study the isotope exchange mechanism between CO_2 and O_3 via $O(^1D)$. As photolysis fluxes were not reported

in their article, we adjusted this parameter in our model to reproduce the time evolution of SM-CO_2 for $\delta^{18}O$.

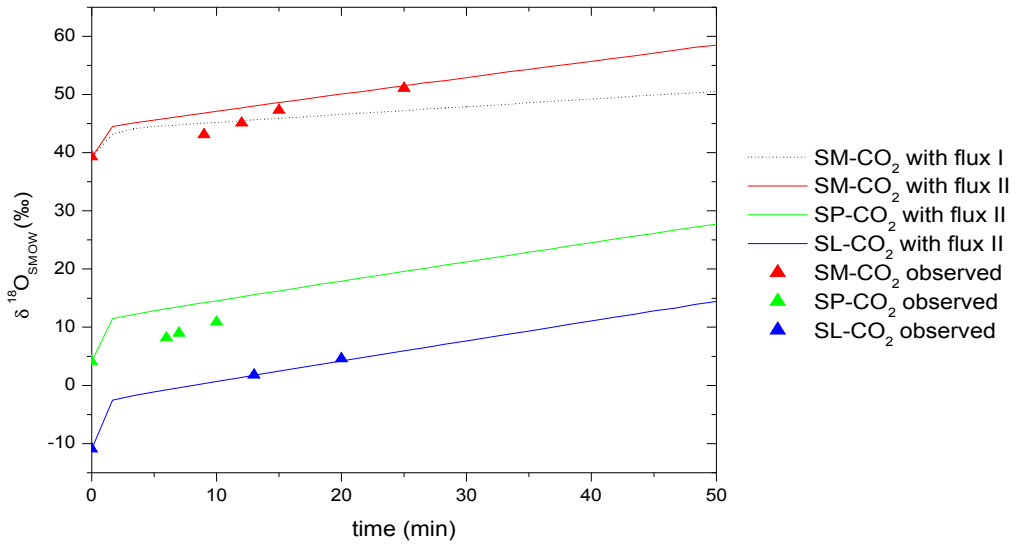

Figure 7.6: Model results of the $\delta^{18}O$ simulations for three different CO_2 gases used to investigate CO_2 isotope exchange with O_3 ($\delta^{17}O$ = 106 ‰ $\delta^{18}O$= 125‰). Solid triangles represent experimental values, dashed line is simulations with Puritech Hg-lamp (JO_3 = 1 x10^{-2}, JO_2 = 4.0 x 10^{-6} measured in our lab). solid lines are simulation with adjusted fluxes for Hg-resonance lamp (JO_3 = 3 x10^{-2}, JO_2 = 6.0 x 10^{-6}) used by Chakraborty and Bhattacharya [2003].

It is evident fromFigure 7.6 that $\delta^{18}O$ of SP-CO2 does not fit the simulation. In order to obtain agreement we need to reduce the photolysis fluxes to values that that can reproduce their results (JO_3 = 0.4 x10^{-2}, JO_2 = 2.0 x 10^{-6}). This change is contrary to their reported rate of increase in ^{18}O enrichments, i.e. SL-CO_2 = 0.88 > SP-CO_2 = 0.68 > SM-CO_2 =0.46. It is dubious that photolysis fluxes need to be adjusted for each CO_2 to obtain the observed enrichment rates. The change in photolysis flux affects O_3 dissociation and secondary O_3 formation in our model simulations, which in turn changes the $O(^1D)$ isotopic composition. Though it is evident form the description of the experimental setup that the same lamp has been employed for O_3 formation and for the investigation of CO_2 and $O(^1D)$ isotope exchange mechanism but this discrepancy remains unclear. Additionally, our model predict further enrichment in SM-CO_2 with increasing exposure of the mixture to UV irradiation, which

could not be observed by these authors even after 130 and 360 minutes of photolysis. The reason behind further enrichment is the production of secondary O_3 even after 3 minutes of photolysis as $O(^3P)$ produced during $O(^1D) + CO_2$ reaction and from O_2 dissociation immediately react with oxygen molecules to produce secondary O_3 ($\delta^{17}O$ = 221 ‰ $\delta^{18}O$ = 258‰).

We reported above detailed model results obtained after including collisional fractionation in the rate constants and now we briefly discuss some salient feature of their results without additional mass dependent collisional fractionation in the reaction scheme Table 7.7. We included both scenarios in the model to get an insight about the effective $O(^1D)$ isotopic composition, because they envisaged this scenario to interpret their data.

Table 7.7: Comparison of observed slopes and model results obtained with and without mass dependent collisional fractionation (CF) in the rate coefficients.

Species	***Slope ($\delta^{17}O/\delta^{18}O$)***			***$\Delta O(^1D)^a$***	
	Observed	without CF	with CF	$\delta^{17}O$	$\delta^{18}O$
SM-CO_2	1.79	1.07	1.03	21.94	42.78
SP-CO_2	1.52	0.96	0.92	21.94	42.78
SL-CO_2	1.29	0.91	0.89	21.94	42.78

a= net increase in $O(^1D)$ isotopic composition after inclusion of mass dependent collisional fractionation in the rate coefficients.

It is interesting to note that slope increases by ~2.5, 1.8 and 1.6% for SM-CO_2, SP-CO_2 and SL-CO_2 respectively in the case where mass dependent collisional fractionation in rate coefficients was not included, which is contrary to the explanation given by these authors.

8 Summary and Conclusions

Owing to the importance of stratospheric CO_2 anomaly, the primary objective of this work is to investigate the isotope exchange mechanism between CO_2 and O_3 via $O(^1D)$. In contrast to earlier, we did not primarily investigate slopes in the three-isotope diagram but approached the problem on a more fundamental level: we determined in detail the photochemical and isotope equilibrium in the exchange mechanism from which other quantities like three-isotope slopes can then be calculated.

For this purpose we carried out a large number of isotope exchange experiments with CO_2 and O_2 gases of widely different isotopic composition, including artificially prepared gases. By combining experiments with various gases in the three-isotope plot, the concept of an isotope equilibrium point could be unequivocally demonstrated using a triangulation method. At room temperature, we established an isotope equilibrium in which CO_2 enriched relative to O_2 by about 130‰ in $\delta^{17}O$ and $\delta^{18}O$. This value is independent of the initial isotopic composition of both the CO_2 and the O_2, including in particular mass independently fractionated CO_2 and O_2 gases. Having established the existence of an isotope equilibrium, we have derived a simple equation to calculate three-isotope slopes from the isotope equilibrium point and the isotopic composition of the initial reactants only.

Since this information is insufficient to explain the observed three-isotope slope in the atmosphere, other effects must contribute to the value of the isotope equilibrium point. Therefore we have investigated and determined the dependence of the isotope equilibrium point on both temperature and pressure for the first time. Results show that CO_2 isotope enrichments at photochemical equilibrium decrease towards lower temperature by -0.19‰/K for $\delta^{17}O$ and -0.28‰/K for $\delta^{18}O$. Since the temperature dependence is stronger for $\delta^{18}O$ than for $\delta^{17}O$, the $\delta^{17}O/\delta^{18}O$ slopes increase towards lower temperatures. Thus low stratospheric temperatures contribute to the fact that the three-isotope slope in the atmosphere is higher than the slopes found in room-temperature laboratory studies in the past.

In one experimental set at low temperatures (220±15K) the isotope equilibrium was also determined by the triangulation method. In addition to measuring CO_2 and O_2 isotope data, O_3 was collected in a specially designed trap at 63K and the isotopic composition of total ozone as well as the asymmetric isotopomer of O_3 was determined, the latter using a new tunable diode laser absorption spectroscopy. The results show that asymmetric O_3 and CO_2 at photochemical equilibrium are linked via a mass dependent relation, i.e., the difference in

$\delta^{18}O$ is twice as large as the difference in $\delta^{17}O$. This is an important result which shows that no additional mass independent fractionation is required in all steps of the exchange sequence that follow ozone formation, in particular the CO_3^* complex itself. Prior studies had concluded that mass independent fractionation steps are necessary in the CO_3^* complex, however, no information about asymmetric ozone was available in those studies. Thus, the experiments here show that mechanism 2 given in the introduction is the most likely scenario in the CO_2-O_3 isotope exchange process. We anticipate that the results presented here, together with additional measurements on asymmetric ozone in future, will soon provide more information about this issue also at other temperatures and pressures to substantiate this point.

The pressure dependence of the isotope equilibrium point was investigated in a series of experiments. The measurements show an inverse pressure dependence of -0.04‰ /mb for ^{17}O and -0.02‰ /mb for ^{18}O in the pressure range of 80 to 1000mb. Thus the pressure dependency is stronger for ^{17}O than for ^{18}O thus the low pressures in the stratosphere will result in higher three-isotope slopes than found in laboratory experiments at ambient pressure.

The temperature and pressure dependencies of the isotope equilibrium point were compared to model predictions for variations of the isotopic composition of asymmetric O_3 with temperature and pressure. In general, the magnitudes of enrichments in CO_2 are similar to those calculated for asymmetric O_3. This indicates that the observed dependencies of the CO_2 isotope equilibrium point, and thus of three-isotope slopes, are to a large part due to variations in the precursor O_3.

However, some experiments also indicate that the isotope equilibrium point of CO_2 versus O_2 depends also on the relative proportions of O_2 and CO_2 in the reaction mixture. At lower O_2 / CO_2 ratios, i.e., at higher CO_2 mixing ratio, the equilibrium enrichments is lower than at low CO_2 mixing ratios. This indicates that CO_2 itself has an effect on the isotope equilibrium point, potentially by directly affecting $O(^1D)$ via a recently discovered non-quenching isotope exchange channel.

A number of our photochemical equilibrium experiment were simulated using a Facsimile model. Using recent rate coefficients data, available for various channels of O_3 formation and assuming mass dependent fractionation in O_3 photolysis we generally achieved good agreement for various sets of experiments. When this model is run with atmospheric input data, the resulting $\delta^{17}O$/ $\delta^{18}O$ slope is 1.5 for stratospheric CO_2. The increase in the slope compared to earlier studies is primarily due to including the pressure and the temperature

dependencies discovered in this work. This increase in the three-isotope slope brings the model results into much better agreement with observations ($\delta^{17}O/\delta^{18}O = 1.7$). The remaining discrepancy may be explained by an effect of photolysis wavelength, as preliminary experiments with a broad band light source produced a higher three-isotope slope than experiments with the Hg lamps. If this effect, although not fully investigated, is added to the model result, then even higher stratospheric three-isotope slopes can be explained. Future studies should attempt to quantify the wavelength dependence of the exchange process. Further work should also concentrate on narrowing the uncertainties in O_3 enrichments at higher pressure and low temperatures, in particular regarding the asymmetric ozone isotopologues.

In addition to the laboratory experiments, oxygen isotope measurements on stratospheric CO_2 samples were carried out in this study. Although the precision is not as good as in some prior studies, a large number of samples from the lower stratosphere are presented that extend the results form earlier balloon samples of mesosphere and stratosphere to the troposphere.

9 Bibliography

Alexander B., M. K. Vollmer, T. Jackson, R. F. Weiss, M. H. Thiemens (**2001**), Stratospheric CO_2 isotopic anomalies and SF_6 and CFC tracer concentration in the Arctic polar vortex, *Geophys. Res. Lett.*, **28** (21), 4103-4106

Anderson S. M., D. Hülsebusch, K. Mauersberger (**1997**), Surprising rate coefficients for four isotopic variants of O + O_2 + M, *J. Chem. Phys.*, **107** (14), 5385-5392

Anderson S. M., J. Morton, K. Mauersberger (**1989**), Laboratory measurements of ozone isotopomers by tunable diode laser absorption spectroscopy, *Chem. Phys. Lett.*, **156** (2,3), 175-180

Aregbe Y., S. Valkiers, K. Mayer, P. De Bievre, R. M. Wessel, A. Alink (**1998**), Measuring amount ratios of gas isotopes by two primary methods, *Metrologia*, **35** (1), 7-16

Assonov S. S., C. A. M. Brenninkmeijer (**2001**), A new method to determine ^{17}O isotopic abundance in CO_2 using oxygen isotope exchange with a solid oxide, *Rapid Commun. Mass Spectrom.*, **15**, 2426-2437

Atkinson R., D. L. Baulch, R. A. Cox, R. F. J. Hampston, J. A. Kerr, M. J. Rossi, J. Troe (**1996**), Evaluated kinetic and photochemical data for atmospheric chemistry, *Atmos. Environ.*, **30** (V), 1125-1600

Bains-Sahota S. K., and M. H. Thiemens (**1987**), Mass-independent oxygen isotopic fractionation in a microwave plasma, *J. Phys. Chem.*, **91**, 4370-4374

Barth V. and A. Zahn, (**1997**), Oxygen isotope composition of carbon dioxide in the middle atmosphere, *J. Geophys. Res.*, **102** (D11), 12995-13007

Baulch D. L., and W. H. Breckenridge (**1966**), Isotopic Exchange of $O(^1D)$ with carbon dioxide, *Trans. Faraday Soc.*, **62**, 2768-2773

Bennet C. J., C. Jamieson, A. M. Mebel, R. I. Kaiser, (**2004**), Untangling the formation of the cyclic carbon trioxide isomer in low temperature carbon dioxide ices, *Phys. Chem. Chem. Phys.*, **6**, 735-746

Bhattacharya S. K., M. H. Thiemens (**1989**), Effect of isotopic exchange upon symmetry dependent fractionation in the O + CO to CO_2 reaction, *Z. Naturforsch.,*, **44**, 811-813

Bigeleisen J. (**1996**), Nuclear size and shape effects in chemical reactions. Isotope chemistry of the heavy elements, *J. Am. Chem. Soc.*, **118** (15), 3676-3680

Bigeleisen J. (**1949**), The relative reaction velocities of isotopic molecules, *J. Chem. Phys.*, **17** (8), 675-678

Bigeleisen J. and M. Wolfsberg (**1958**), Theoretical and experimental aspects of isotope effects in chemical kinetics, *Adv. Chem. Phys.*, **1**, 15-76

Bigeleisen J., M. G. Mayer (**1947**), Calculation of equilibrium constants for isotope exchange reactions, *J. Chem. Phys.*, **15** (5), 261-267

Blake A. J., S. T. Gibson, D. G. McCoy (**1984**), Photodissociation of $^{16}O^{18}O$ in the atmosphere, *J. Geophys. Res.*, **89**, 7277-7284

Boering K. A., S. C. Wofsy, B. C. Daube, H. R. Schneider, M. Loewenstein, J. R. Podolske and I. J. Conway (**1996**), Stratospheric mean ages and transport rates from observations of carbon dioxide and nitrous oxide, *Science*, **274**, 1340-3

Boering K. A., T. Jackson, K. J. Hoag, A. S. Cole, M. J. Perri, M. Thiemens, E. Atlas (**2004**), Observations of the anomalous oxygen isotopic composition of carbon dioxide in the lower stratosphere and the flux of the anomaly to the troposphere, *Geophys. Res. Lett.*, **31**, L03109, doi:10.1029/2003GL018451

Brasseur G. and S. Solomom (**1986**), Aeronomy of the Middle Atmosphere, D. Reidel Publication Co. Dordrecht, Holland, 247-291 pp

Brasseur G. P., J. J. Orlando, G. S. Tyndall (**1999**), Atmospheric Chemistry and Global Change, Oxford Univ. Press, New York, 655 pp

Brenninkmeijer C. A. M., and T. Röckmann (**1999**), Mass spectrometry of the intramolecular nitrogen isotope distribution of environmental nitrous oxide using fragment ion analysis, *Rapid commun. Mass Spectrom.*, **13** (20), 2028-2033

Brenninkmeijer C. A. M., C. Janssen, J. Kaiser, T. Röckmann, T. S. Rhee, and S. S. Assonov (**2003**), Isotope effects in the chemistry of atmospheric trace compounds, *Chem. Rev.*, **103**, 5125-5161

Brenninkmeijer C. A. M., T. Röckmann (**1998**), A rapid method for the preparation of O_2 from CO2 for mass spectrometric measurement of $^{17}O/^{16}O$ ratios, *Rapid Commun. Mass Spectrom.*, **12** (8), 479-483

Cantrell C. A., R. E. Shetter, J. G. Calvert (**1994**), Branching Ratios for the $O(^1D) + N_2O$ reaction, *J. Geophys. Res.*, **99** (D2), 3739-3743

Chakraborty S. and S. K. Bhattacharya (**2003**), Experimental investigation of oxygen isotope exchange between CO_2 and $O(^1D)$ and its relevance to the stratosphere, *J. Geophys. Res.*, **108** (D23), 4724,doi: 10.1029/2002JD002915

Ciais P., A. S. Denning, P. P. Tans, J. A. Berry, D. A. Randall, G. J. Collatz, P. J. Sellers, J. W. C. White, M. Trolier, H. A. J. Meijer, R. J. Francy, P. Monfray, M. Heimann (**1997**), A three-dimensional synthesis of $\delta^{18}O$ in atmospheric CO_2. 1. Surface fluxes, *J. Geophys. Res.*, **102** (D5), 5857-5872

Ciais P., P. P. Tans, J. W. C. White, M. Trolier, R. J. Francy, J. A. Berry, D. R. Randell, P. J. Sellers, J. G. Collatz, D. S. Schimel (**1995b**), Partioning of ocean and land uptake of CO_2 as inferred by $\delta^{13}C$ measurements from the NOAA Climate Monitoring and Diagnostic Laboratory Global Air Sampling Network, *J. Geophys. Res. Atmos.*, **100**, 5051-5070

Ciais P., P. P. Tans, M. Trolier (**1995a**), A large northern-hemisphere terrestrial CO_2 sink indicated by the $^{13}C/^{12}C$ ratio of atmospheric CO_2, *Science*, **269**, 1098-1102

Cicerone R. J., and J. L. McCrumb (**1980**), Phtodissociation of isotopically heavy O_2 as a source of atmospheric O_3, *Geophys. Res. Lett.*, **7** (4), 251-254

Clayton R. N. and T. K. Mayeda (**1996**), Oxygen isotope studies of achondrites, *Geochim. Cosmochim. Acta*, **60**, 1999-2017

Clayton, R. N., L. Grossman, T. K. Mayeda (**1973**), A component of primitive nuclear composition in carbonaceous meteorites, *Science*, **182**, 485-488

Cliff S.S, and M. H. Thiemens (**1997**), The $^{18}O/^{16}O$ and $^{17}O/^{16}O$ ratios in nitrous oxide: A mass independent anomaly, *Science*, **278** (5344), 1774-1776

Cobos C., R. Castellano and H J Schumacher (**1983**), The kinetic and the mechanism of ozone photolysis at 253.6 nm, *J. Photochem.*, **21**, 291-312

Cuntz M., P. Ciais, G. Hoffmann, C. E. Allison, R. J. Francy, W. Knorr, P. P. Tans, J. W. C. White, I. Levine (**2003b**), A comprehensive global three dimensional model of $\delta^{18}O$ in atmospheric CO_2: 2. Mapping the atmospheric signal, *J. Geophys. Res.*, **108** (D17), 4528, doi: 10.1029/2002JD003153

Cuntz M., P. Ciais, G. Hoffmann, W. Knorr (**2003a**), A comprehensive global three dimensional model of $\delta^{18}O$ in atmospheric CO_2: 1. Validation of surface processes, *J. Geophys. Res.*, **108** (D17), 4527, doi: 10.1029/2002JD003153

Davidson J. A., C. M. Sadowski, H. I. Schiff, G. E. Streit, C. J. Howard, D. A. Jennings, A. L. Schmeltekopf (**1976**), Absolute rate constant determinations for the deactivation of O (^1D) by time resolved decay of $O(^1D)$ $O(^3P)$ emission, *J. Phys. Chem.*, **64** (11), 57-62

DeMore W. B. and C. Dede, (**1970**), Pressure dependence of carbon trioxide formation in the

gas- phase reaction of O(^{1}D) with carbon dioxide, *J. Phys. Chem.*, **74** (15), 2621-2625

DeMore, W. B., S. P. Sander, D. M. Golden, R. F. Hampson, M. J. Kurylo, C. J. Howard, A. R. Ravishankara, C. E. Kolb, M. J. Molina (**1997**), Chemical kinetics and photochemical data for use in stratospheric modeling, Jet Propul. Lab., Pasadena, California, USA.

Farquhar G. D., J. Lloyd, J. A. Taylor, L. B. Flangen, J. P. Syvertsen, K. T. Hubick, S. C. Wong and J. R. Ehleringer (**1993**), Vegetation effects on the isotope composition of oxygen in atmospheric CO_2, *Nature*, **363**, 439-443

Fleurat-Lessard P., S. Yu. Grebenshchikov, R. Schinke, C. Janssen, D. Krankowsky (**2003**), Isotope dependence of the O+O_2 exchange reactions: Experiment and theory, *J. Chem. Phys.*, **19** (9), 4700-4712

Franchi I. A., I. P. Wright, A. S. Sexton, C. T. Pillinger (**1999**), The oxygen-isotopic composition of Earth and Mars, *Meteorit. Planet. Sci.*, **34**, 657-661

Francy R. J. and P. P. Tans (**1987**), Latitudinal variation in oxygen-18 of atmospheric CO_2, *Nature*, **327**, 495-497

Francy R. J., P. P. Tans, C. E. Allison (**1995**), Changes in oceanic and terrestrial carbon uptake since 1982, *Nature*, **373**, 326-330

Friedli H. and U. Siegenthaler (**1988**), Influence of N_2O on isotope analysis in CO_2 and mass-spectrometeric determination of N_2O in air samples, *Tellus*, **40B**, 129-133

Fujii T., T. Yamamoto, J. Inagawa, K. Watanabe, K. Nishizawa (**1998**), Influence of nuclear size and shape and nuclear spin on chemical isotope effect of zirconium-crown complex, *Ber. Bunsen-Ges. Phys. Chem.*, **102** (4), 663-669

Gamo T., M. Tsutsumi, H. Skai, T. Nakazawa, T. Matchida, H. Honda, T. Itoh, (**1995**), Long term monitoring of carbon and oxygen isotope ratios of stratospheric CO_2 over Japan, *Geophys. Res. Lett.*, **22** (4), 397-400

Gosh P., and W. A. Brand (**2004**), The effect of N_2O on the isotopic composition of air-CO_2 samples, *Rapid commun. Mass Spectrom.*, **18**, 1830-1838

Günther J, B. Erbacher, D. Krankowsky, K. Mauersberger (**1999**), Pressure dependence of two relative ozone formation rate coefficients, *Chem. Phys. Lett.*, **306**, 209-213

Günther J, D. Krankowsky, K. Mauersberger (**2000**), Third body dependence of rate coefficients for ozone formation in ^{16}O-^{18}O mixtures, *Chem. Phys. Lett.*, **324**, 31-36

Hoag, K. J., C. J. Still, I. Y. Fung, K. A. Boering (**2005**), Triple oxygen isotope composition of tropospheric carbon dioxide as a tracer of terrestrial gross carbon flux, *Geophys. Res. Lett.*, **32**, L02802, doi:10.1029/2004GL021011

Hoefs J. (**1997**), Stable Isotope Geochemistry, Springer-Verlag, Berlin, 201 pp

Hulston J. R. and H. G. Thode (**1965**), Variations in S^{33}, S^{34} and S^{36} contents of meteorites and their relation to chemical and nuclear effects, *J. Geophys. Res.*, **70**, 3475-3484

Janssen C. (**2005**), Intramolecular isotope distribution in heavy ozone ($^{16}O^{18}O^{16}O$ and $^{16}O^{16}O^{18}O$), *J. Geophys. Res.*, **110** (D08308), 1-9, doi:10.1029/2004JD005479

Janssen C., J. Guenther, D. Kranskowsky, K. Maueresberger (**1999**), Relative formation rates of $^{50}O_3$ and $^{52}O_3$ in ^{16}O-^{18}O, *J. Chem. Phys.*, **111** (16), 7179-7182

Janssen C., J. Guenther, K. Mauersberger, D. Krankowsky (**2001**), Kinetic origin of the ozone isotope effect: a critical analysis of enrichments and rate coefficients, *Phys. Chem. Chem. Phys.*, **3**, 4718-4721

Johnson M. S., Feilberg K. L., von Hessberg P., Nielsen O. J., (**2002**), Isotopic processes in atmospheric chemistry, *Chem. Soc. Rev.*, **31**, 313-323

Johnston J. C., M.H. Thiemens (**1997**), The isotopic composition of tropospheric ozone in three environments, *J. Geophys. Res.*, **102** (D21), 25395-25404

Johnston, J. C., T. Röckmann, C. A. M. Brenninkmeijer, (**2000**), CO_2 + $O(^1D)$ isotopic exchange: Laboratory and modeling studies, *J. Geophys. Res.*, **105** (D12), 15213-15229

Kaiser J., Röckmann T., Brenninkmeijer C. A. M. (**2002**), Temperature dependence of isotope fractionation in N2O photolysis, *Phys. Chem. Chem. Phys.*, **4** (18), 4420-2002

Katakis D. and H. Taube, (**1962**), Some photochemical reactions of O_3 in the gas phase, *J. Chem. Phys.*, **36** (2), 416-422

Kaye J. A., and D. F. Strobel (**1983**), Enhancement of heavy ozone in the Earth's atmosphere, *J. Geophys. Res.*, **88** (13), 8447-8452

Keeling C. D., R. B. Bacastow, A. F. Carter, S. C. Piper, T. P. Whorf, M. Heimann, W. G. Mook, H. Roleoffzen (**1989**), A three-dimensional model of atmospheric CO2 transport based on observed winds:1. Analysis of observed data, *Geophysical Monograph*, **55**, 165-236

Keeling C. D., R. B. Bacastow, P. P. Tans (**1980**), Predicted schift in the ^{13}C-^{12}C ratio of atmospheric carbon dioxide, *Geophys. Res. Lett.*, **7**, 505-508

Keeling C. D., T. P. Whorf, M. Wahlen, J. van der Plicht (**1995**), Interannual extremes in the rate of atmospheric carbon dioxide since 1980, *Nature*, **375**, 666-670

Krankowsky D., F. Bartecki, G. G. Klees, K. Mauersberger, K. Schellenbach, J. Stehr (**1995**), Measurement of heavy isotope enrichment in tropospheric ozone, *Geophys. Res. Lett.*, **22** (13), 1713-1716

Krankowsky D., P. Lämmerzahl, K. Mauersberger (**2000**), Isotopic measurements of stratospheric ozone, *Geophys. Res. Lett.*, **27** (17), 2593-2595

Krankowsky D., P. Lämmerzahl, K. Mauersberger (**2001**), Stratospheric ozone isotope enrichments-revisited, *Geophys. Res. Lett.*, **28** (16), 3155-3158

Krankowsky D., C. Janssen, K. Mauersberger (**2003**), Comments on "low-pressure dependencyof the isotopic enrichment in ozone: Stratospheric implications" by S. K. Bhattacharya et al. -art. no. 4503, *J. Geophys. Res.* **108**(D16), 4503-4507

Lämmerzahl P., T. Röckmann, C. A. M. Brenninkmeijer, D. Krankowsky, K. Mauersberger (**2002**), Oxygen isotope composition of stratospheric carbon dioxide, *Geophys. Res. Lett.*, **29** (12), 1582, 23(1-4)

Lee C. C. -W., and M. H. Thiemens (**2001**), The $\delta^{17}O$ and $\delta^{18}O$ measurements of atmospheric sulfate from a coastal and high alpine region: A mass independent anomaly, *J. Geophys. Res.*, **106** (D15), 17,359-17,373

Li W. J., and H.A. J. Meijer (**1998**), The use of electrolysis for accurate $\delta^{17}O$ and $\delta^{18}O$ isotope measurements in water, *Iso. Env. Health Stud.*, **34**, 349-369

Luz B., E. Barkan, M. L. Bender, M. H. Thiemens, K. A. Boering (**1999**), Triple isotope composition of atmospheric O_2 as a tracer of biosphere productivity, *Nature*, **400**, 547-550

Maiss M., L. P. Steele, R. J. Francy, P. J. Fraser, R. L. Langenfelds, N. B. A. Trivett, I. Levin (**1996**), Sulfur hexafluoride- a powerful new atmospheric tracer, *Atmos.Env.*, **30** (10/11), 1621-1629

Matsuhisa Y., J. R. Goldsmith, R. N. Clayton (**1978**), Mechanism of hydrothermal crystallization of quartz at 250°C and 15kbar, *Geochimica and Cosmochimica Acta*, **42**, 173-182

Mauersberger K. (**1981**), Measurement of heavy ozone in the stratosphere, *Geophys. Res. Lett.*, **8** (8), 935-937

Mauersberger K. (**1987**), Ozone isotope measurements in the stratosphere, *Geophys. Res. Lett.*, **14** (1), 80-83

Mauersberger K., B. Erbacher, D. Krankowsky, J. Gunther, R. Nickel (**1999**), Ozone isotope

enrichment: isotopomer-specific rate coefficients, *Science*, **283**, 370-372

Mauersberger K., D. Krankowsky, C. Janssen (**2003**), Oxygen isotope processes and transfer reactions, *Space Sci. Rev.*, **106**, 265-279

Mauersberger K., J. Morton, B. Schueler, J. Steher, S. M. Anderson (**1993**), Multi-isotope study of ozone: Implications for the heavy ozone anomaly, *Geophys. Res. Lett.*, **20**, 1031-1034

Mebel A. M., M. Hayashi, V. V. Kislov, S. H. Lin (**2004**), Isotpic exchange of the excited oxygen atoms with $C^{18}O_2$ and their collisional deactivation, *J. Phys. Chem. A*, **2004**, 7983-7994

Minschwaner K., R. J. Salawitch, M. B. McElroy (**1993**), Absorption of solar radiation by O_2, implication for O_3 and lifetimes of N_2O, $CFCl_3$ and CF_2Cl_2, *J. Geophys. Res.*, **98** (D6), 10543-10561

Mook W. G. (**2000**), Environmental isotopes in the hydrological cycle: Principles and applications,UNESCO, Paris

Mook W. G. and S. van der Hoek (**1983**), The N_2O correction in the carbon and oxygen isotopic composition analysis of atmospheric CO_2, *Isot. Geosci.*, **1**, 237-242

Moore H. (**1974**), Isotopic measurement of atmospheric nitrogen compounds, *Tellus*, **26** (1-2), 169-174

Morton J., B. Schuker, K. Mauersberger (**1989**), Oxygen fractionation of ozone isotopes $^{48}O_3$ through $^{54}O_3$, *Chem. Phys. Lett.*, **154** (2), 143-145

Müller P. (**1997**), Ozonolysis of non methane hydrocarbons as a source of the mass independent oxygen isotope enrichment in tropospheric CO, *Science*, **278** (5344), 1774-1776

Omidvar K., J. E. Fredrick (**1987**), Atmospheric odd oxygen production of ordinary and isotopic molecular oxygen, *Planet. Space Sci.*, **35**, 769-784

Perri M. J., A. L. Van Wyngarden, J. J. Lin, Y. T. Lee, K. A. Boering, (**2004**), Energy dependence of oxygen isotope exchange and quenching in the $O(^1D) + CO_2$ reactions: A crossed molecular beam study, *J. Phys. Chem. A*, (108), 7995-8001

Richet P., Y. Bottinga, M. Javoy (**1977**), A review of hydrogen, carbon, nitrogen, oxygen, sulphur, and chlorine stable isotope fractionation among gaseous molecules, *Ann. Rev. Earth Planet. Sci.*, **5**, 65-110

Riley W. J., (**2003**), ^{18}O composition of CO_2 and H_2O ecosystem pools and fluxes: Simulations and comparisons to measurements, *Global ChangeBiol.*, **9**, 1567-1581

Röckmann T., C. A. M. Brenninkmeier, P. Neeb, P. J. Crutzen (**1998a**), Ozonolysis of non methane hydrocarbons as a source of the mass independent oxygen isotopeenrichment in tropospheric CO, *J. Geophys. Res.*, **103** (D1), 1463-1470

Röckmann T., J. Kaiser, C. A. M. Brenninkmeijer, J. N. Crowly, R. Borchers, W. A. Brand, P. J. Crutzen (**2001**), The isotopic enrichment of nitrous oxide ($^{15}N^{14}NO$, $^{14}N^{15}NO$, $^{14}N^{14}N^{18}O$) in the stratosphere and in the laboratory, *J. Geophys. Res.*, **106** (D10), 10,403-10,410

Santrock J., S. A. Studley, J. M. Hayes (**1985**), Isotopic analysis based on mass spectrum of carbon dioxide, *Anal. Chem.*, **57**, 1444-1448

Savarino, J. and M. H. Thiemens (**1999b**), Mass-independent oxygen isotope (^{16}O, ^{17}O, ^{18}O) fractionation found in H_x, O_x reactions, *J. Phys. Chem. A*, **103**, 9221-9229

Sedlacek A. J., D. R. Harding, R. E. Weston, Jr., T. G. Kreutz, G. W. Flynn (**1989**), Probing the $O(^1D) + CO_2$ reaction with second-derivative modulated diode laser spectroscopy, *J. Chem. Phys.*, **91** (12), 7550-7556

Sehested J., O. J. Nielsen, H. Egsgaard, N. W. Larsen, T. J. Anderson, T. Pedersen (**1998**),

Kinetic study of the formation of isotopically substituted ozone in argon, *J. Geophys. Res.*, **103** (D3), 3545-3552

Sheppard M. G., R. B. Walker (**1983**), Wigner method studies of ozone photodissociation, *J. Chem. Phys.*, **78**, 7191-7199

Sirignano C., R. E. M. Neubert, H. A. J. Meijer (**2004**), N_2O influence on isotopic measurements of atmospheric CO_2, *Rapid commun. Mass Spectrom.*, **18**, 1839-1846

Takahashi K. S., S. Hayashi, Y. Matsumi, N. Taniguchi, S. Hayashida (**2002**), Quantum yield of O(1D) formation in the photolysis of ozone between 230 and 308 nm, *J. geophys. Res.*, **107** (D20), 4440, doi: 10.1029/2001JD002048

Tans P. P. (**1998**), Oxygen isotopic equilibrium between carbon dioxide and water in soils, *Tellus*, **50B**, 163-178

Tans P. P., J. A. Berry, R. F. Keeling (**1993**), Oceanic $^{13}C/^{12}C$ observations- a new window on ocean CO_2 uptake, *Global Biogeochemical Cycles*, **7**, 353-368

Tans P. P., Y. Fung, T. Takahashi (**1990**), Observational constraints on the global atmospheric CO_2 budget, *science*, **247**, 1431-1438

Thiemens M. H., and J. E. Heidenreich III (**1983**), The mass-independent isotope fractionation of oxygen: a novel isotope effect and its possible cosmochemical implications, *Science*, **219**, 1073-1075

Thiemens M. H., T. Jackson, E. C. Zipf, P. W. Erdman, C. van Egmond (**1995a**), Carbon dioxide and oxygen Isotope anomalies in the mesosphere and stratosphere, *science*, **270**, 969-972

Thiemens M. H., T. Jackson, K. Mauersberger, B. Schueler, J. Morton (**1991**), Oxygen isotope fractionation in stratospheric CO_2, *Geophys. Res. Lett.*, **18** (4), 669-672

Thiemens, M. H., T. Jackson, C. A. M. Brenninkmeijer (**1995b**), Observation of a mass independent oxygen isotopic composition in terrestrial stratospheric CO_2, the link to ozone chemistry and the possible occurrence in the Martian atmosphere, *Geophys. Res. Lett.*, **22**, 255-257

Trolier M., J. W. C. White, P. P. Tans, K. A. Masarie, P. A. Gemery (**1996**), Monitoring the isotopic composition of atmospheric CO_2 measurements from NOAA Global Air Sampling Network, *J. Geophys. Res. Atmos.*, **101**, 25897-25916

Tuzson B., (**2005**), Symmetry specific study of ozone isotopomer formation, *Ph.D. Thesis*, Ruprecht-Karls University Heidelberg

Urey H. C. (**1967**), The thermodynamic properties of isotopic substances, *J. Chem. Soc.*, , 562-581

Wen J. and M. H. Thiemens, (**1993**), Multi-isotope study of the $O(^1D) + CO_2$ isotope exchange and stratospheric consequences, *J. Geophys. Res.*, **98** (D7), 12801-12808

Werner R. A., M. Rothe, W. A. Brand (**2001**), Extraction of CO_2 from air samples for isotopic analysis and limits to ultra high precision $\delta^{18}O$ determination in CO_2 gas, *Rapid commun. Mass Spectrom.*, **15**, 2152-2167

Werner R. A., W. A. Brand (**2001**), Referencing strategies and techniques in stable isotope ratio analysis, *Rapid Commun. Mass Spectrom.*, **15**, 501-519

Weston R. E. Jr. (**1999**), Anomalous or mass-indpendent isotope effects, *Chem. Rev.*, **99**, 2115-2136

Yamazaki H. and R. J. Cvetanovic, (**1963**), Isotpic exchange of the excited oxygen atoms with $C^{18}O_2$ and their collisional deactivation, *J. Chem. Phys.*, **40** (2), 582-585

Yang J. M., and S. Epstein (**1987b**), The effect of pressure and excitation energy on the isotopic fractionation in the formation of ozone by discharge of O_2*, *Geochim. Cosmochim. Acta*, **51**, 2019-2024

Yang J. M., and S. Epstein (**1987a**), The effect of the isotopic composition of oxygen on the non mass-dependent isotopic fractionation in the formation of ozone by discharg in O_2*, *Geochim. Cosmochim. Acta*, **51**, 2011-2017

Young E. D., Galy A., Nagahara H. (**2002**), Kinetic and equilibrium mass-dependent isotope fractionation laws in nature and their geochemical and cosmochemical significance, *Geochimica et Cosmochimica Acta*, **66** (6), 1095-1104

Yung Y. L., A. Y. T. Lee, F. W. Irion, W. B. DeMore, J. Wen (**1997**), Carbon dioxide in the atmosphere: Isotopic exchange with ozone and its use as a tracer in the middle atmosphere, *J. Geophys. Res.*, **102**, 10,857-10,866

Yung Y. L., W. B. DeMore, J. P. Pinto (**1991**), Isotopic exchange between carbon dioxide and ozone via O(^{1}D) in the stratospher, *Geophys. Res. Lett.*, **18**, 13-16

Zipf E. C., and P. W. Erdmann (**1994**), Studies of trace constituents in the upper atmosphere and mesosphere using cryogenic whole air sampling techniques, NASA's Upper-Atmospher Research Programme (UARP) and Analysis Programme (AMAP) Research summaries 1992-1993, Environ. Prot. Agency, Washington, D.C.

Appendix I

Table 1: Stratospheric CO_2 samples collected with balloon-borne sampler and with Whole Air Sampler (WAS) mounted on Geophysica during EUPLEX-03 campaign at Kiruna, Sweden.

Sample No.	***Sampling date***	***Altitude (km)***	***Latitude ^oN***	***Longitude ^oE***	***T-Pot (K)***	***N_2O (ppb)***	***Ln f***	***$\delta\,^{13}C$ (‰)***	***$(\delta\,^{17}O)^a$ (‰)***	***$(\delta\,^{18}O)^a$ (‰)***	***$(\Delta)^b$ (‰)***
BL40-5	06/03/03	30.02	67.3	24.8	870.5	18.9	-2.81	-8.07	32.22	47.66	7.62
BL40-8		28.37	67.2	25.1	776.4	19.1	-2.79	-7.85	30.71	47.46	6.21
BL40-14		25.26	67.1	25.5	647.2	12.8	-3.20	-8.09	36.73	50.79	10.52
BL40-12		22.50	67.0	25.8	547.7	3.5	-4.48	-8.05	35.27	49.44	9.76
BL40-1		21.05	67.0	26.0	504.4	18.1	-2.85	-8.06	30.69	46.01	6.95
BL40-4		19.72	66.9	26.3	470.5	61.2	-1.63	-8.01	27.89	45.07	4.63
BL40-7		18.27	66.9	26.5	443.1	133.6	-0.85	-7.97	24.41	43.07	2.18
BL40-10		15.45	66.8	26.8	393.4	234.6	-0.29	-8.11	23.52	41.54	2.08
BL40-3		14.05	66.8	27.0	372.8	270.8	-0.15	-7.82	21.41	41.02	0.24
BL39-1	23/10/02	28.67	43.5	0.8	764.5	103.8	-1.11	-8.10	23.31	42.40	1.43
BL39-7		27.02	43.5	0.9	712.5	143.9	-0.77	-7.62	32.11	46.85	7.93
BL39-4		25.21	43.5	1.0	657.8	-	-	-7.76	23.03	42.24	1.23
BL39-13		20.68	43.5	1.0	524.6	-	-	-8.03	24.54	42.62	2.54
BL39-9		17.63	43.5	1.1	453.8	257.2	-0.20	-7.77	20.67	40.39	-0.16
BL38-2	11/10/01	31.44	44.0	-0.7	866.0	96.8	-1.17	-8.26	27.04	42.76	4.97
BL38-5		30.21	44.0	-0.8	806.0	108.7	-1.05	-9.42	24.57	42.54	2.62
BL38-11		27.02	44.0	-0.9	682.6	143.8	-0.77	-8.31	24.26	41.13	3.03
BL38-6		24.19	44.0	-1.0	599.9	178.7	-0.56	-8.01	22.22	40.51	1.32
BL38-12		22.65	44.0	-1.0	553.1	208.0	-0.41	-8.01	21.67	40.93	0.54

BL38-1		21.48	44.0	-1.0	526.7	240.3	-0.27	-8.12	21.19	41.49	0.56
BL38-4		20.08	44.0	-1.1	498.7	231.0	-0.31	-8.01	20.79	39.78	0.26
BL38-13		17.33	44.1	-1.1	440.4	284.2	-0.10	-8.09	20.14	40.17	-0.58
BL38-3		14.74	44.1	-1.2	393.3	292.3	-0.07	-8.01	20.38	40.30	-0.41
EU02-01	19/01/03	16.84	69.3	20.8	416.2	274.5	-0.14	-8.10	23.43	40.57	2.49
EU03-03	23/01/03	17.66	70.9	16.1	442.2	215.7	-0.37	-7.95	24.78	42.26	2.97
EU03-05		17.64	73.5	16.0	433.4	163.6	-0.65	-7.99	26.77	43.12	4.52
EU04-06	26/01/03	17.81	73.4	23.0	438.3	141.1	-0.80	-8.33	26.91	42.67	4.90
EU07-13	06/02/03	19.58	69.1	12.0	434.2	131.9	-0.86	-8.00	25.29	42.91	3.14
EU07-12		19.52	71.9	9.8	436.6	122.0	-0.94	-8.00	25.39	42.61	3.40
EU07-11		19.45	72.5	9.1	436.9	120.0	-0.96	-7.98	25.14	42.38	3.27
EU07-10		18.96	72.7	9.6	427.0	147.5	-0.75	-8.11	25.61	42.46	3.69
EU07-04		18.50	65.6	14.8	418.6	165.1	-0.64	-8.02	25.36	42.99	3.18
EU07-05		18.49	65.9	14.4	420.8	157.6	-0.68	-7.98	25.88	42.85	3.76
EU07-09		18.48	70.1	12.0	420.3	163.2	-0.65	-7.86	24.69	41.83	3.10
EU07-07		18.47	69.1	12.7	419.9	160.5	-0.67	-7.82	24.97	42.22	3.18
EU07-08		18.47	69.6	12.4	420.2	160.5	-0.67	-8.10	25.66	42.65	3.65
EU07-18		17.08	67.0	17.3	397.1	202.1	-0.44	-8.05	24.72	42.28	2.91
EU07-19		15.03	67.7	19.4	370.4	260.6	-0.19	-8.03	23.16	41.54	1.72
EU08-17	08/02/03	20.47	70.8	21.8	452.0	100.7	-1.13	-8.14	26.00	43.40	3.60
EU08-16		20.41	71.1	20.2	452.5	103.3	-1.11	-8.03	26.09	43.46	3.66
EU08-13		20.25	68.7	16.5	452.5	200.4	-0.45	-8.10	23.63	41.78	2.07
EU08-12		20.13	67.6	21.5	445.6	205.5	-0.42	-7.98	25.17	41.42	3.80
EU08-10		20.03	67.2	23.6	441.9	196.1	-0.47	-8.18	25.35	41.56	3.90

EU08-07		19.87	67.4	24.8	439.0	182.2	-0.54	-8.05	24.21	41.89	2.59
EU08-08		19.80	67.1	26.1	435.9	191.7	-0.49	-8.08	25.43	42.54	3.48
EU08-06		19.52	68.8	17.9	439.8	225.7	-0.33	-8.02	23.12	40.82	2.06
EU08-05		19.14	69.1	16.3	433.8	210.7	-0.40	-7.97	25.82	42.72	3.78
EU08-03		15.76	68.1	17.7	389.0	286.9	-0.09	-7.95	22.97	41.42	1.59
EU09-18	09/02/03	19.81	68.7	29.0	447.9	227.9	-0.32	-8.10	22.87	40.97	1.73
EU09-12		19.81	72.1	46.0	439.2	170.2	-0.61	-8.38	25.03	41.27	3.73
EU09-17		19.80	69.1	30.1	447.6	222.2	-0.34	-8.01	23.87	41.98	2.21
EU09-16		19.80	69.4	31.2	445.8	217.7	-0.36	-8.04	23.58	41.12	2.36
EU09-11		19.79	71.9	47.4	439.6	159.0	-0.68	-8.15	27.56	43.89	4.91
EU09-10		19.79	71.7	48.8	437.8	146.3	-0.67	-8.14	25.59	41.86	3.98
EU09-13		19.78	71.6	39.1	439.8	146.3	-0.76	-8.18	24.76	41.34	3.42
EU09-14		19.78	71.4	37.7	440.1	177.2	-0.57	-8.09	24.87	41.53	3.44
EU09-15		19.78	71.1	36.4	441.5	217.3	-0.36	-8.18	22.68	41.24	1.40
EU09-08		18.67	72.1	42.6	420.6	216.6	-0.37	-8.04	23.65	41.63	2.17
EU09-05		18.46	70.0	32.8	420.7	248.3	-0.23	-7.99	25.58	41.55	4.14
EU09-04		18.46	69.6	31.7	420.5	257.4	-0.20	-7.90	23.27	41.19	2.02
EU09-06		18.46	70.5	33.8	420.8	239.7	-0.27	-8.00	23.92	40.78	2.88
EU09-03		16.84	68.3	25.9	405.3	276.1	-0.13	-7.71	23.33	41.16	2.09
EU09-19		15.92	68.1	23.5	394.3	286.1	-0.10	-7.95	22.52	40.56	1.59
EU09-02		15.20	68.2	24.8	382.5	304.7	-0.03	-7.94	22.64	40.94	1.51
EU10-11	11/02/03	18.53	69.9	12.1	438.2	270.7	-0.15	-8.19	24.07	40.86	2.98
EU10-05		12.62	70.0	25.6	343.9	305.0	-0.03	8.08	23.37	40.24	2.60

$a = 1000\ln(1+\delta^{i}O/1000)$

$b = \Delta = 1000\ln(1+\delta^{17}O/1000) - 0.516 * 1000\ln(1+\delta^{18}O/1000)$

Acknowledgements

As I started my way through the world of the invisible gas molecules for the first time in my life, I happened to encounter ozone- a most reactive molecule as it is called rather I would say "most aggressive molecule". During this doctoral work, I happened to break some of my glass equipment, but Prof. T. Röckmann encouraged me to think critically and more importantly to make every thing safe. I consider it a distinct privilege to work with Prof. T. Röckmann, as I learned from him, how to apply chemical principles, how to define a scientific problem, design an experiment and above all how to scrutinize and squeeze the utmost information out of my data. Like wise, I gained much in association with Dr. C. Janssen. I particularly value his ever ready nature to discuss the issues and his willingness to solve them. He shaped my approach to science and to intellectual pursuit in general.

During my work I could profit much from Prof. K. Mauersberger's experience, his way of thinking and questioning things and especially his way, how he was looking at elementary reactions of great significance. The combination of all these experienced people in their field, Prof. T. Röckmann, Prof. K. Mauersberger, P.D. Dr. C. Janssen and Dr. D. Krankowsky created a very stimulating scientific environment. I learned in the atmospheric physics group that best science is not much of worth when it cannot be presented in an appropriate way. I remember the particular sessions with our group before meetings and conferences. The idea was never to simply criticize the work, rather the comments were always constructive. I think as a scientist we all need a constructive feed back from colleagues to further improve and widen our horizon.

I feel fortunate to have Prof. W. Kräetschmer as my co-supervisor because he has a wonderful quality of instilling confidence- an attribute for which I am grateful. Thanks to Zsuzsanna for keeping my chaotic work table fresh with wonderful flowers from her garden and lovely hugs to brighten my day.

During my stay at the Max Planck Institute, a friendly and collegial atmosphere prevailed because of my friends Joachim, Ruth and Ute. Their friendship has been a source of satisfaction for me and I take great pleasure in the kind and caring friends they have always been.

Special thanks are due to M. Brass to carefully solve the software problems. His calm nature has inspired me sometimes. I really appreciate the way, he can spend hours and hours to solve

every problem step by step. I particularly must thank my colleague Dr. P. Franz for extending help in all sort of problems and B. Knape who skillfully maintained high standards of mass spectrometers. Last but not least, F. Kepler is acknowledged for useful discussions.

This work would have been incomplete without the assistance of Dr. B. Tuzson who measured the ozone isotopomers with his highly precise TDLAS and shared some of his recent unpublished work which I used in the modeling section.

I wish to thank our glass blowers, P. Mögel, E. Borger and the librarian G. Vogt and other staff at the Max Planck Institute for Nuclear Physics, Heidelberg for their unfailing assistance.

I am thinking of many people who have influenced and shaped my scientific path over the past years, among them Dr. M. H. Naqvi, Dr. Javed Akhter, Dr. Mohsin Iqbal, Dr. Haseebullah, Dr. Mohammad Afzal and Dr. Shaukat Hassan are few to name. Back in Switzerland, I am thankful to Dr. K. Wilkinson and Dr. N. Rouiller for their assistance to step forward for doctoral work.

I am indeed pleased to mention Dr. S. H. Mujtaba Naqvi, Ingy Abdel-Aziz and Nasrin Marzban who always inspired me to look ahead. I gratefully acknowledge Fr. Petra Ziegler and Dr. Martina Schade for providing superb administrative assistance at the Faculty of Chemistry, University of Heidelberg, Germany.

Thus far in my career I have been blessed with the prayers of my parents and my grandmother. I am really grateful to them for their permission to pursue my studies abroad and apologize whole heartedly for being not able to visit them on this long winding road. In fact, it took more than half a decade for me to make the journey from plant science to atmospheric physics and chemistry.

This acknowledgment would not be complete without mentioning my aunt Huma Soofi and uncle Ali Soofi whose encouragement enabled me to pass through the thicks and thins of life. I wish to thank my all family members for their loving support through my entire education.

In closing, I would like to thank my friends, Nicole, Birgit, both Verena's, Iffat Hassan, Asma and Rubina that they have always reminded me some of other important aspect of life except work. In this context, I wish to thank Christof Janssen and Birgit Müller for many social events and that they always welcomed me so warmly.